DYNAMIC ANALYSIS OF CONSTRAINED RIGID PAVEMENT SUBJECTED TO MOVING LOAD

MAJOR-II PROJECT REPORT

SUBMITTED IN PARTIAL FULFILLMENT OF THE REQUIREMENTS

FOR THE AWARD OF THE DEGREE

OF

MASTER OF TECHNOLOGY

IN

GEOTECHNICAL ENGINEERING

Submitted by:

Yakshansh Kumar

2K18/GTE/018

Under the supervision of

Professor Ashutosh Trivedi

DEPARTMENT OF CIVIL ENGINEERING

DELHI TECHNOLOGICAL UNIVERSITY
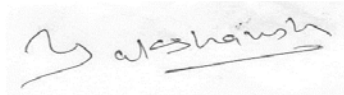
(Formerly Delhi College of Engineering)

Bawana Road, Delhi-110042

July 2020

DELHI TECHNOLOGICAL UNIVERSITY

(Formerly Delhi College of Engineering)

Bawana Road, Delhi-110042

CANDIDATE'S DECLARATION

I, Yakshansh Kumar, Roll no. 2K18/GTE/018 student of M.Tech., Geotechnical Engineering, hereby declare that the Dissertation titled "**Dynamic analysis of constrained rigid pavement subjected to moving load**" which is submitted by me to the Department of Civil Engineering, Delhi Technological University, Delhi in partial fulfillment of the requirement for the award of the Master of Technology is original and not copied from any source without proper citation. This work has not previously formed the basis for the award of any Degree, Diploma Associateship, Fellowship, or other similar title or recognition.

Place: Delhi **(YAKSHANSH KUMAR)**

Dated: 26/10/2020

DEPARTMENT OF CIVIL ENGINEERING

DELHI TECHNOLOGICAL UNIVERSITY

(Formerly Delhi College of Engineering)

Bawana Road, Delhi-110042

CERTIFICATE

I hereby certify that the Project Dissertation titled "**Dynamic analysis of constrained rigid pavement subjected to moving load**" which is submitted by Yakshansh Kumar, Roll no. 2K18/GTE/018 [Civil Engineering], Delhi Technological University, Delhi in the partial fulfillment of the requirement for the award of the degree of Master of Technology, is a record of the project work carried out by the student under my supervision. To the best of my knowledge this work has not been submitted in part or full for any degree or diploma to this University or elsewhere.

Place: Delhi **(Prof. ASHUTOSH TRIVEDI)**

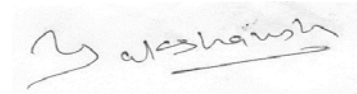Dated: 26/10/2020 **SUPERVISOR**

ABSTRACT

In the present study velocity-induced displacement, stress, and stiffness response of rigid pavement subjected to moving mass is captured using a numerical program. The implicit integration scheme is used to carry out dynamic analysis of rigid pavement supported by granular fill confined by retaining walls. A comparative solution to the problem of velocity induced loading, displacement, stress, and stiffness response is obtained using numerical algorithms. The dynamic amplification factors are calculated as a function of velocity in the vertical as well as in the lateral direction. The maximum value of dynamic displacement observed in the vertical direction was 31% higher than that of the static displacement and 57% higher than that of static displacement in the lateral direction. The maximum dynamic magnification was observed to be 70% higher than that of the static load for the selected velocities considered in this study. Numerical damping was introduced while computing velocity induced magnifications. The dynamic displacement contour showed levitation effects for the higher range of velocities. The model is validated by performing mesh convergence tests and results are compared within the output obtained using numerically varied algorithms. The evaluation of numerical damping, load and displacement magnification, and dynamic stiffness of the pavement along with velocity induced stress variation subjected to moving mass set an important milestone in the dynamic analysis of rigid pavements supporting the transportation network.

ACKNOWLEDGMENT

I thank god almighty for bestowing his blessings and grace in the completion of this thesis.

I express my sincere thanks to the University Management.

As I write this acknowledgment, I must clarify that this is not just a formal acknowledgment but also a sincere note of thanks and regards from my side. I feel a deep sense of gratitude and affection for those who were associated with the project and without whose co-operation and guidance this project could not have been conducted properly. Words fail me to express my regards towards my project guide, Prof. A. Trivedi Dean (IRD) Department of Civil Engineering, Delhi Technological University, Delhi for allowing me to work under his guidance, which instilled in me the requisite confidence. I also express my deep gratitude to the Department of Civil Engineering and all the Faculty member of Civil Engineering Delhi Technological University, Delhi for the pains taken by him to go through the manuscript and giving his useful suggestions. Last but not the least, I would like to thank my family and friends who stimulated me to bring this work to a successful close.

YAKSHANSH KUMAR

Roll No. 2K18/GTE/018

Department of Civil Engineering

Delhi Technological University

CONTENT

LIST OF FIGURES

LIST OF TABLES

Chapter 1

Introduction

Practically the problem of finding exact values of displacement for moving load is very difficult in the field as it involves various field complexities. An attempt is made using commercialized software package Abaqus in an implicit integration scheme to solve this problem numerically. A non-dimensional displacement factor is obtained to evaluate the increased values of displacement due to the moving load in terms of the ratio of displacement due to the moving load to the displacement due to the static load.

The finite element algorithm used to evaluate the dynamic displacement factor uses an 8-node linear brick element in full integration scheme. The whole analysis is divided into 2 steps for analysis i.e., the first step is for applying the load gradually and the second step is for observing the effects of moving load. By default, hex dominated mesh is used to reach out to exact results. A numerical noise is unavoidably introduced when we are solving the problem, these operators account for different numerical noise in terms of numerical damping for stabilizing the algorithm.

Further studies are carried out to check the stability of these operators. Response for each algorithm is recorded in tabular form and their stability check is performed by comparing their dynamic displacement factor.

CHAPTER 2
REVIEW OF LITERATURE

In the present study velocity-induced loading, displacement, stress, and stiffness response of rigid pavement subjected to moving mass are captured using a numerical program. A comparative solution to the problem of velocity induced loading, displacement, and stiffness response is obtained using a numerical algorithm. The vehicle-pavement interaction effects are critically acclaimed to be crucially significant for exploration of the dynamic response of rigid pavements subjected to moving mass type of loading (Lewis and Harr, 1969; Chiu et al.,1971; Taheri et al., 1990). In classic pavement engineering, the design criteria for concrete pavements were based on analytical solutions. An exploring study for the dynamic anatomization of beams and plates because of moving loads employing classical approaches was discussed by Fryba (1972). Timoshenko's beam theory was used for obtaining the analytical solution for an infinite dimensioned beam and the foundation soil was modelled as linear viscoelastic solid considering the Kelvin model (Achenbach and Sun, 1965). Using the same ideology for the infinite dimensioned plate, Thompson (1963) analytically presented the steady-state solution for the same dynamic displacement value problem. Several attempts were made by incorporating two-dimensional (2D) FE algorithms to observe the dynamic displacement. In classical literature, Yoshida and Weaver (1971) introduced a 2D finite-element algorithm to study the dynamic analysis of rigid pavements. An improved 2D finite element algorithm which studied the transient response under arbitrary boundary conditions with the moving load was then introduced (Taheri and Ting, 1989,1990). Zaman et al. (1991) used thick plate theory to capture the dynamic response of pavement and observed the dynamic effects due to transverse shear deformation. These aforesaid 2D FE algorithms have been proven to be satisfactorily validated with other theoretical solutions but there are limitations associated with these, namely thickness of the pavement, oversimplified boundary conditions, absence of realistic frictional effect, dynamic load creation, and so on. To accomplish a more accurate, precise, and comprehensive analysis of the soil subgrade pavement system's behaviour. So, it is imperative to create a 3-D finite element algorithm. Many 3-D models were created and used to run the simulation problem concerning subgrade stress effects in pavement (Ioannides and Donnelly, 1988). Wu (1996) proposed a 3-D finite-element algorithm that was used to analyse the behaviour of concrete pavements concerned with moving loads. Moving state equations

were derived using Hamilton's principle in the formulation and the linear viscoelastic model was used to model the soil foundation to consider the linear foundational damping profile. Dynamic behaviour and interaction effects between moving load and pavement-subgrade-soil systems contain severe mathematical complexities. So, mathematical modelling for static loading alone cannot be used to analyse the response of concrete pavement subjected to fast-moving vehicular loading (Kim and McCullough, 2003; Wang and Yang, 2008). Using the classical approach, the mass-spring-dashpot model for the moving load with constant velocity or acceleration over concrete pavement was created by Ding et al, (2014). Kumari and Trivedi (2020) examined the semi-dynamic control technique for retaining structure and the pressure strain reaction of the PZT framework comprises holding a PZT fix between the retaining structure and granular inlay had been dissected. The variety of stress-strain reaction with modulus proportion of holding retaining wall and PZT fix was introduced graphically. A model was introduced to inspect the impact of retaining wall and PZT framework on vibration incited in retaining structure because of even powerful contrasted vertical shaking conditions. Hilber et al, (1977) presented the importance of studying the numerical noise introduced while computing a problem numerically and obtained the values to be assigned in terms of non-dimensional factor-alpha to define operators corresponding to numerical damping. Tang et al., (2020) observed the variation of displacement and stress variation for different saturation and permeability conditions.

It has been observed in the literature so far that very little attention was given to dynamic displacement profile, dynamic stiffness changes, and stress variation. So, there is a great need to study the displacement and stiffness response along with stress variations induced due to velocity. Practically the solution to the displacement response for moving load is very difficult in the field as it involves various field complexities. Thus, an attempt was made using a numerical program. An implicit integration scheme is used to carry out the dynamic analysis. The whole analysis was divided into 2 steps namely the loading step and the moving step. The first step was for applying the load gradually and the second step was for observing the effects of moving load. The dynamic amplification factors are calculated as a function of velocity in the lateral as well as in the vertical direction. Amplification factors along the depth were obtained on the pavement top. The pavement in the vertical direction is constrained with boundary conditions simulating the problem of retaining wall in the field, using this

assumption, in the lateral direction amplification factors were obtained on the retaining wall. The non-dimensional stiffness factor showed hardening and softening effects.

CHAPTER 3
DYNAMIC DISPLACEMENT FACTOR AND METHODOLOGY ADOPTED

3.1 INTRODUCTION

Researchers study the amplification due to dynamic effects in terms of load factor but this study is believed to carry out in terms of dynamic displacement and static displacement and amplification are recorded in terms of dynamic displacement factor.

This study was carried out in terms of load, displacement, and stiffness responses further their corresponding amplifications are recorded in terms of dynamic magnification factor (DMF), dynamic displacement factor (DDF), and non-dimensional stiffness factor (NDSF) respectively.

DDF is defined as the ratio of displacement obtained using inertial frame analysis (dynamic displacement) to the displacement obtained using non-inertial frame analysis (static displacement). DMF is defined as the ratio of dynamic load to the static load and NDSF is defined as the ratio of DMF to DDF.

$$\text{DDF} = \frac{\text{Dynamic displacement}}{\text{Static displacement}}$$

$$\text{DMF} = \frac{\text{Dynamic load}}{\text{Static load}}$$

$$\text{NDSF} = \frac{\text{DMF}}{\text{DDF}}$$

$$(1)$$

3.2 MODELING ASSEMBLY

For the problem statement assembly of different layers is done with general and hard contact profile and the value of frictional coefficient between moving mass and pavement surface to be 0.3. The commercialized software package Abaqus was used to model the concrete pavement-subgrade-subbase assembly for the investigation concerned with moving mass

problems (e.g., Wang and Chen, 2006; Liao and Huang, 2008; Zhuang et al., 2009; Wang and Fu, 2010).

Reduced dimensional analysis considering numerous tire model for modelling the quarter portion and half portion of the car is done by Yang et al. (2013). Base on the studies of Yang et al. (2013) author has considered the half model for symmetry to reduce the computation time. Consequently, dimensions were reduced to half, and analysis was performed. Dimensions related to pavement, subgrade, and subbase are tabulated in Table 1.

Table 1: Dimensional specification of the pavement-subgrade-subbase model.

Material specification	Dimensions (m)		
	Length (L)	Breadth (B)	Height (H)
Concrete pavement layer	10.00	1.75	0.15
Granular subgrade layer	10.00	2.50	0.25
Subbase layer	10.00	3.00	6.00

Figure 1 shows the line diagram of the problem statement in the sectional and isometric view. Constrained boundary condition representing the retaining structure condition as shown in the sectional view diagram (not drawn to scale). Half symmetric line diagram of the model (not drawn to scale) consisting of an isometric view of the soil-subgrade-pavement system in which face ABCD, EFGH, and IJKL are constrained faces. Assembly of the pavement-subgrade-subbase system was done with general and hard contact profile. The value of the frictional coefficient between moving mass and pavement surface was defined to be 0.3. Boundary conditions are taken to be fixed on the bottom and boundary condition on the sides to be symmetric about the axis. The lateral dimension was constrained with boundary conditions simulating to retaining wall conditions. Figure 2 represents the CAE view of the modal assembly with half symmetry.
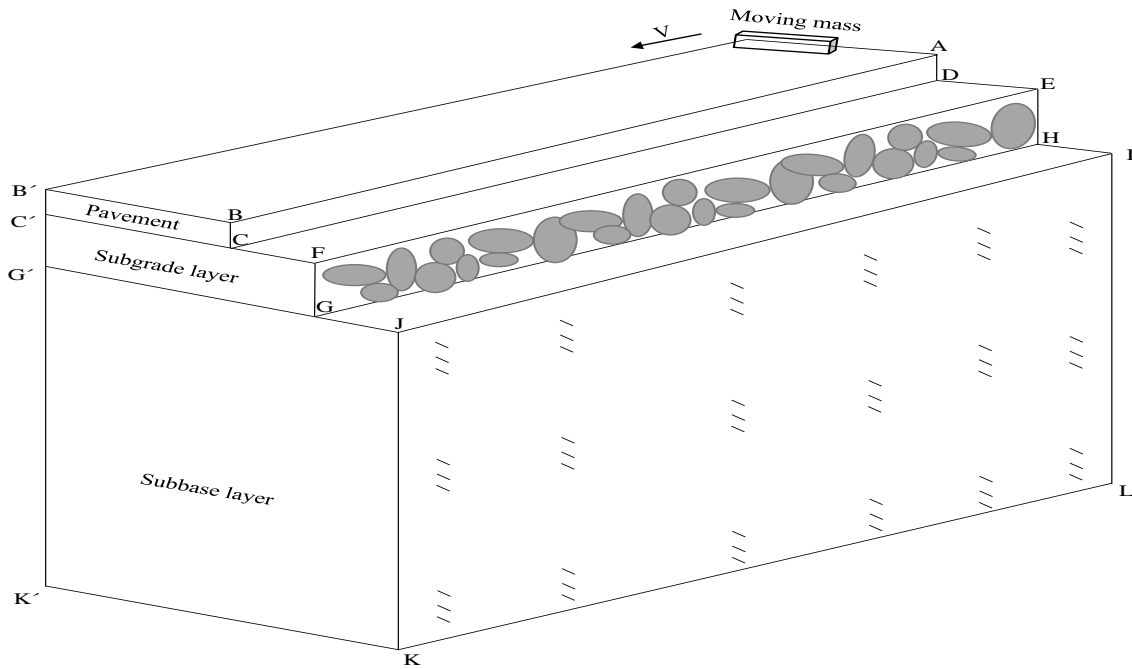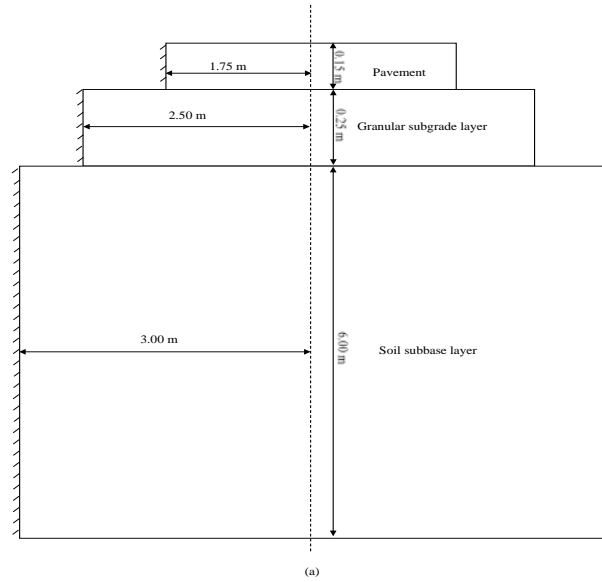
Figure 1: Line diagram (a) Representative line diagram (not drawn to the scale) consisting of sectional front view of the soil-subgrade-pavement system with dimension of pavement, granular subgrade and soil subbase considered half taking symmetry about center are (10.00m X 1.75m X 0.15m), (10.00m X 2.50m X 0.25m), and (10.00m X 3.00m X 6.00m) respectively constrained by boundary condition representing the retaining structure condition as shown. and (b) Half symmetric model line diagram (not drawn to scale) consisting of isometric view of the soil-subgrade-pavement system where face ABCD, EFGH and IJKL are constrained by boundary condition representing the retaining structure condition.
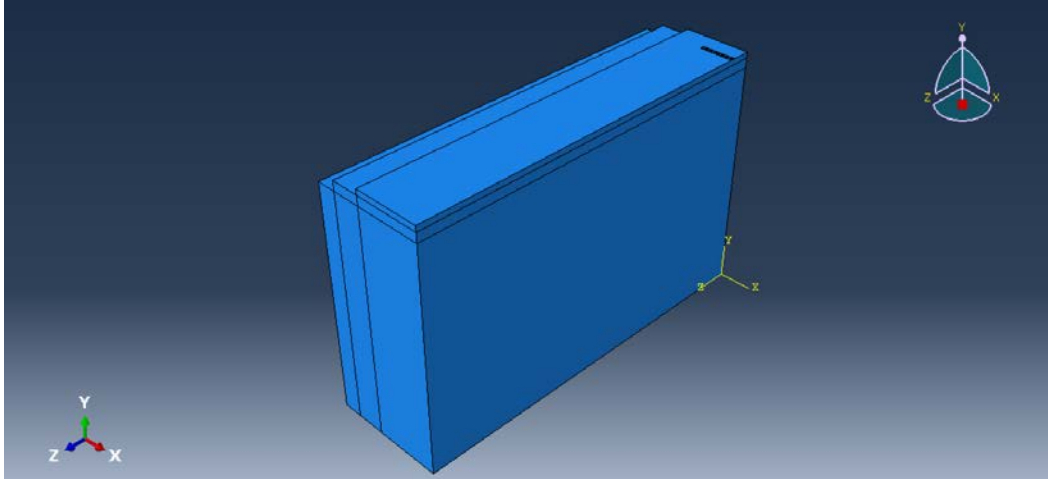
Figure 2: Idealized pavement subgrade base model in ABAQUS

3.3 STEPS INVOLVED IN THE ANALYSIS AND MATERIAL PROPERTY

The whole analysis is divided into two steps, loading and moving step. In the loading step, gradual loading on the pavement top surface, and in the second step, this loaded mass is moved with different velocities. The material properties were adopted from Bowls (1996). Specifications for layers according to their density, Young's modulus, and Poisson's ratio are presented in tabular form as shown in Table 2.

Table 2: Material properties adopted from Bowls (1996).

Parameter (symbol)	Material	unit	Value
	Concrete		2.48×10^7
Elastic modulus (E)	Granular material	MPa	2.76×10^5
	Dense uniform sand		5.15×10^4
	Concrete		0.15
Poisson's ratio (v)	Granular material	-	0.30
	Dense uniform sand		0.40
	Concrete		23.24
Density (ρ)	Granular material	kN/m^3	17.60
	Dense uniform sand		18.40

3.4 LOAD DEFINATION AND MESHING

Meshing is done using a global seeding tool. An 8-node linear brick element under reduced integration with hourglass control is used in meshing. Results are obtained by performing mesh convergence tests as tabulated in Table 3.

Table 3: Mesh size corresponding to global seeding.

Global seeding	Mesh size (L X B X H)		
	Dense uniform sand	Granular layer	Pavement
0.5	20 X 6 X 12	20 X 5 X 1	20 X 4 X 1
0.4	25 X 7 X 15	25 X 6 X 1	25 X 4 X 1
0.3	33 X 10 X 20	33 X 8 X 1	33 X 6 X 1
0.2	50 X 16 X 30	50 X 13 X 1	50 X 9 X 1

As discussed earlier whole analysis is carried out using two steps i.e., Loading step and Moving step. In loading step load is applied gradually using Abaqus stranded static general step till the maximum static load is reached. Then this loading is maintained in moving step typically defined as heave side step loading function.

Mathematically load function is defined as,

$$f_m(t) = U(t_m - t_l) \qquad (2)$$
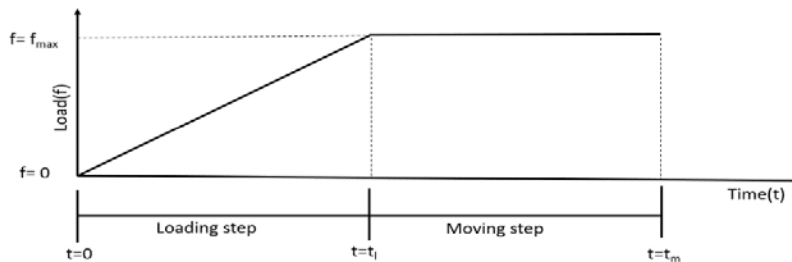
Figure 3: Load definition

CHAPTER 4

FINITE ELEMENT ALGORITHM AND EQUATION OF MOTION

A 3-Dimensional 8-node linear brick element in full integration scheme is adopted for modeling the dynamic behavior of pavement. The nodal displacement distributions of the pavement-subgrade-soil system is tabulated in Table 4. The detailed information about the interpolator (shape function) is specified in Hinton and Owen (1979).

Table 4: Nodal specifications

Local Node Number	x_i	y_i	z_i
1	-1	-1	-1
2	1	-1	-1
3	1	1	-1
4	-1	1	-1
5	-1	-1	1
6	1	-1	1
7	1	1	1
8	-1	1	1
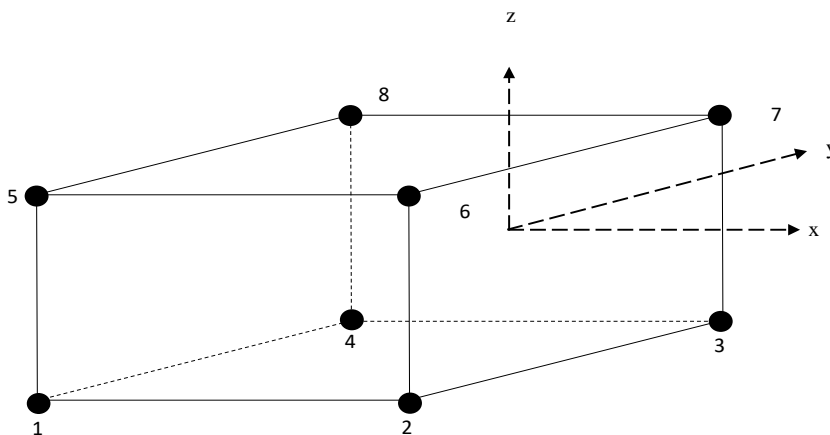
Figure 4: 8- node linear brick element

4.1 Static analysis

Displacement independent of time frame i.e., Static displacement is calculated in static analysis.

Static analysis is accomplished using a time-independent integration scheme using static general steps in the Abaqus standard.

Equation of motion for this can be written as,

$$[K] \times [x] = [F] \tag{3}$$

where,

[K] = Global stiffness matrices

[x]= nodal displacement vectors

[F]= externally applied force vectors

4.2 Dynamic analysis

Moving vehicle load effects were captured using the time-dependent direct integration scheme.

Displacement depending on time frame is captured using D'Allembert principal and motion equation is given by,

$$[M]\{\ddot{x}\} + [C]\{\dot{x}\} + [K]\{x\} = \{F_E\} \tag{4}$$

where [M], [C], and [K] are corresponding mass matrix, damper matrix, and stiffness matrix respectively. $\{\ddot{x}\}$ is the acceleration vector associated with the mass matrix, $\{\dot{x}\}$ is the velocity vector associated with the damper matrix, $\{x\}$ is the displacement vector associated with the stiffness matrix, and $\{F_E\}$ is the externally prescribed force vector.

Equation of motion in terms of externally prescribed force and body force related to elemental volume is given by,

$$\{Q_B\} + [\rho]\{\ddot{x}\} = \{Q_E\} \tag{5}$$

where $\{Q_B\} = \frac{[C]\{\dot{x}\} + [K]\{x\}}{v}$ is body force terms in terms of elemental volume (v), $\{Q_E\} = \frac{\{F_E\}}{v}$ is the externally prescribed force in terms of elemental volume.

11

Equation of work done in terms of body force (Q_B) and externally applied force (Q_E) is given by,

$$\iiint Q_B.\delta v \; dv - \iiint (\rho.\ddot{x}).\delta v \; dv \;=\; \iiint Q_E.\delta v \; dv \qquad (6)$$

with regards to initial reference volume v_0 and initial reference density ρ_0, D'Allembert force term can be rewritten as $\iiint (\rho_0\ddot{x}).\delta v \; dv_0$ and correspondingly equation of work done takes the form as,

$$\iiint Q_B.\delta v \; dv_0 \;-\; \iiint (\rho_0\ddot{x}).\delta v \; dv_0 \;=\; \iiint Q_E.\delta v \; dv_0 \qquad (7)$$

where $\ddot{x}$ is calculated using the time integration operator.

The nodal displacement distributions of the pavement-subgrade-soil system are given by:

$$x = N_i^N x^N \qquad (8)$$

$$N_i^N(x, y, z) = \frac{1}{8}(1+x_i x)(1+y_i y)(1+z_i z) \qquad (9)$$

The detailed information about the interpolator (shape function) is specified in Hinton and Owen (1979). The interpolator (N_i^N), independent of displacement vectors approximates the displacement at a given by,

$$x = N_i^N x^N \qquad (10)$$

and nodal acceleration is given by,

$$\ddot{x} = N_i^N \ddot{x}^N \qquad (11)$$

D'Allembert force term assuming interpolation can be written as ($\iiint \rho_0 N_i^N N_i^M \; dv_0)\ddot{x}^M$ and the corresponding equation of work done is given by,

$$\iiint \rho_0 N_i^N N_i^M \, dv_0 \, \ddot{x}^M + \iiint \beta^N{:}\sigma \, dv_o = \iint N_i^N \, t \, ds + \iiint N_i^N \, Q_E \, dv \qquad (12)$$

where ρ_0 is initial reference density, v_0 is initial reference volume, N_i^N and N_i^M are interpolation function associated with n^{th} and m^{th} node, and $\ddot{x}^M$ acceleration vector associated with m^{th} node. $\beta^N{:}\sigma$ is the nth node extension field degree of the stress extension field calculating the inertial force vector. Using the interpolation assumption, the body force term was calculated as a product of mass matrix formulated by consistent use of interpolation times the nodal acceleration.

Consistent use of interpolation assists in maintaining a constant value of mass to avoid the violation of the law of conservation of mass. Finally, the equation of motion is given by,

$$[M_C^{NM}]\{\ddot{x}\} + [I_F^N] = [Q_F^N] \qquad (13)$$

where $M_C^{NM} = \iiint \rho_0 N_i^N N_i^M \, dv_0$ is mass matrices obtained by consistent use of interpolation between n^{th} node to m^{th} node,

$I_F^N = \iiint \beta^N{:}\sigma \, dv_0$ is inertial force vector associated with n^{th} node, and

$Q_F^N = \iint N_i^N \, t \, ds + \iiint N_i^N \, Q_E \, dv$ is the external force vector associated with n^{th} node

4.3 Damper controlled numerical solution

A numerical solution to the problem of moving mass on the assembly of pavement subgrade and subbase is obtained by modifying the Newmark's β method. In the process of time integration, a small amount of high-frequency numerical noise unwantedly gets introduced and the numerical noise was removed by numerical damping to stabilize the algorithm. The actual equilibrium equation of motion is replaced by the operator with balanced D'Allembert forces. The weighted average was taken for the static forces at the start and termination of each time step. Now, the equation of motion is given by,

$$[M_{DC}^{NM}]\{\ddot{x}\,|_{t+\Delta t}\} + \{R_F^N\,|_{t+\Delta t}\} - \Phi\{R_F^N\,|_t\} = 0 \qquad (14)$$

where, M_{DC}^{NM} is the damped consistent mass matrix,

13

$R_F^N |_{t+\Delta t} = [\frac{\{I_F^N |_{t+\Delta t}\} - \{Q_F^N |_{t+\Delta t}\}}{L^N |_{t+\Delta t}}]$ and $R_F^N |_t = [\frac{\{I_F^N |_t\} - \{Q_F^N |_t\}}{L^N |_{t+\Delta t}}]$ are the resultant force vector associated

with the nth node at time $t + \Delta t$ and time t in which $L^N |_{t+\Delta t}$ is the summation of all Lagrange multiplier forces corresponding to the nth node at time $t + \Delta t$.

Further, modified Newmark's formula for displacement and velocity integration is given by,

$$\{x |_{t+\Delta t}\} = \{x |_t\} + \Delta t.\{\dot{x} |_t\} + \Delta t^2.(\psi).\{\ddot{x} |_t\} + \left(\frac{1}{2} - \psi\right).\{\ddot{x} |_{t+\Delta t}\}) \tag{15}$$

$$\{\dot{x} |_{t+\Delta t}\} = \{\dot{x} |_t\} + \Delta t.((\omega).\{\ddot{x} |_t\} + (1 - \omega).\{\ddot{x} |_{t+\Delta t}\}) \tag{16}$$

where $\ddot{x} |_{t+\Delta t}$, $\dot{x} |_{t+\Delta t}$, and $x|_{t+\Delta t}$ is the acceleration, velocity, and displacement vector at time $t + \Delta t$ and $\ddot{x} |_t$, $\dot{x} |_t$, and $x|_t$ is the acceleration, velocity and displacement vector at time t and the limits of non-dimensional damping factors have been derived for equation (14), equation (15), equation (16) as:

$$-1 < \Phi < 0, \, 4\psi = 2 - \left(\frac{1}{1+\Phi}\right)^2, \text{ and } \omega = \frac{1}{2}\left(\frac{1+3\Phi}{1+\Phi}\right)$$

4.4. Stress calculation

The velocity induced total nodal stress for the problem of moving mass over rigid pavement is obtained as,

$$\sigma_T^N = \sigma_{11}^N + \sigma_{22}^N + \sigma_{33}^N \tag{17}$$

Nodal stress at time integration step was obtained by formulating isotropic elastic model for stress-strain in a constitutive model given as,

$$
\begin{pmatrix} \varepsilon_{11}^N \\ \varepsilon_{22}^N \\ \varepsilon_{33}^N \\ \varepsilon_{12}^N \\ \varepsilon_{13}^N \\ \varepsilon_{23}^N \end{pmatrix} =
\begin{bmatrix}
1/E & -v/E & -v/E & 0 & 0 & 0 \\
-v/E & 1/E & -v/E & 0 & 0 & 0 \\
-v/E & -v/E & 1/E & 0 & 0 & 0 \\
0 & 0 & 0 & 1/G & 0 & 0 \\
0 & 0 & 0 & 0 & 1/G & 0 \\
0 & 0 & 0 & 0 & 0 & 1/G
\end{bmatrix}
\begin{pmatrix} \sigma_{11}^N \\ \sigma_{22}^N \\ \sigma_{33}^N \\ \sigma_{12}^N \\ \sigma_{13}^N \\ \sigma_{23}^N \end{pmatrix} \tag{18}
$$

where $\varepsilon_{11}^N, \varepsilon_{22}^N, \varepsilon_{33}^N, \varepsilon_{12}^N, \varepsilon_{13}^N, \varepsilon_{23}^N$, are the elastic normal and shear strain components for n^{th} node, $\sigma_{11}^N, \sigma_{11}^N, \sigma_{11}^N, \sigma_{11}^N, \sigma_{11}^N, \sigma_{11}^N$ are the elastic normal and shear stress components for n^{th} node, and $G = E/2(1+v)$.

4.5. Computation algorithm

Figure 5: Flow chart

The computation is carried out using commercialized software package Abaqus under Abaqus standard solver technique, the flowchart for which is shown in Figure 5.

1. Analysis for static and dynamic loading is carried out under Abaqus standard solver considering initial input parameters for pavement-subgrade-subbase. The damper controlled nodal dynamic behavior of moving mass is observed using equation (14) and hence the dynamic displacement is obtained using equation (15).

2. Taking dynamics of moving mass into account the dynamic nodal stress behavior of system is obtained using equation (18) and total nodal stress is calculated using equation (17).

3. Using this aforementioned equation in step 1 and 2 the displacement and stress calculation is repeated and the whole process is cycled towards the finer mesh size until the desired convergence is achieved for the present study.

4. With these converged valued results of displacement and loading, the velocity induced amplification is determined using equation (1) and dynamic profile is presented over the observation line of pavement and retaining wall considered in the present study.

CHAPTER 5

Model Validation and result discussion

The numerical model presented in this study is validated by a mesh convergence test and result comparison with available literature. The present study was carried out on mesh sizes from coarse to finer mesh sizes. Variation of mesh size with global seeding was studied in volumetric terms. The variation of the mesh size for the model considered in the present study is depicted in Figure 6. A decrease in global seeding indicated towards the finer mesh size and vice versa.
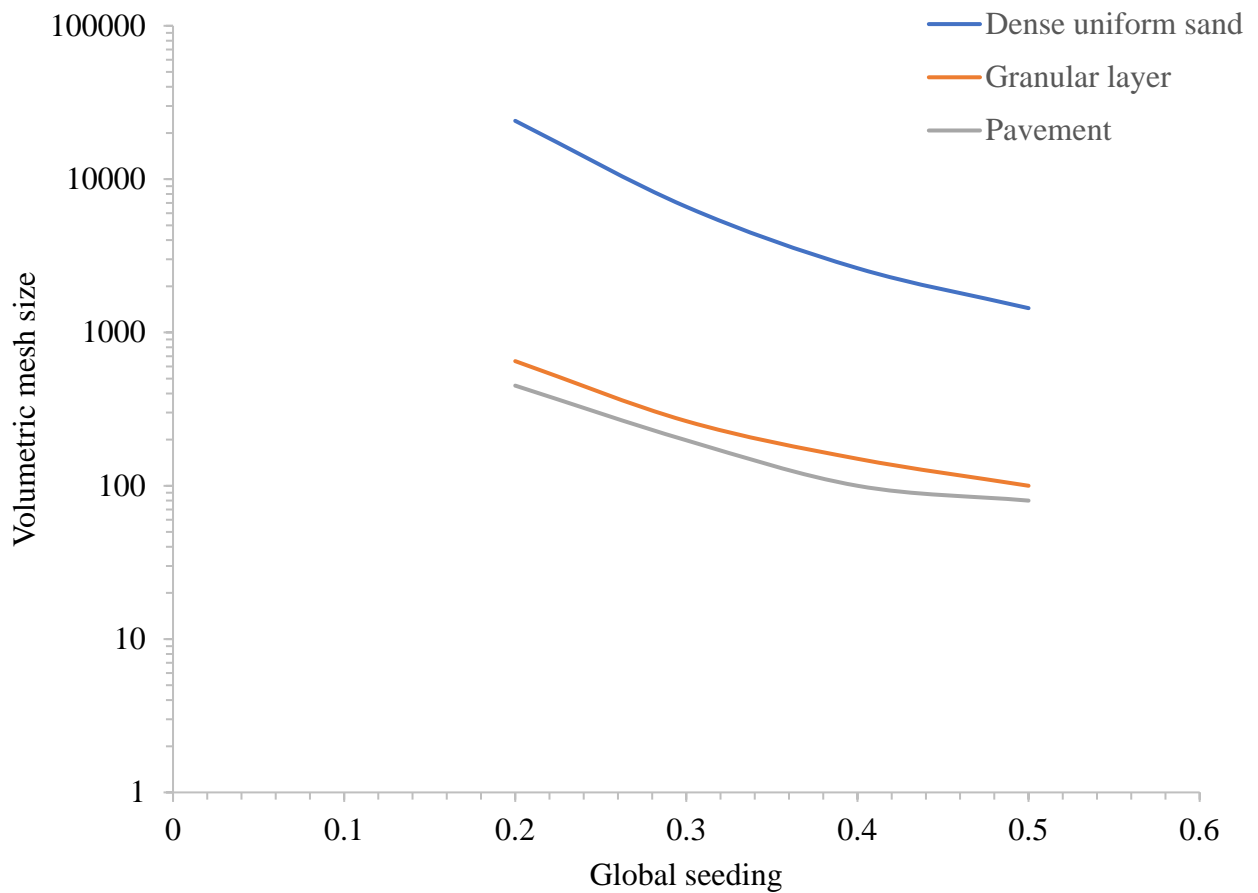

Figure 6: Volumetric mesh size vs global seeding showing mesh size variation from coarse to fine used in mesh convergence test.

Central deflection in the vertical direction with the position of moving load at the center of pavement for global seeding of 0.5 to 0.2 is shown in Figure 7. It is concluded from Figure 7

that deviation in the results for global seeding value of 0.3 and 0.2 is very small (less than 0.1%). So, the present study was carried out for mesh size corresponding to a global seeding value of 0.2.
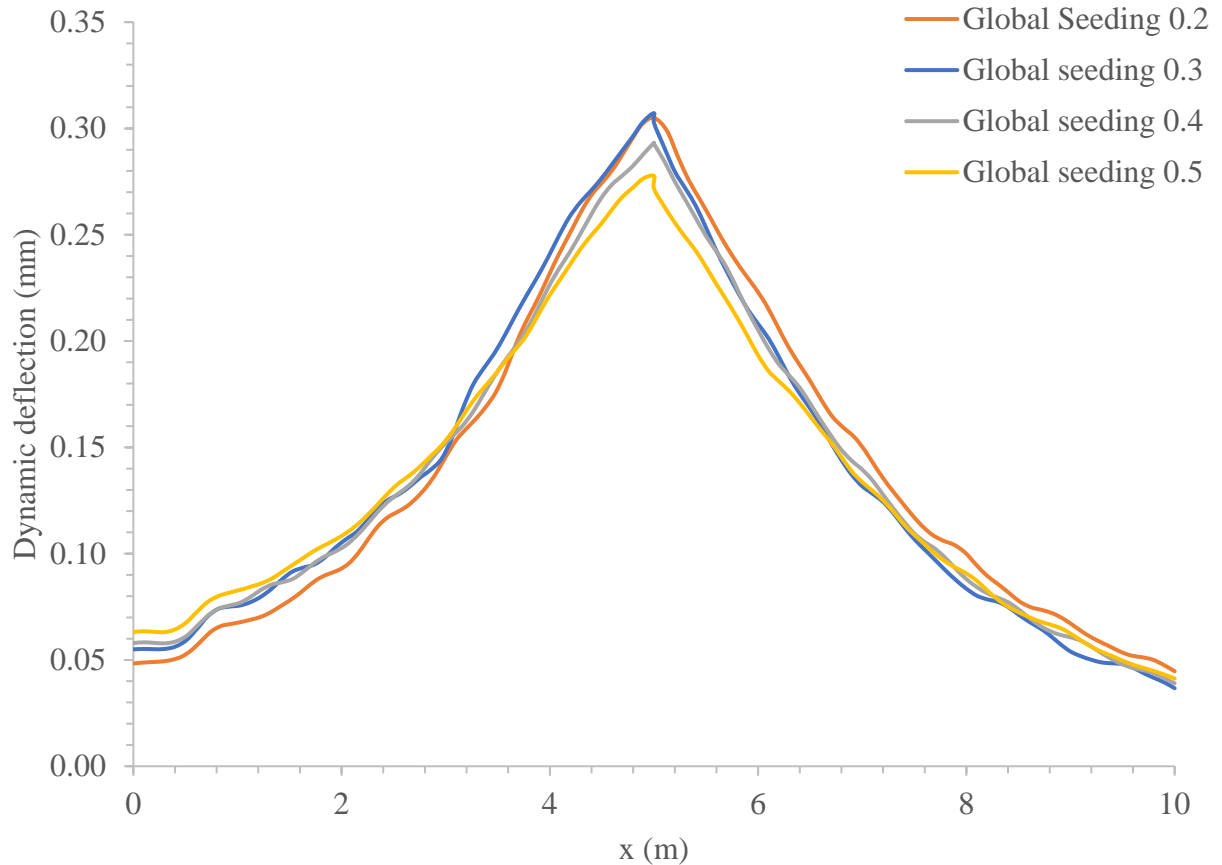

Figure 7: Central deflection in the vertical direction along the pavement length with the position of moving load at the center of pavement and global seeding of 0.5 to 0.2.

In the present study, a non-dimensional time factor (τ) was obtained in terms of the ratio of step time increment to the total time to introduce the corresponding numerical damping associated with time integration. During the time integration procedure, numerical damping is added to remove the numerical noise. Figure 8 shows the variation of numerical damping ratio (ξ_n) with a non-dimensional time factor(τ).
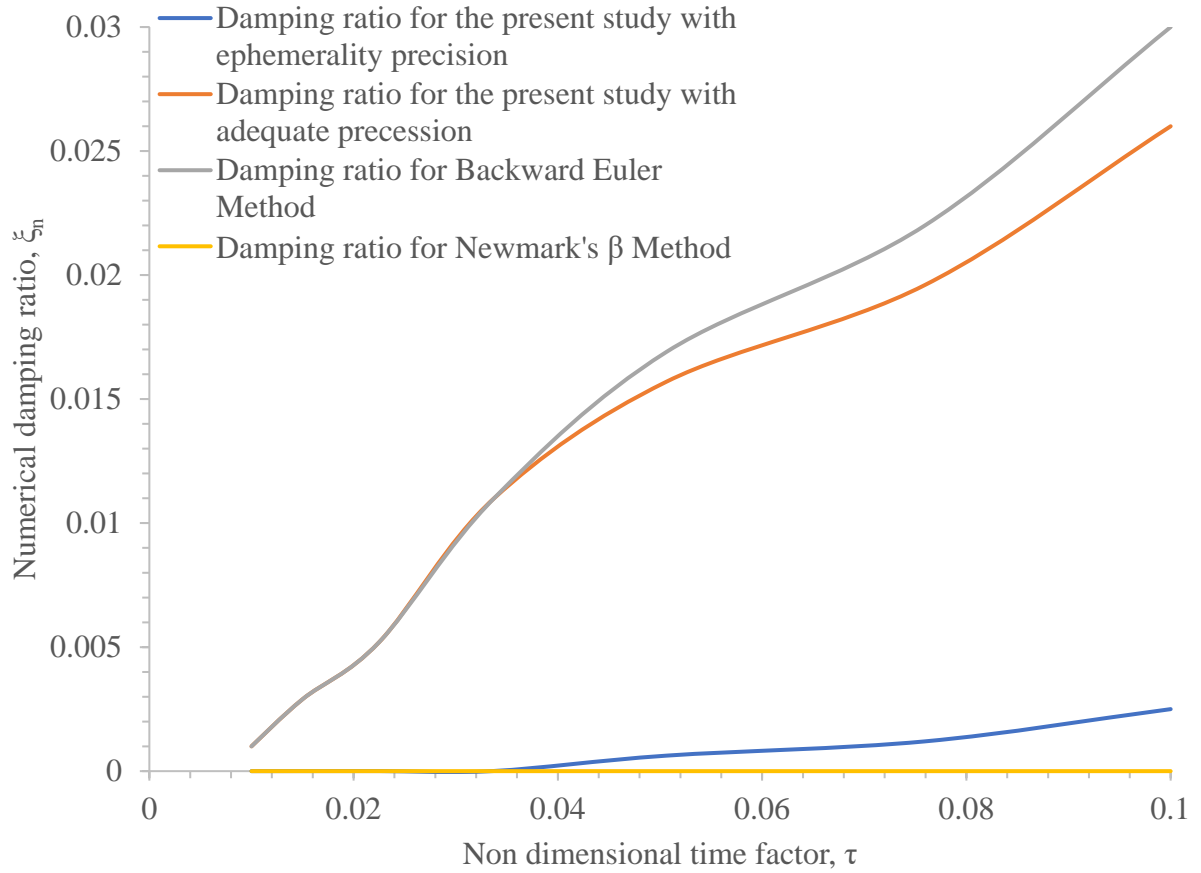
Figure 8: Variation of damping ratio with the non-dimensional time factor

For the present study numerical damping relates to the precision delivered in the numerical model. Figure 8 shows that no numerical damping is associated with Newmark's beta method.

Table 5: Input parameters of the present study compared with Newmark's β method and Backward Euler Method

Methodology		Input parameter			Numerical damping ratio (ξ_n) corresponding to τ (= Δt/t)
		Φ	Ψ	Ω	
Backward Euler Method		-	-	-	0.001 to 0.03
Present study	Adequate precession	-0.7	-2.41	-1.91	0.001 to 0.025
	Ephemerality precession	-0.05	0.22	0.44	0 to 0.0025
Newmark's β method		0	0.25	0.5	0

In the present study for low damping has a maximum of 0.0025 numerical damping and adequate damping has a maximum of 0.025 numerical damping ratio specified using numerical parameters shown in Table 5. In the Backward Euler method, the maximum numerical damping introduced in terms of numerical damping ratio was and 0.03.

5.1 Velocity induced load magnification

To observe the load magnification due to variation in velocity, a dimensionless factor is obtained stated earlier as DMF. DMF is calculated as a multiplier to static loading to account for the dynamics associated with the moving load. The results obtained for the dynamic magnification factor are tabulated in Table 6 which comes in great conjugation with available literature.

Table 6: Variation of dynamic magnification factor in vertical direction contrasted with available literature.

Velocity (m/sec)	Dynamic magnification factor (DMF)				
	Present study		Wu (1996)	Taheri and Ting (1990)	Yoshida and Weiver (1971)
	Ephemerality precession	Adequate precession			
15.6	1.004	1.052	1.059	1.049	1.055
31.9	1.135	1.172	1.120	1.121	1.112
62.38	1.245	1.320	1.256	1.266	1.252
124.76	1.631	1.708	1.698	1.703	1.700

The results for load magnification obtained using adequate precision were observed to be 4.8%, 3.7%, 7.5%, and 6.7% higher than that of the results obtained by ephemerality precision for velocity values of 15.16 m/s, 31.19 m/s, 62.38 m/s and 124.76 m/s respectively. It was observed that at a lower range of velocity, 15.6 m/s moving load gives a response similar to that of static loading. As velocity starts increasing the value of the dynamic magnification factor shows a parabolic behaviour for velocities of 31.19 m/s and 62.38 m/s. The maximum

value in DMF was observed to be 70 % higher than that of static loading for the velocity of 124.76 m/s as shown in Figure 9.
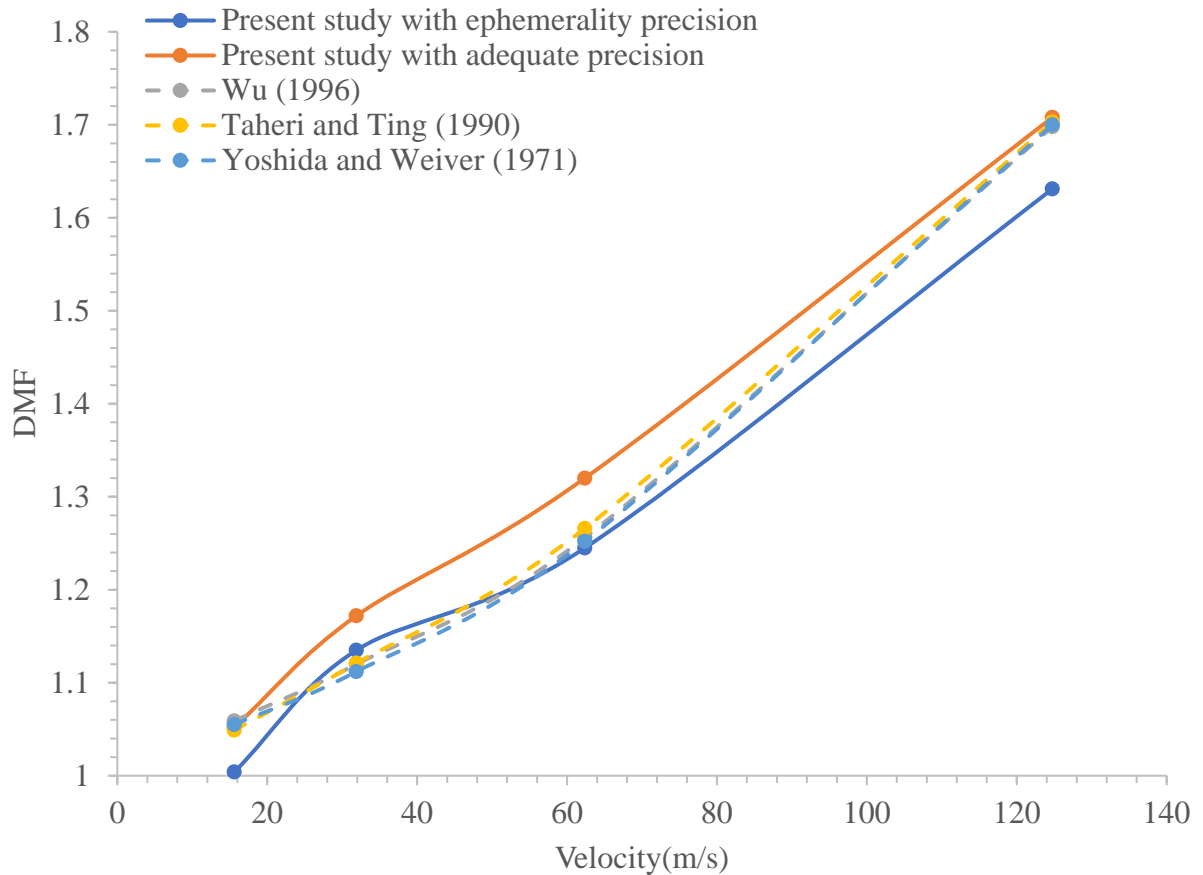

Figure 9: Variation of DMF (the function of loading) with velocity presenting the result of the present study with contrast to the available literature.

5.2 Velocity induced displacement response

The minimum wave velocity in the homogenous isotropic elastic system is defined as critical wave velocity V_{cr} ($V_{cr} = \sqrt[4]{\frac{4kEI}{\rho^2}}$). The model considered for the present study is subjected to a moving load of 25 kN.
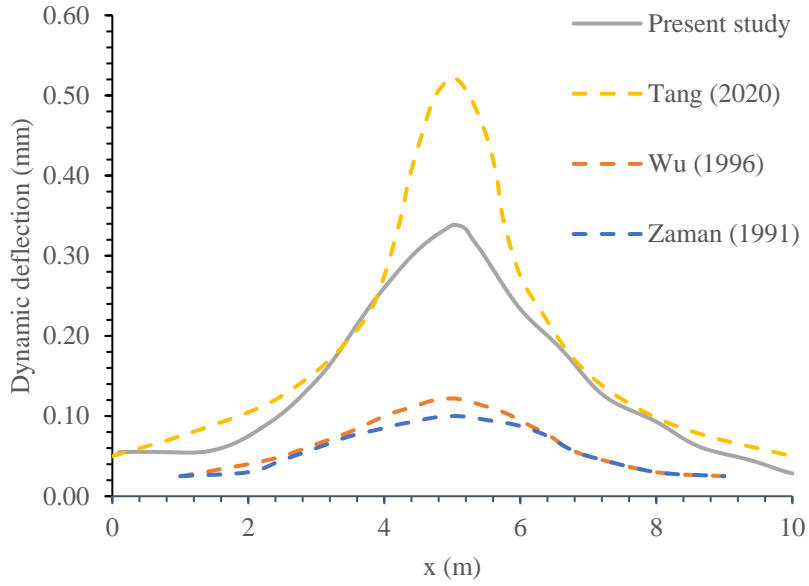
Figure 10: Variation of central deflection along the pavement length for $V/V_{cr} = 0.3$ in comparison with available literature.

Figure 10 shows the central deflection at midspan for moving load at the center for $V/V_{cr} = 0.3$ in comparison with the available literature. Figure 11 and Figure 12 shows the variation central deflection at $V/V_{cr} = 0.3$ and 0.6 and $\xi_n = 0.01$, 0.02, and 0.03.
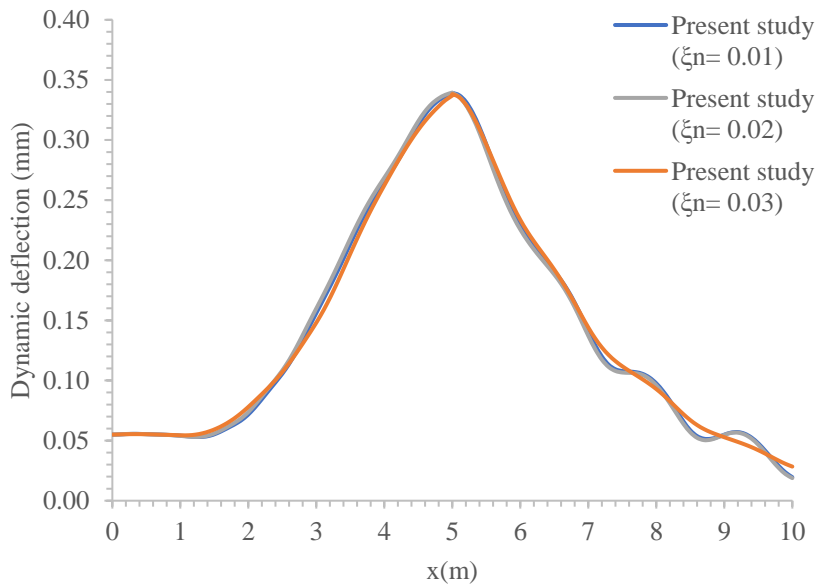
Figure 11: Variation of central deflection along the pavement length for numerical damping ratio (ξ_n) of 0.01, 0.02, and 0.03 and $V/V_{cr} = 0.3$.
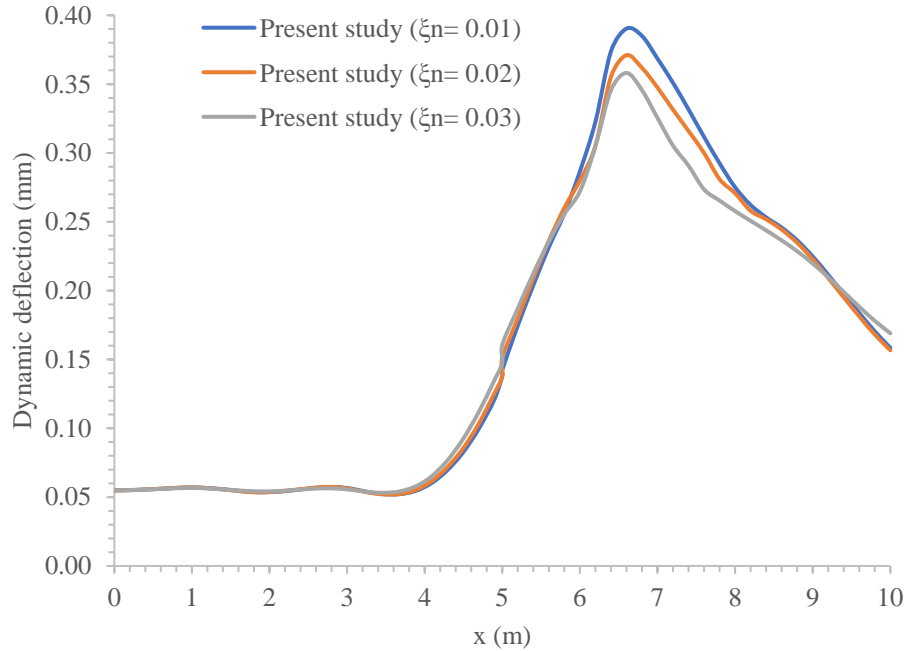
Figure 12: Variation of central deflection along the pavement length for numerical damping ratio (ξ_n) of 0.01, 0.02, and 0.03 and $V/V_{cr} = 0.6$.

Variation of dynamic displacement factor in the vertical direction and the lateral direction is tabulated in Table 7. It is observed from Figure 10 to Figure 12 and Table 6 that solution presented to the problem of moving mass is in great conjugation with the available literature.

Table 7: Variation of dynamic displacement factor (DDF) in the vertical direction (on pavement top) and in the lateral direction (retaining wall).

Velocity	Dynamic displacement factor (DDF)							
(m/sec)		Pavement top				Retaining wall		
	Backward Euler Method	Present study		Newmark's β Method	Backward Euler Method	Present study		Newmark's β Method
		Adequate precession	Ephemerality precision			Adequate precession	Ephemerality precession	
15.6	1.003	1.003	1.009	1.002	1.013	1.004	1.005	1.011
31.9	1.018	1.013	1.018	1.015	1.059	1.057	1.058	1.054
62.38	1.115	1.125	1.133	1.118	1.411	1.415	1.419	1.421
124.76	1.315	1.368	1.387	1.368	1.57	1.563	1.616	1.555

For the lower ranges of velocities, the response observed was pretty much similar to that of static loading. For velocities value of 62.38 m/s and 124.76 m/s, the highest difference in variation of displacement magnification was observed to be 29.6% and 25.5% respectively.
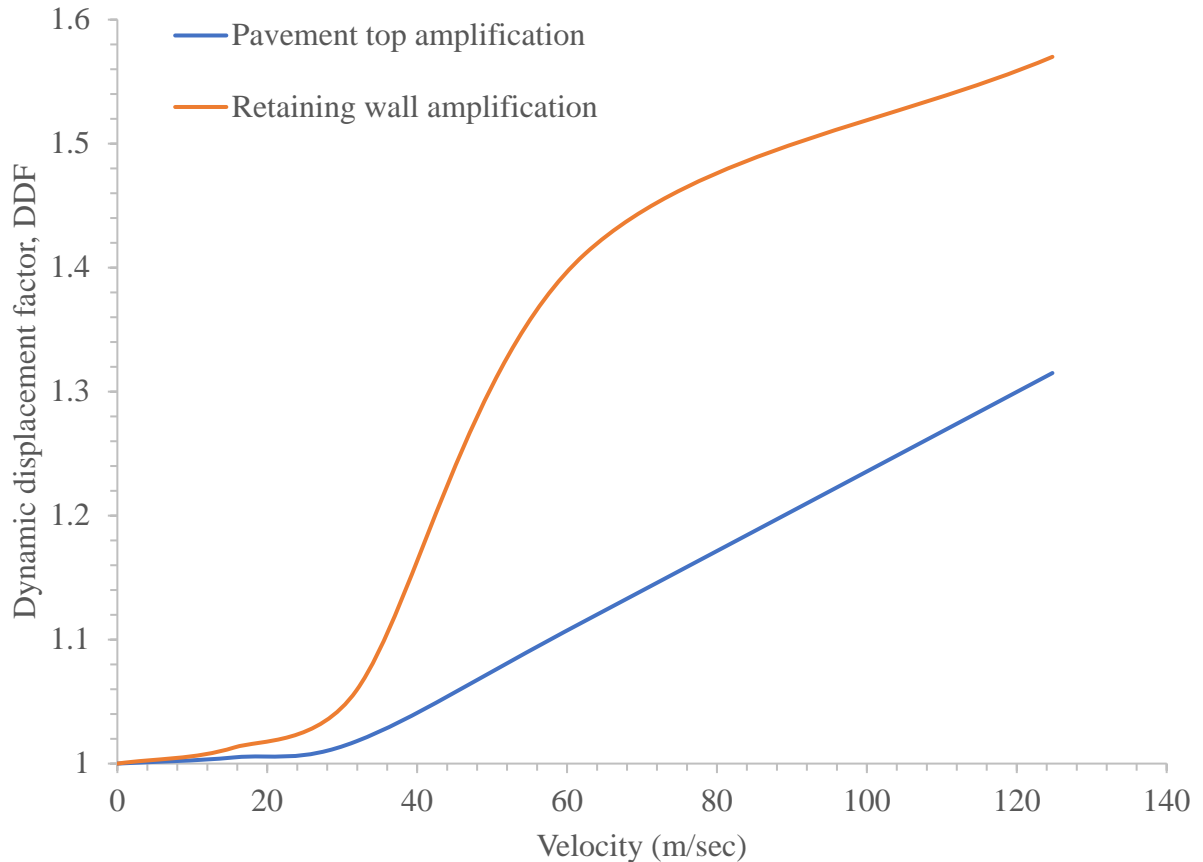
Figure 13: Variation of dynamic displacement factor with velocity for pavement top constrained by retaining wall shown in the figure as retaining wall amplification (amplification in the lateral direction) and amplification on the center of pavement top shown in the figure as pavement top amplification (amplification in the longitudinal direction).

Figure 13 shows the variation of dynamic displacement factor with velocity for pavement top constrained by retaining wall shown in the figure as retaining wall amplification (amplification in the lateral direction) and amplification on the center of the pavement top is shown in the figure as pavement top amplification (amplification in the vertical direction). A maximum of 31% higher dynamic displacement than static displacement was observed in vertical direction whereas Wu (1996) observed an 18% increase in displacement. In the lateral direction maximum of 57% higher dynamic displacement than static displacement was observed.
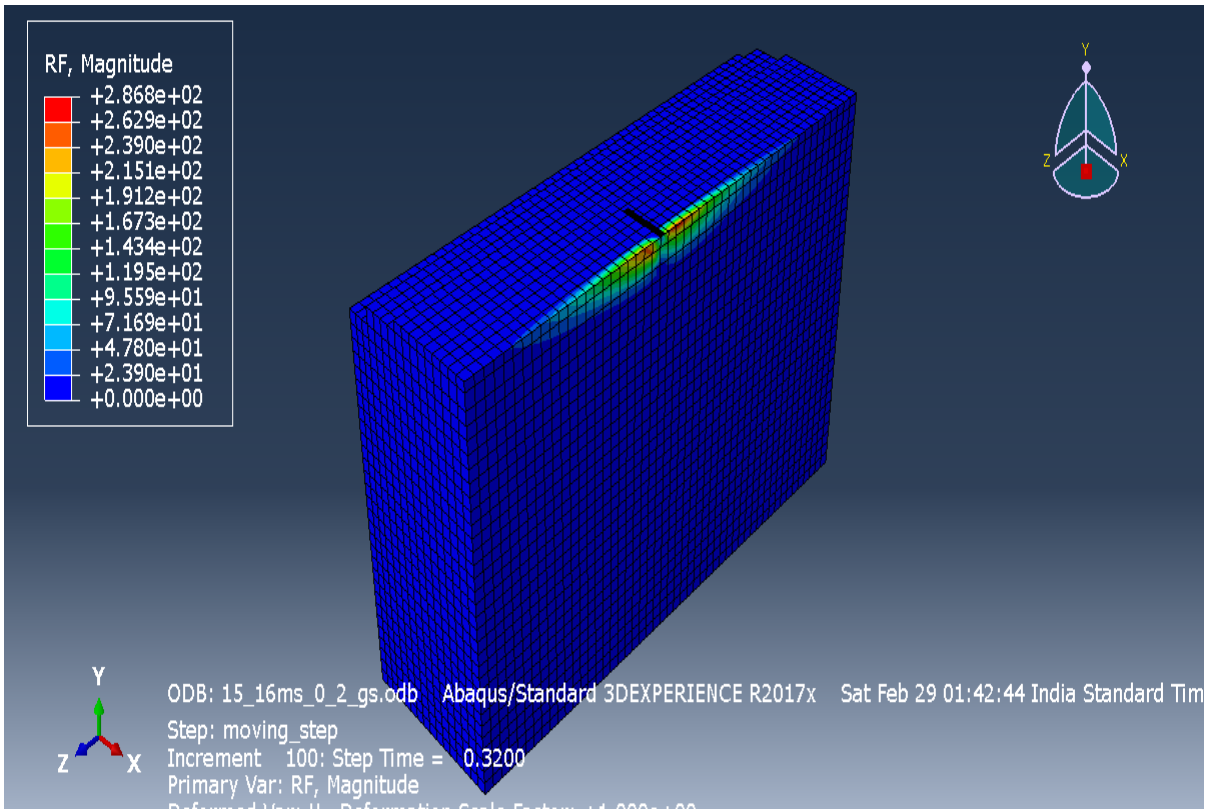
Figure 14 (a)
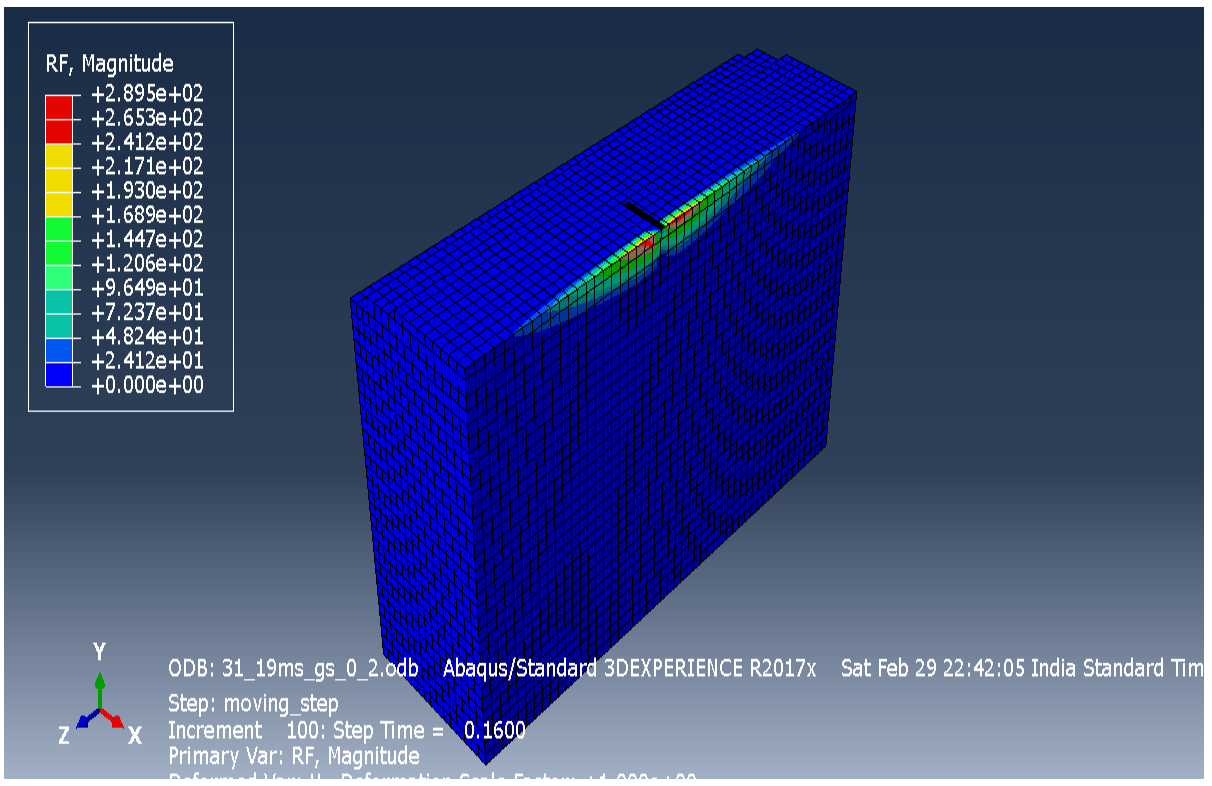
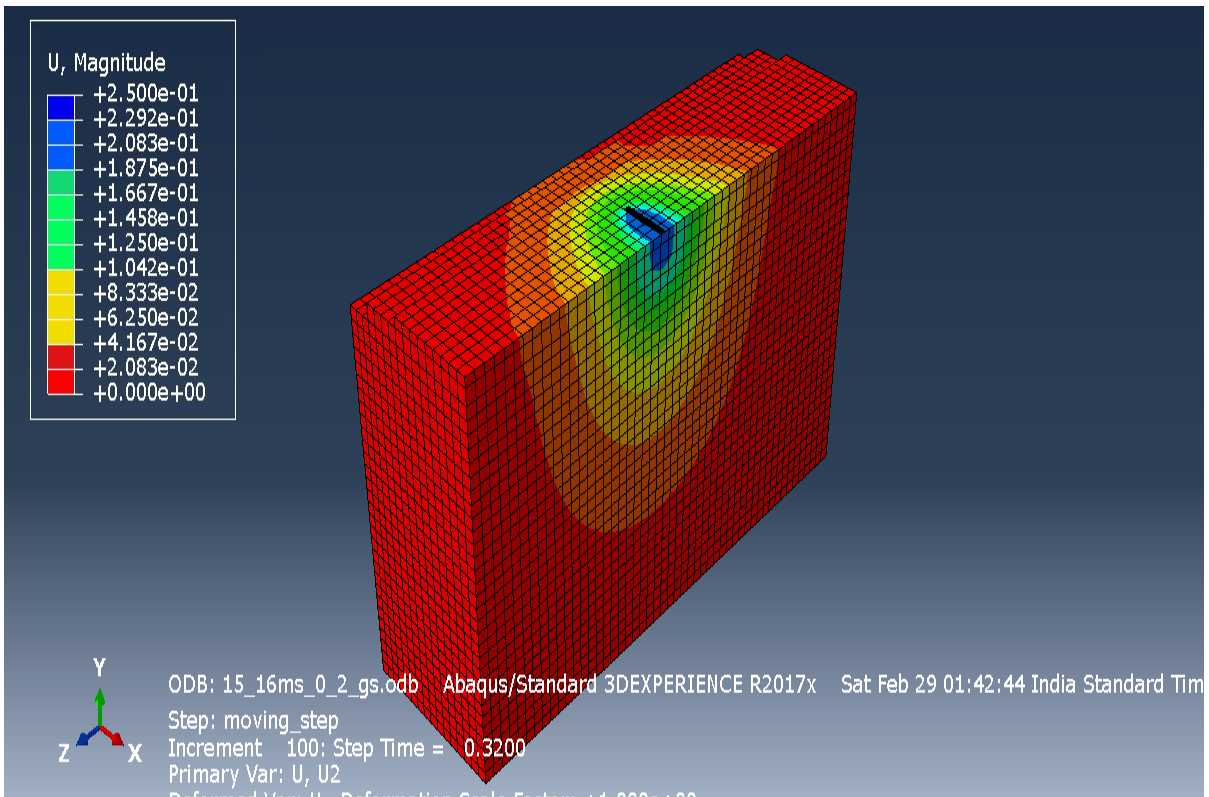
Figure 14 (b)
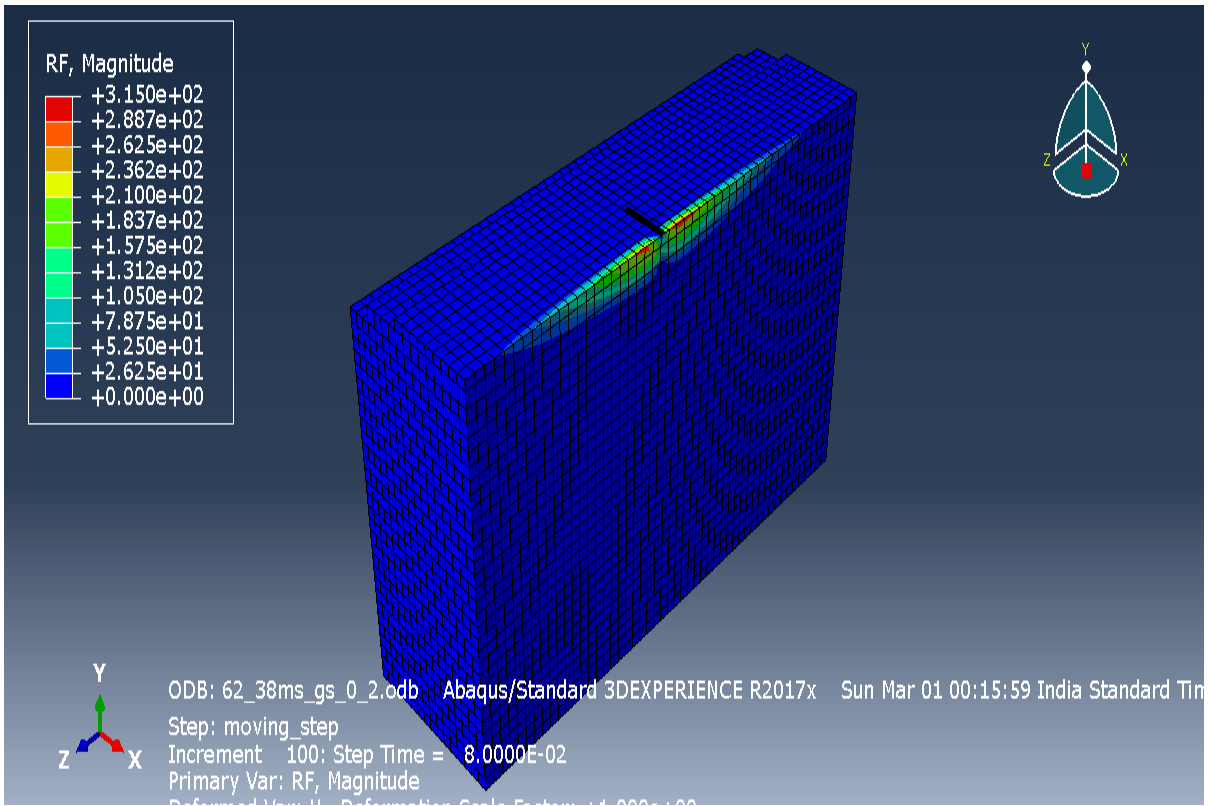
Figure 14 (c)
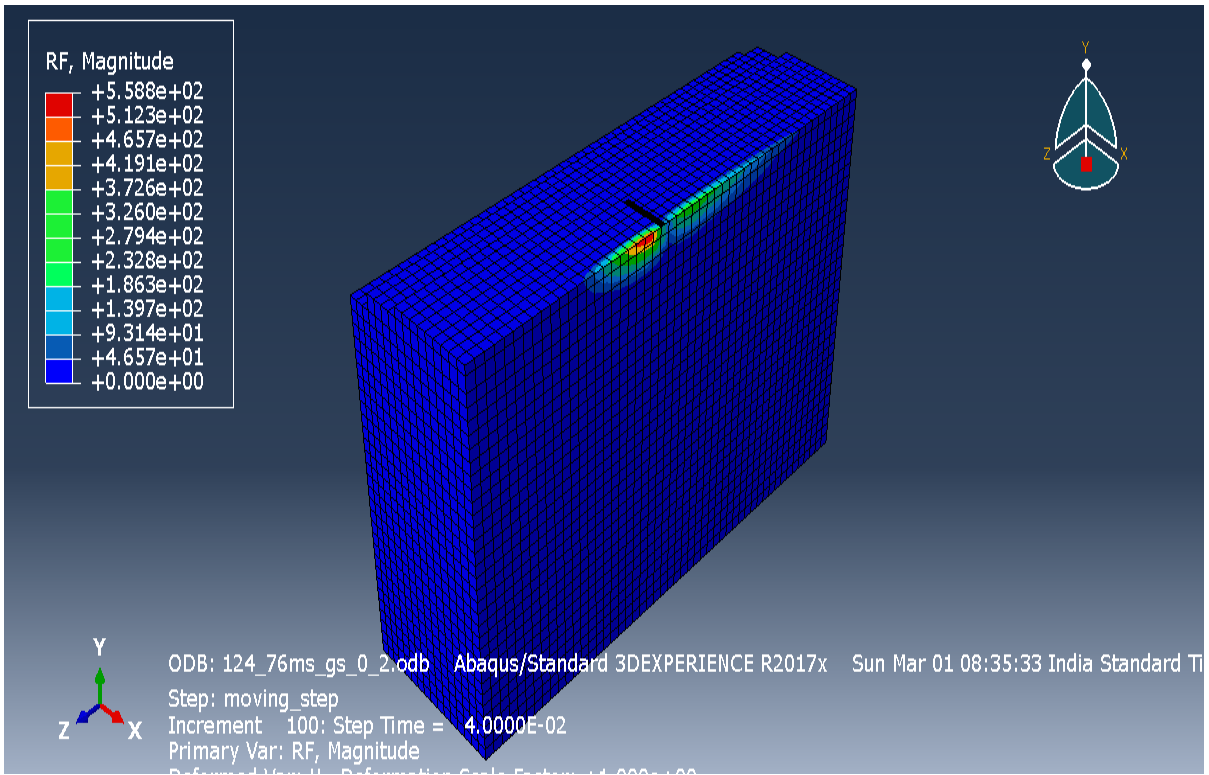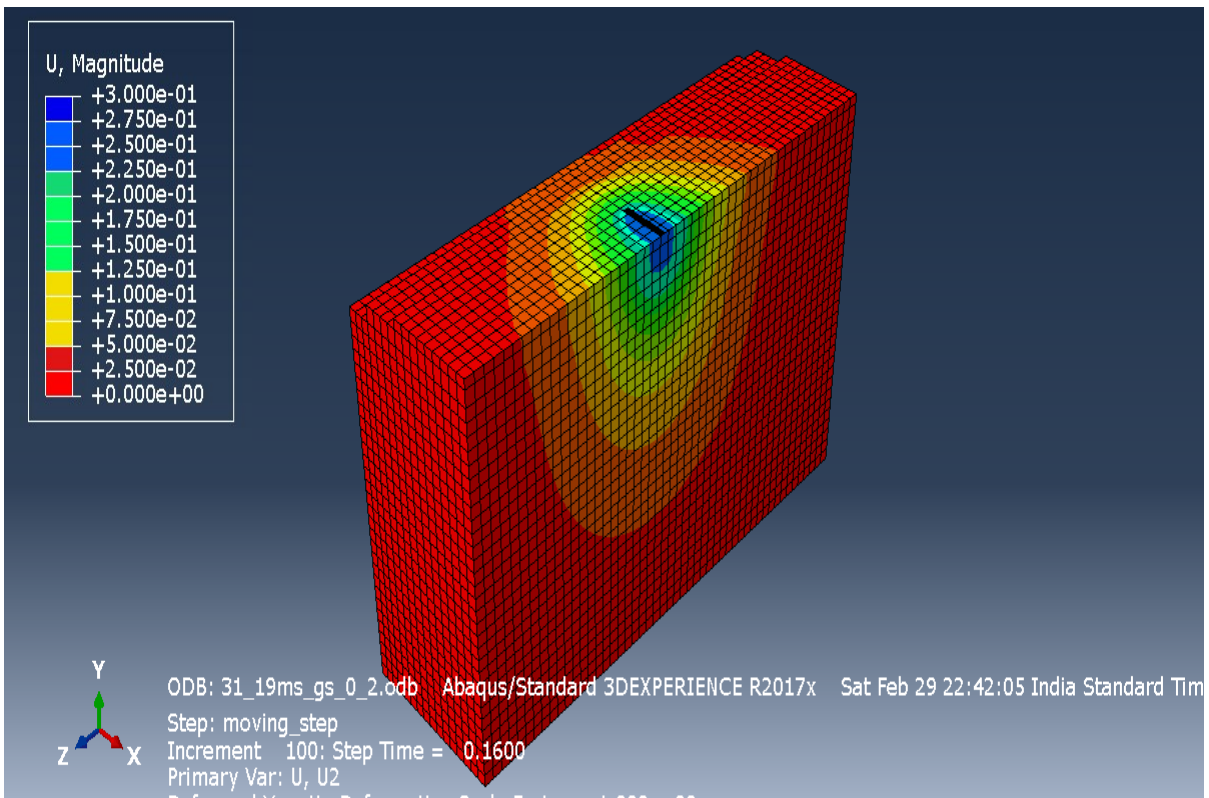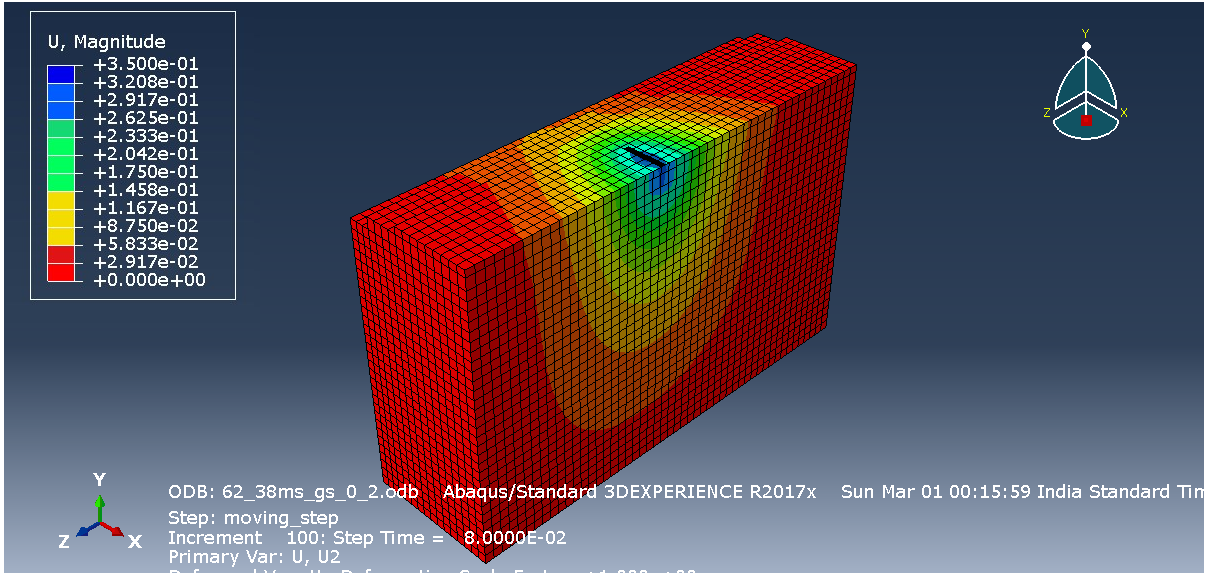

Figure 14 (d)

Figure 14 (e)
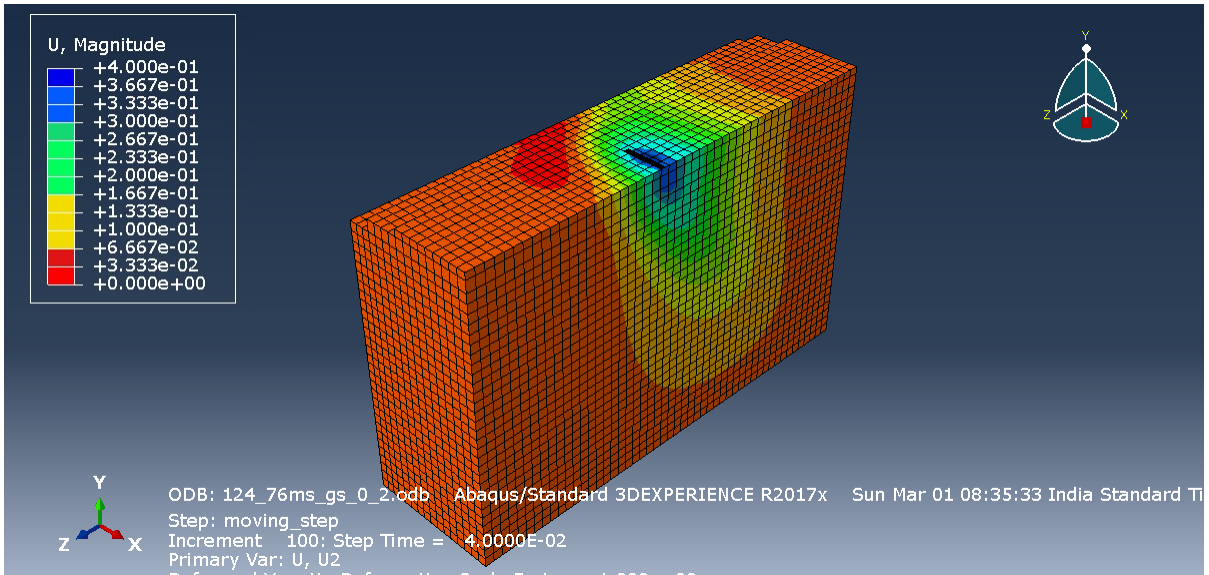

Figure 14 (f)

Figure 14 (g)

Figure 14 (h)

Figure 14: Variation of dynamic loading and displacement showed for mesh size corresponding to global seeding 0.2 accordingly in as (a) Dynamic loading contour at Velocity of 15.16 m/s,(b) Dynamic loading contour at Velocity of 31.19 m/s, (c) Dynamic loading contour at Velocity of 62.38 m/s and (d) Dynamic loading contour at Velocity of 124.76 m/s, (e) Dynamic displacement contour at Velocity of 15.16 m/s, (f) Dynamic displacement contour at Velocity of 31.19 m/s, (g) Dynamic displacement contour at Velocity of 62.38 m/s and (h) Dynamic displacement contour at Velocity of 124.76 m/

Figure 14 shows the viewports presenting the loading and displacement contours obtained for the finest mesh sizes corresponding to the global seeding of 0.2 at $\xi n = 0.025$ presenting the magnified displacement and loading contour. Central deflection decreases with the increase in depth contrasting to classical theories of soil mechanics. As shown for velocity profile of 15.16 m/s, 31.19 m/s and 62.38 m/s. An unusual contour pattern is recorded for the velocity of 124.76 m/s indicating the effects of the extreme side of constrained pavement dynamics with lagging contour profile. It is because the time integration of the motion equation is so rapid that it leads to an unusual displacement dominated zone representing the levitation phenomena showing the extreme side of constrained pavement dynamics. Additional damper control should be done at a velocity of 124.76 m/s for the maximum amount of energy harvesting.

5.3 Stiffness response

The effect of moving mass on stiffness property was observed in a non-dimensional stiffness factor in the vertical as well as in the lateral direction depicted in Figure 15. The maximum value of dynamic stiffness was observed to be 24% higher than that of static stiffness in the vertical direction and 15% higher dynamic stiffness compared to static stiffness observed in the lateral direction. In the lateral direction, curve path A to B and A´ to B´shows stiffness hardening, curve path B to C, and B´ to C´shows stiffness softening.
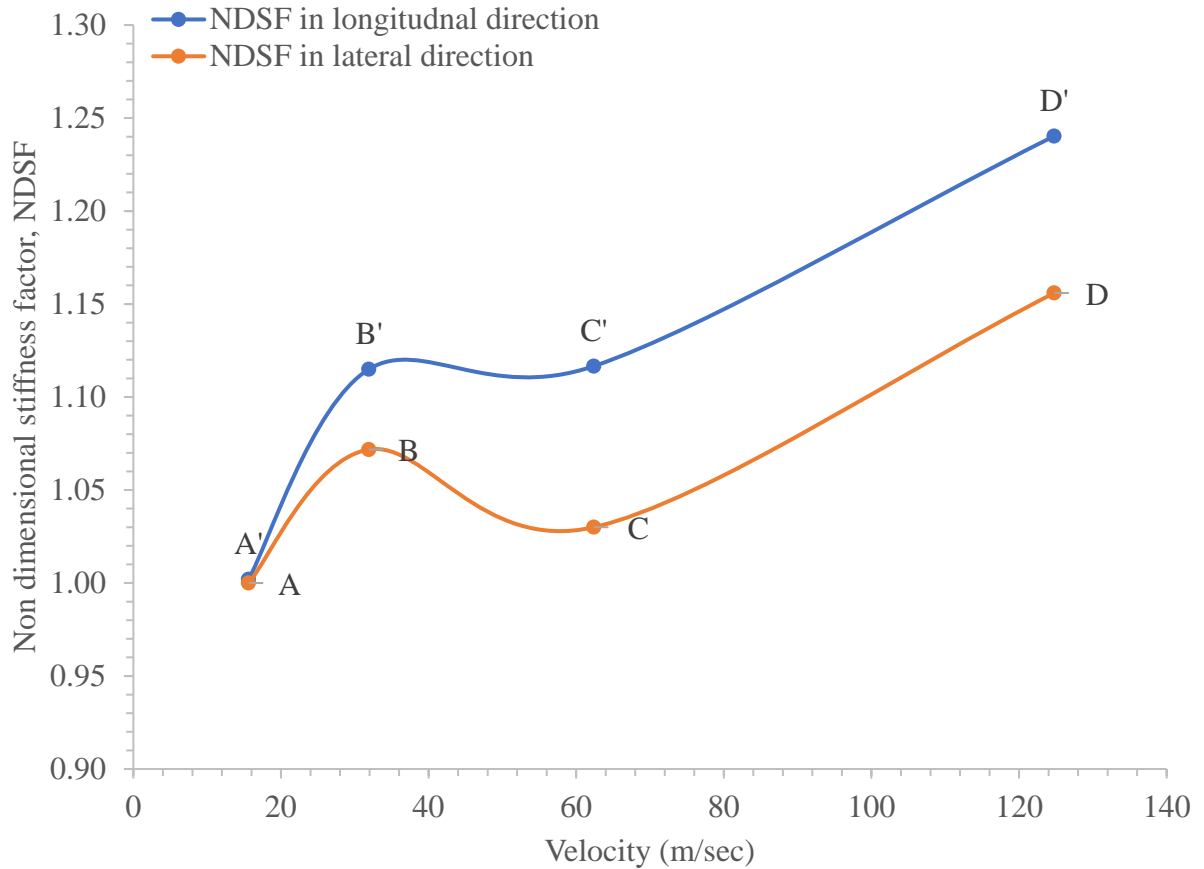
Figure 15: Variation of NDSF with velocity in the vertical and lateral direction is obtained, curve path AB, CD, A′B′ and C′D′ shows incrementing effect, curve path BC and B′C′shows stiffness decrementing effect.

5.4 Velocity induced stress variation

The effect of velocity on stress is recorded along the pavement length. Figure 16 shows that stress remains unchanged for the lower velocity profile at the numerical damping ratio corresponding to 0.001 compared with the studies of Tang et al., (2020).
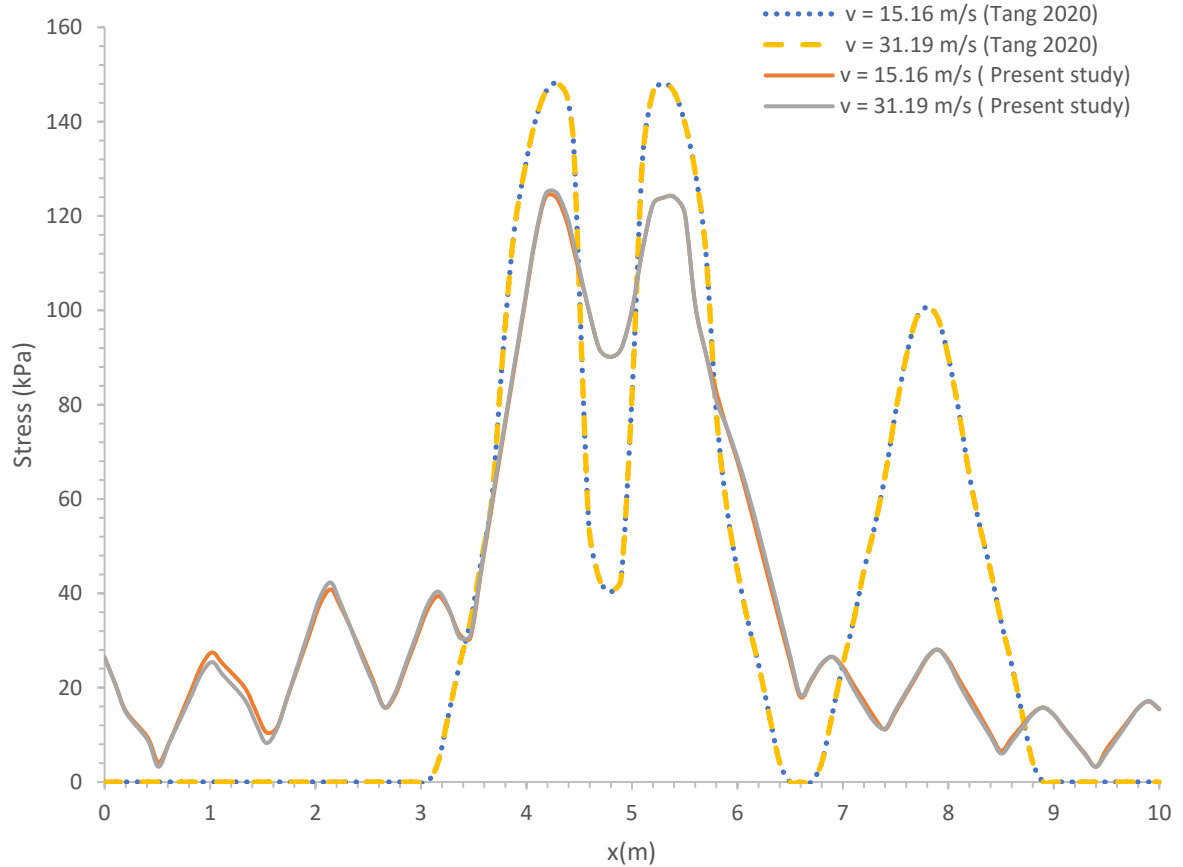
Figure 16: Variation stress along the pavement length for the velocity of 15.16 m/s and 31.19 m/s in comparison with available literature.

Figure 17 and Figure 18 show the increasing velocity effects with damping control. It was observed that with an increase in numerical damping stress reduces and vice versa. An increase in the velocity increase in the value of stress was observed. Further, a harmonic response is observed as we move away from the pavement to the edges of the pavement indicating the dynamic stress response. A maximum of dynamic stress for the velocity range of 100 km/hr recorded by Tang et al., (2020) was 145 kPa whereas the present study with low damping recorded a dynamic stress value of 125 kPa. For low damping maximum stress value observed was 147 kPa for a velocity value of 124.76 m/s and a maximum of 140 kPa stress value was observed for a velocity value of 124.76 m/s indicating that with an increase in numerical

damping stress value decreases.
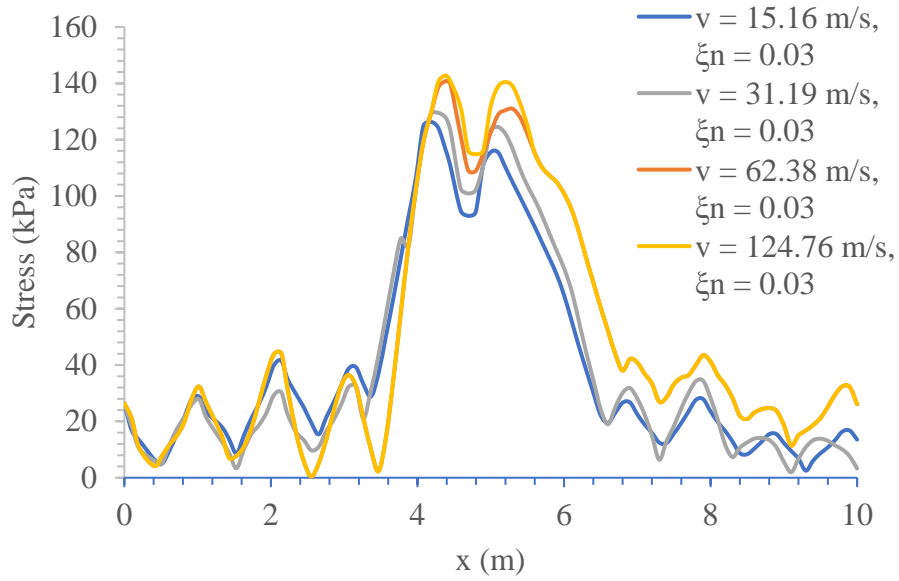
Figure 17: Variation of stress along the pavement length for adequate numerical damping corresponding to numerical damping ratio 0.03.
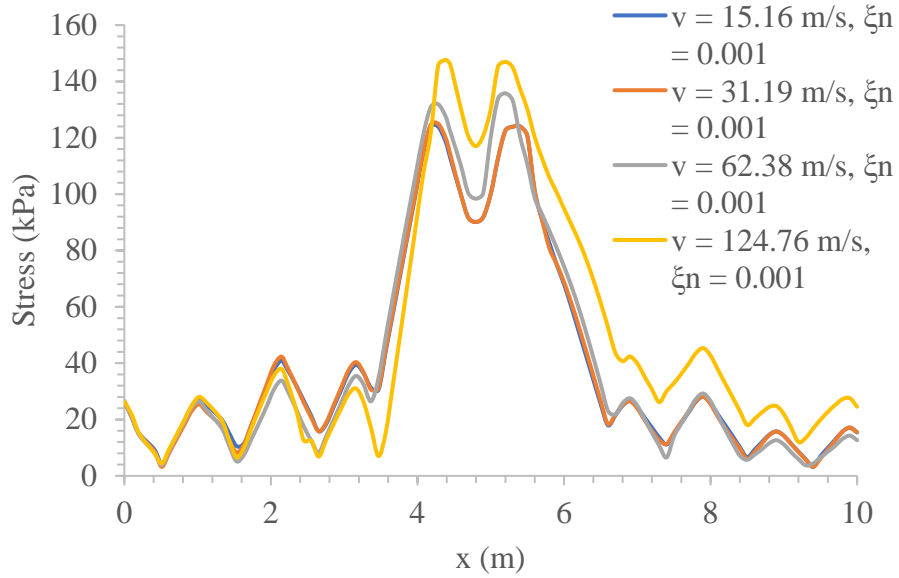
Figure 18: Variation of stress along the pavement length for low numerical damping corresponding to numerical damping ratio of 0.001.

5.4 Displacement – Data convergence

Data sets obtained for numerical operators were all together set up to the convergence as shown in Figure 19 to Figure 26.

Mesh convergence along with data convergence is termed as data convergence test (DCT). A new numerical testing technique is developed to take both factors into consideration mesh sizes as well as all data sets together for convergence.

Data convergence test (DCT) is performed to validate the model in both vertical direction and lateral direction. Variation of mesh size with global seeding was studied in volumetric terms. The variation of the displacement with mesh size for the model considered in the present study is depicted in Figure 7. DCT in the vertical direction is performed as shown in Figure 19 to Figure 22.
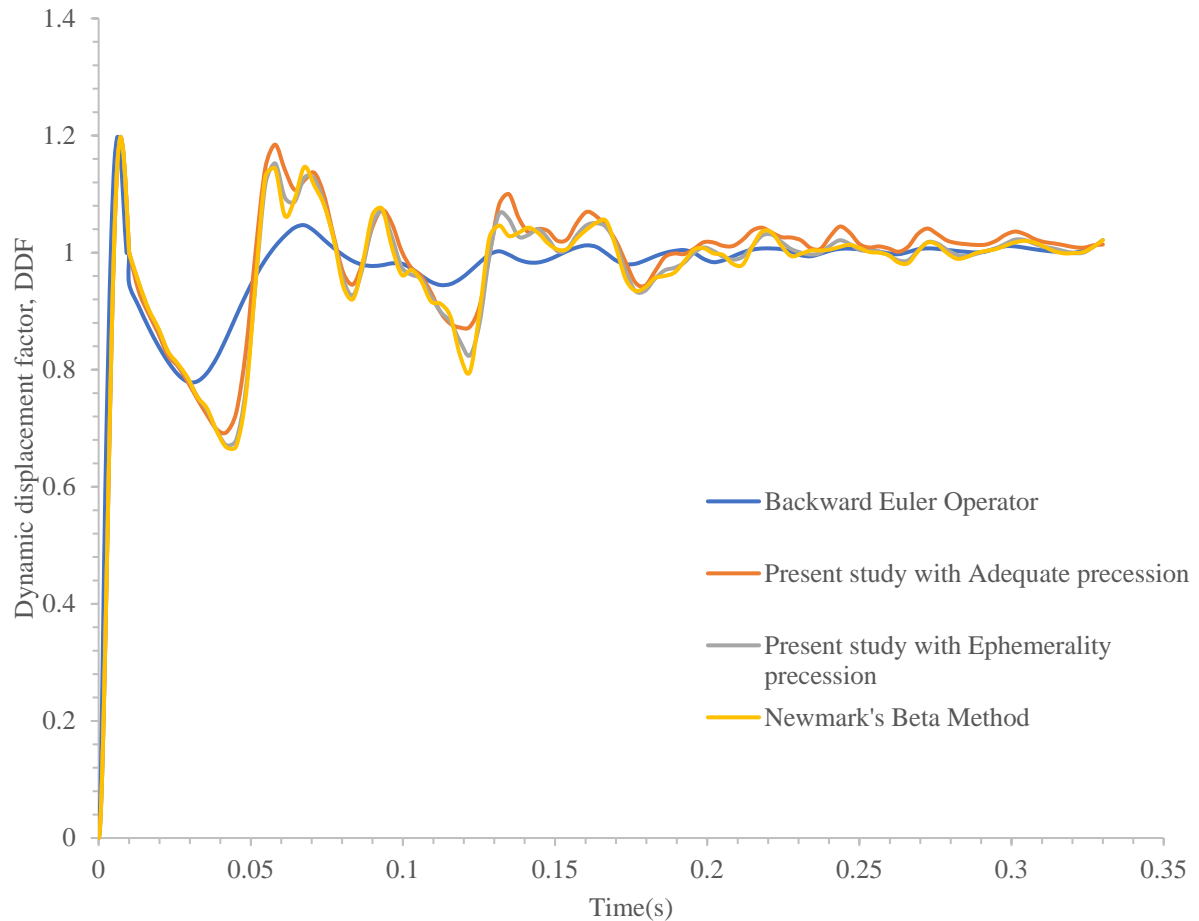
Figure 19 (a)
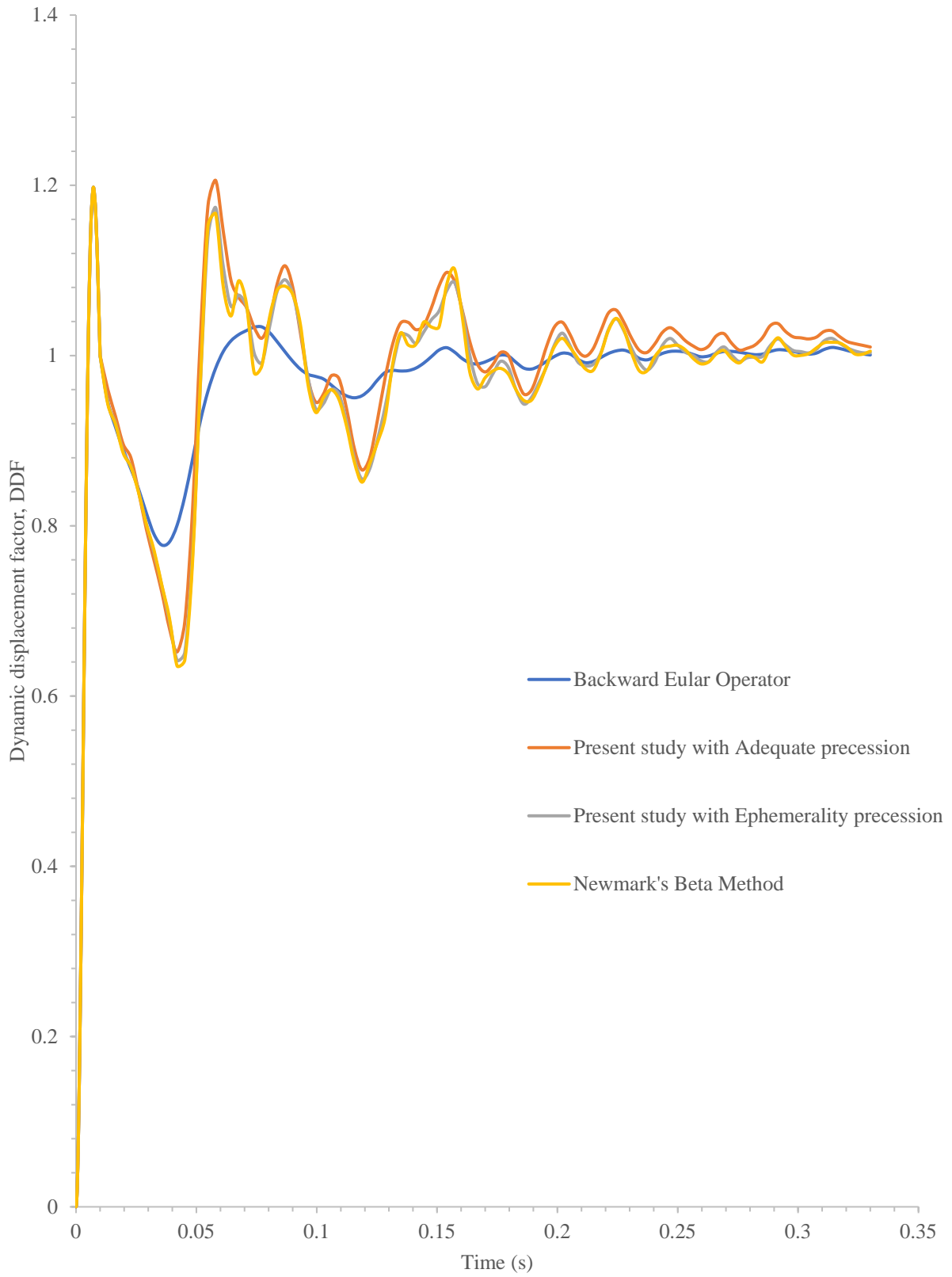
Figure 19 (b)
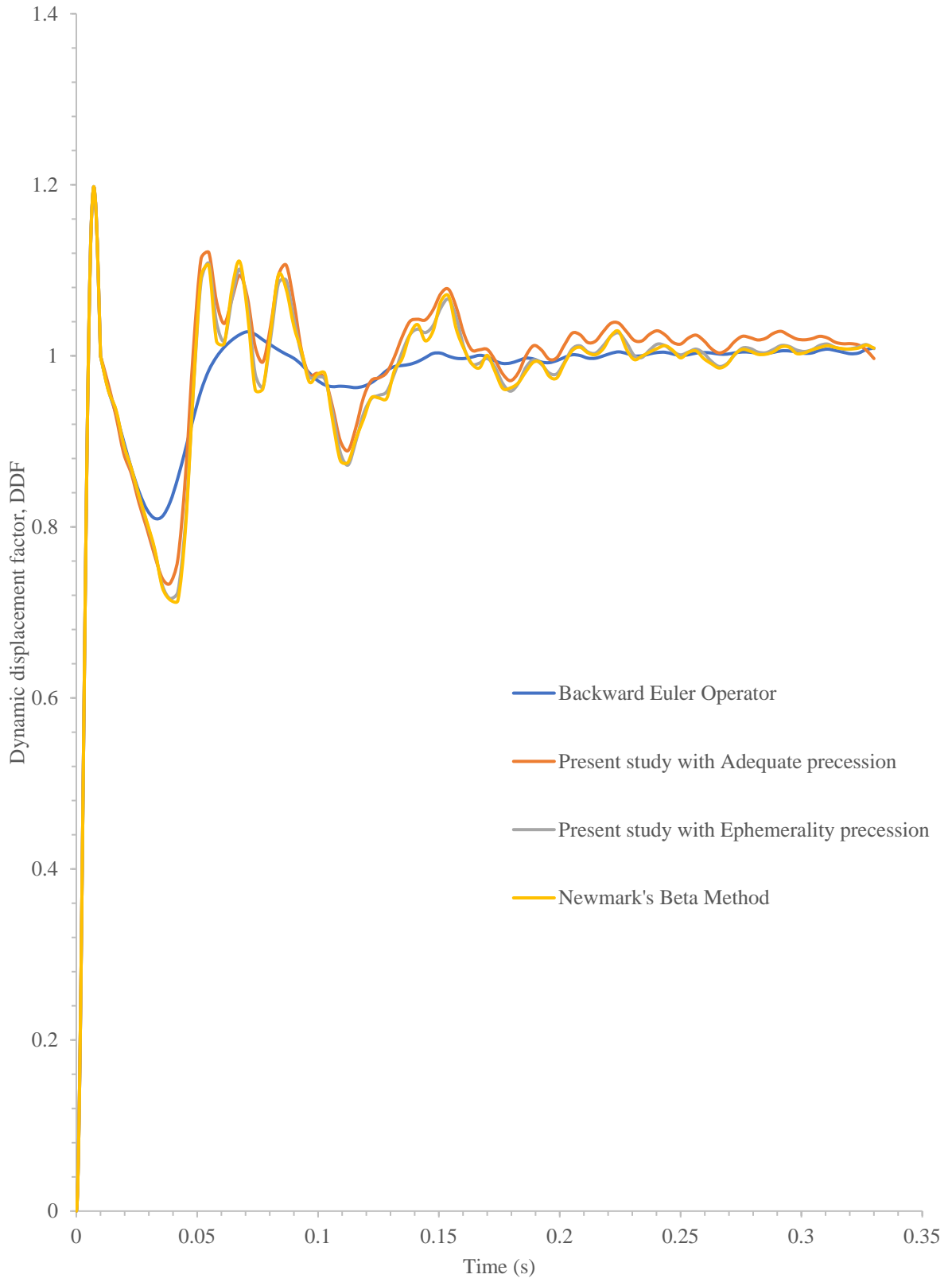
Figure 19 (c)
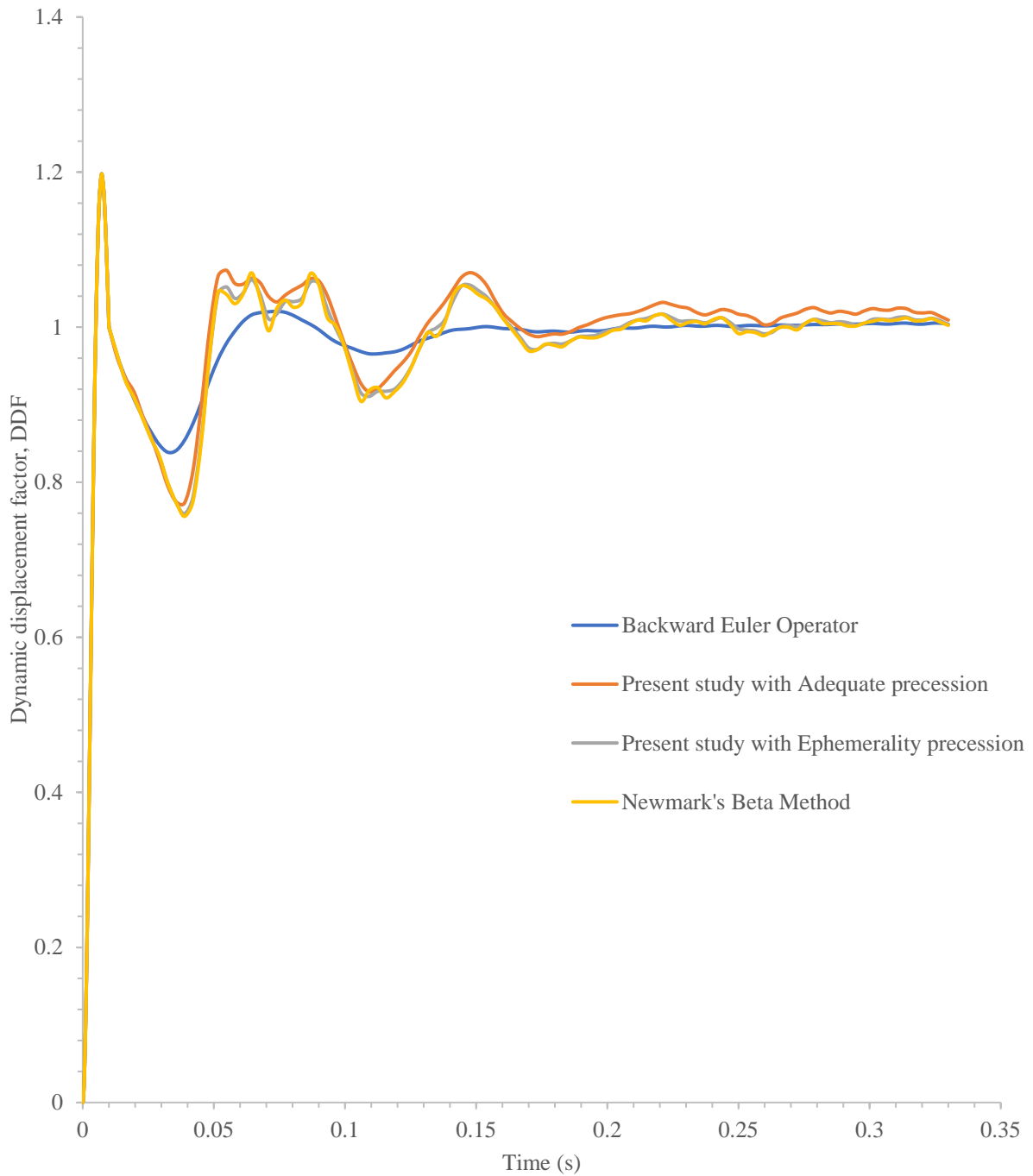
Figure 19(d)

Figure 19: Variation of DDF with time on pavement top at a velocity of 15.16 m/s using Backward Euler operator, HHT moderate dissipation operator, HHT transient fidelity operator, and Newmark's beta method for the present study in data convergence test as per global seeding mesh profile shown in figures (a) Global seeding 0.5, (b) Global seeding 0.4, (c) Global seeding 0.3, and (d) Global seeding 0.2.
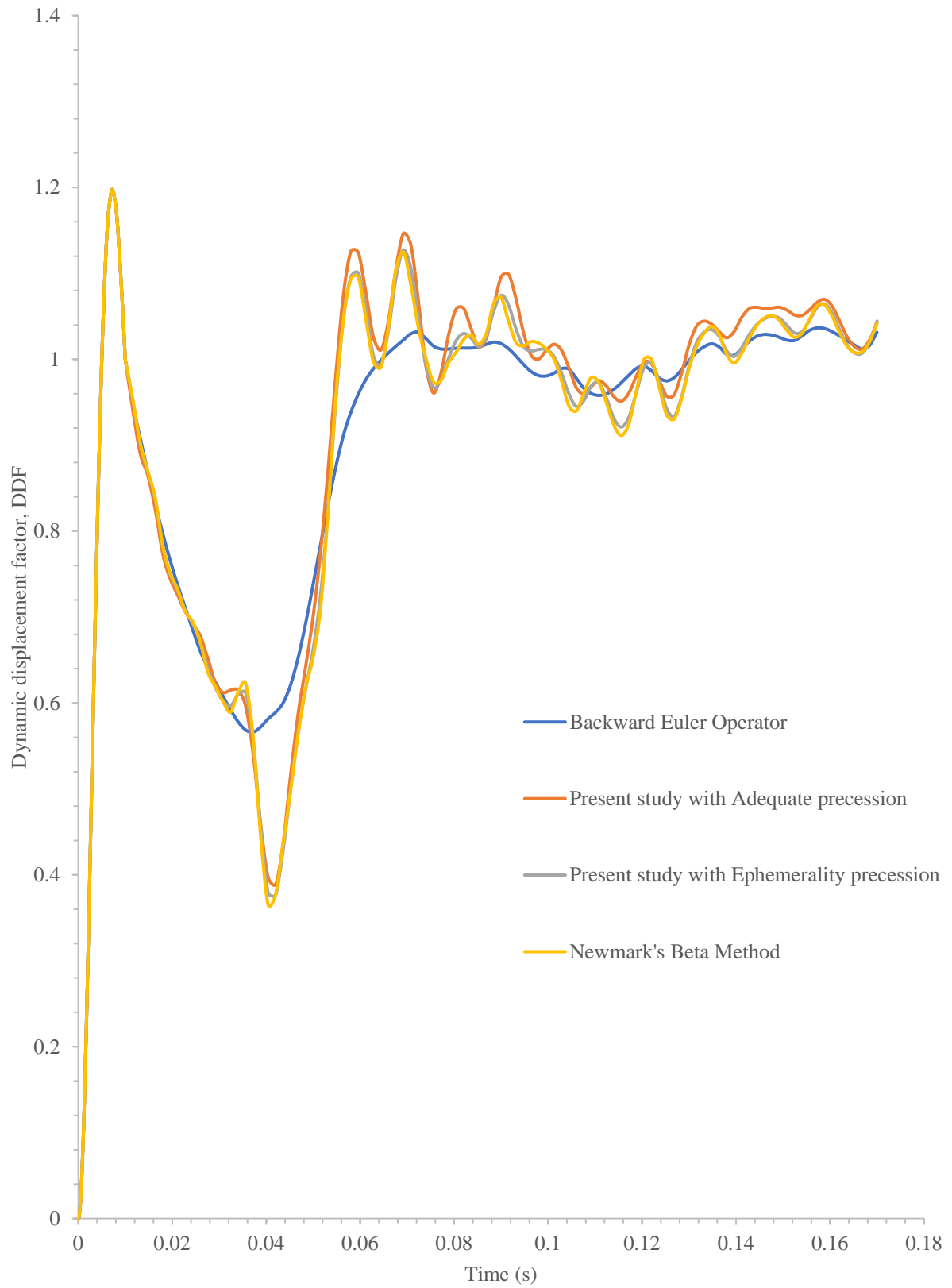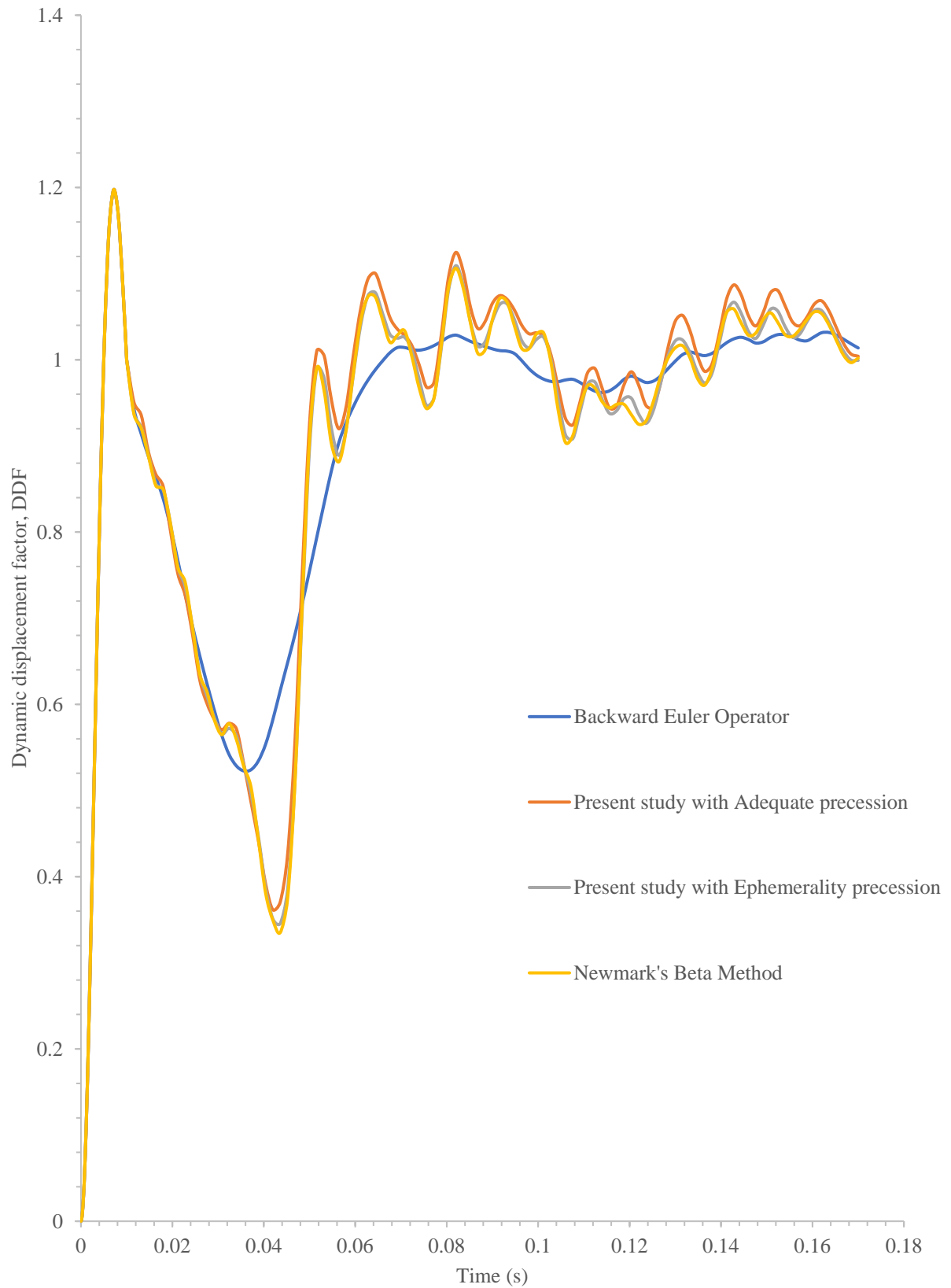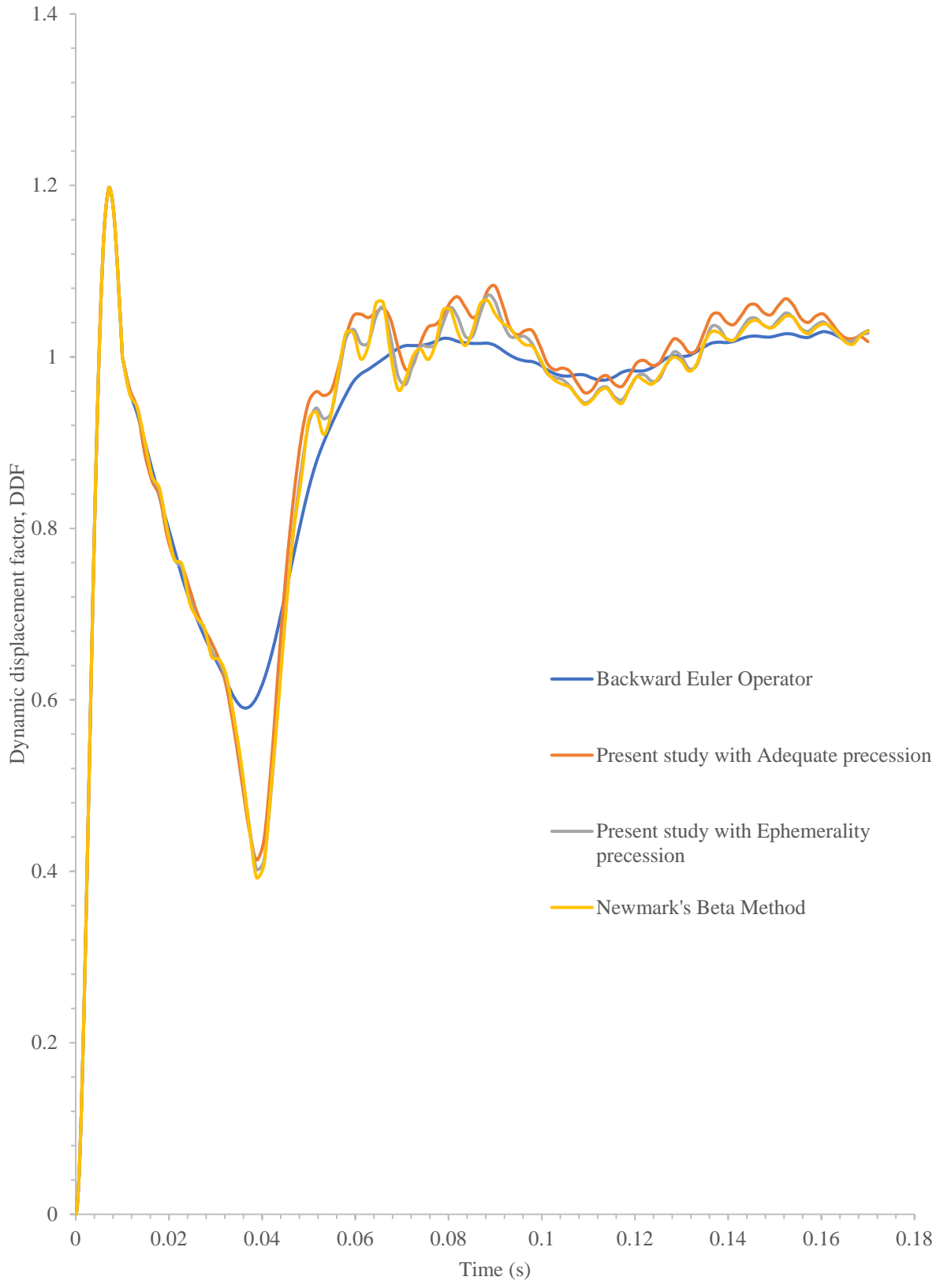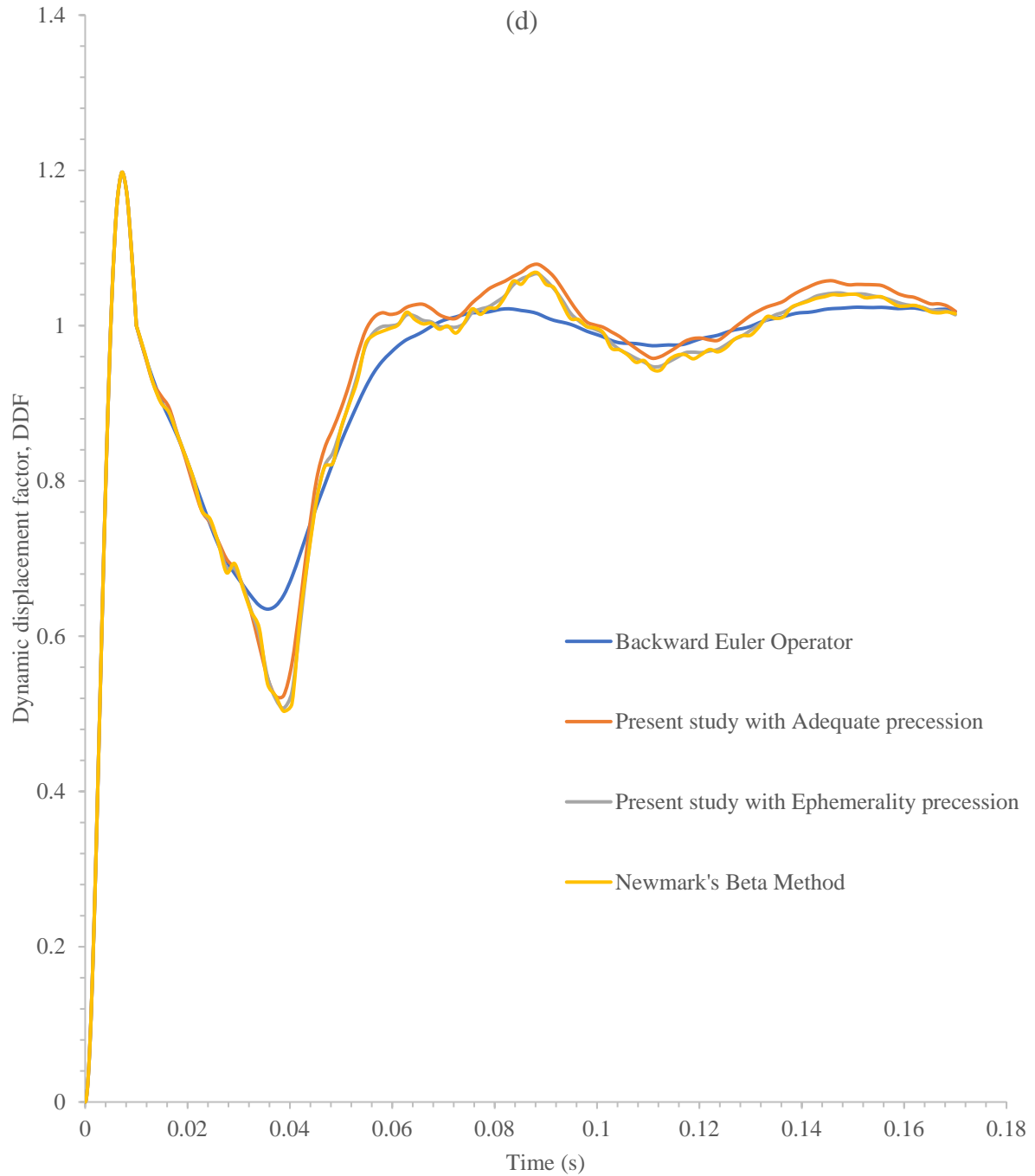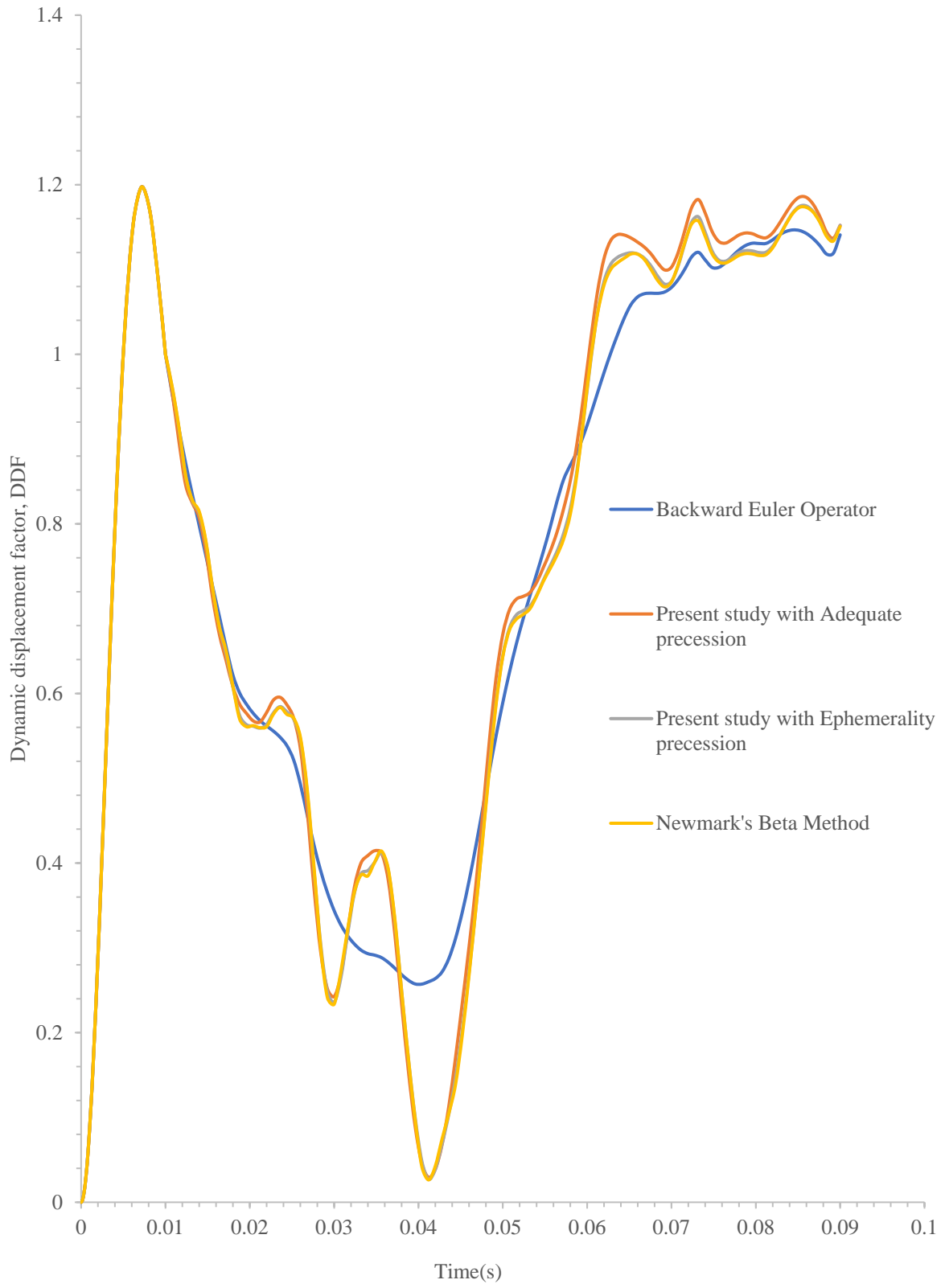
Figure 20 (a)

Figure 20(b)

38

Figure 20 (c)

(d)

Figure 20: Variation of DDF with time on pavement top at a velocity of 31.19 m/s using Backward Euler operator, HHT moderate dissipation operator, HHT transient fidelity operator, and Newmark's beta method for the present study in data convergence test as per global seeding mesh profile shown in figures (a) Global seeding 0.5, (b) Global seeding 0.4, (c) Global seeding 0.3, and (d) Global seeding 0.2.
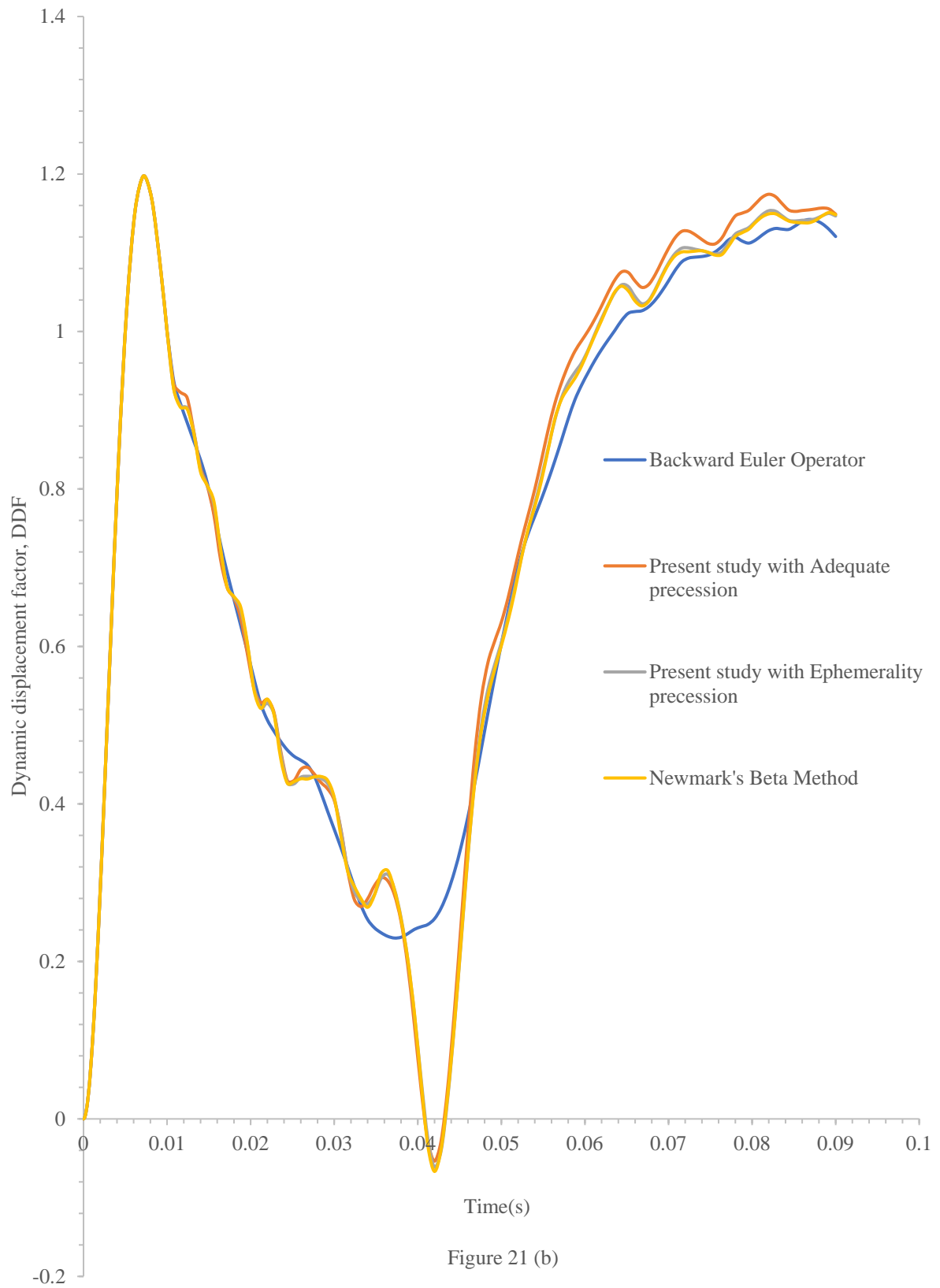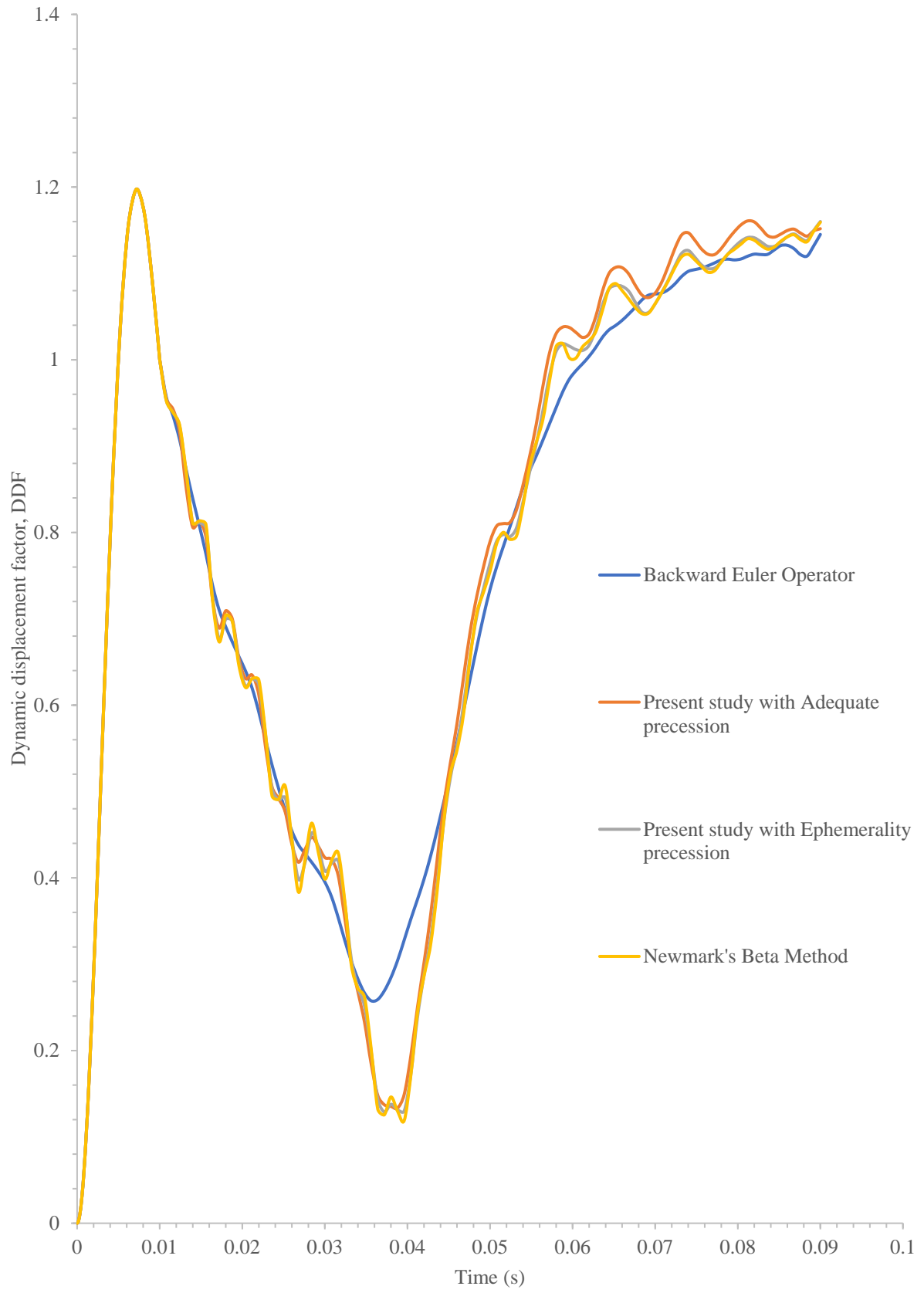
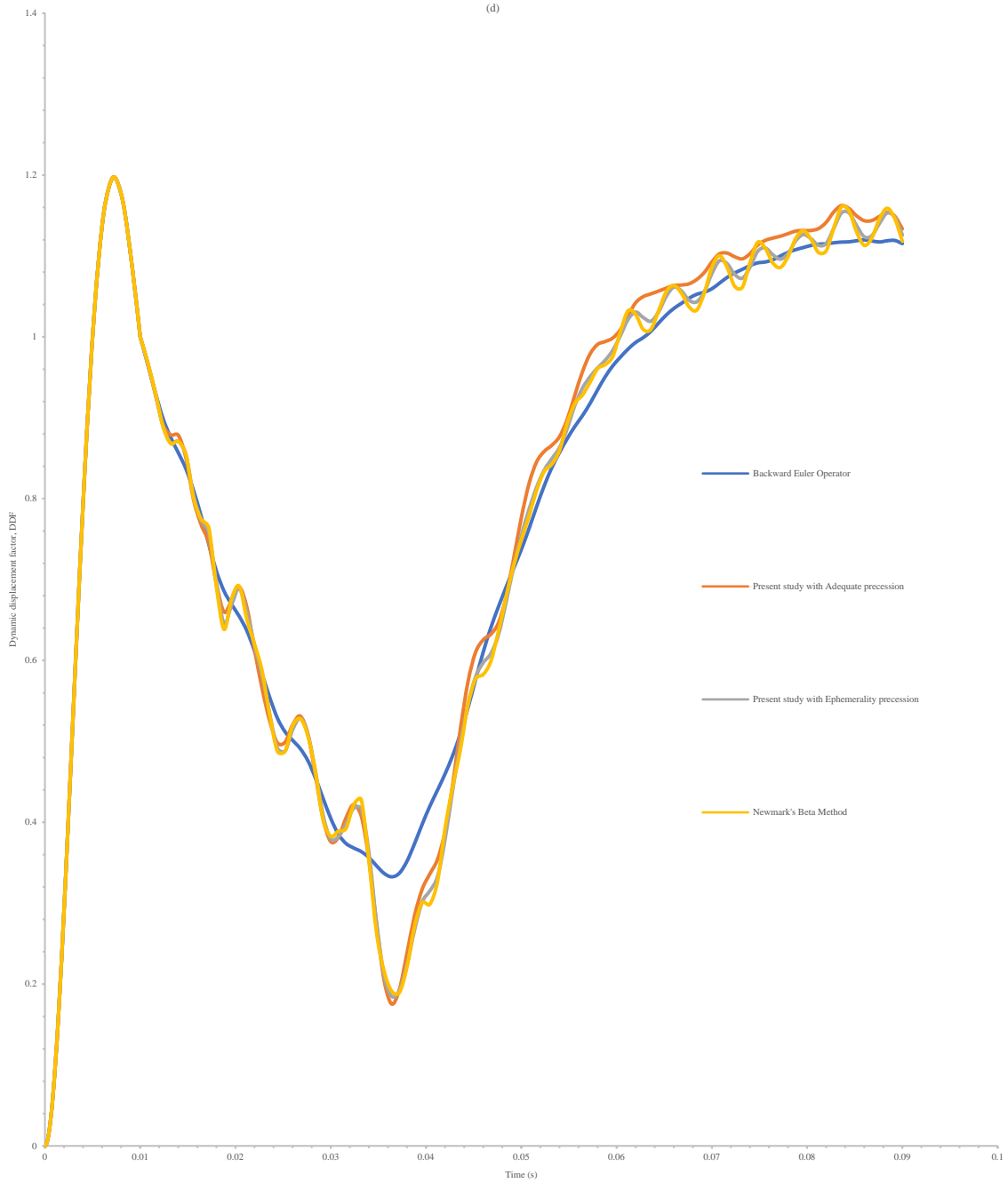Figure 21 (a)

Figure 21 (b)

(c)

Figure 21: Variation of DDF with time on pavement top at a velocity of 62.38 m/s using Backward Euler operator, HHT moderate dissipation operator, HHT transient fidelity operator, and Newmark's beta method for the present study in data convergence test as per global seeding mesh profile shown in figures (a) Global seeding 0.5, (b) Global seeding 0.4, (c) Global seeding 0.3, and (d) Global seeding 0.2.
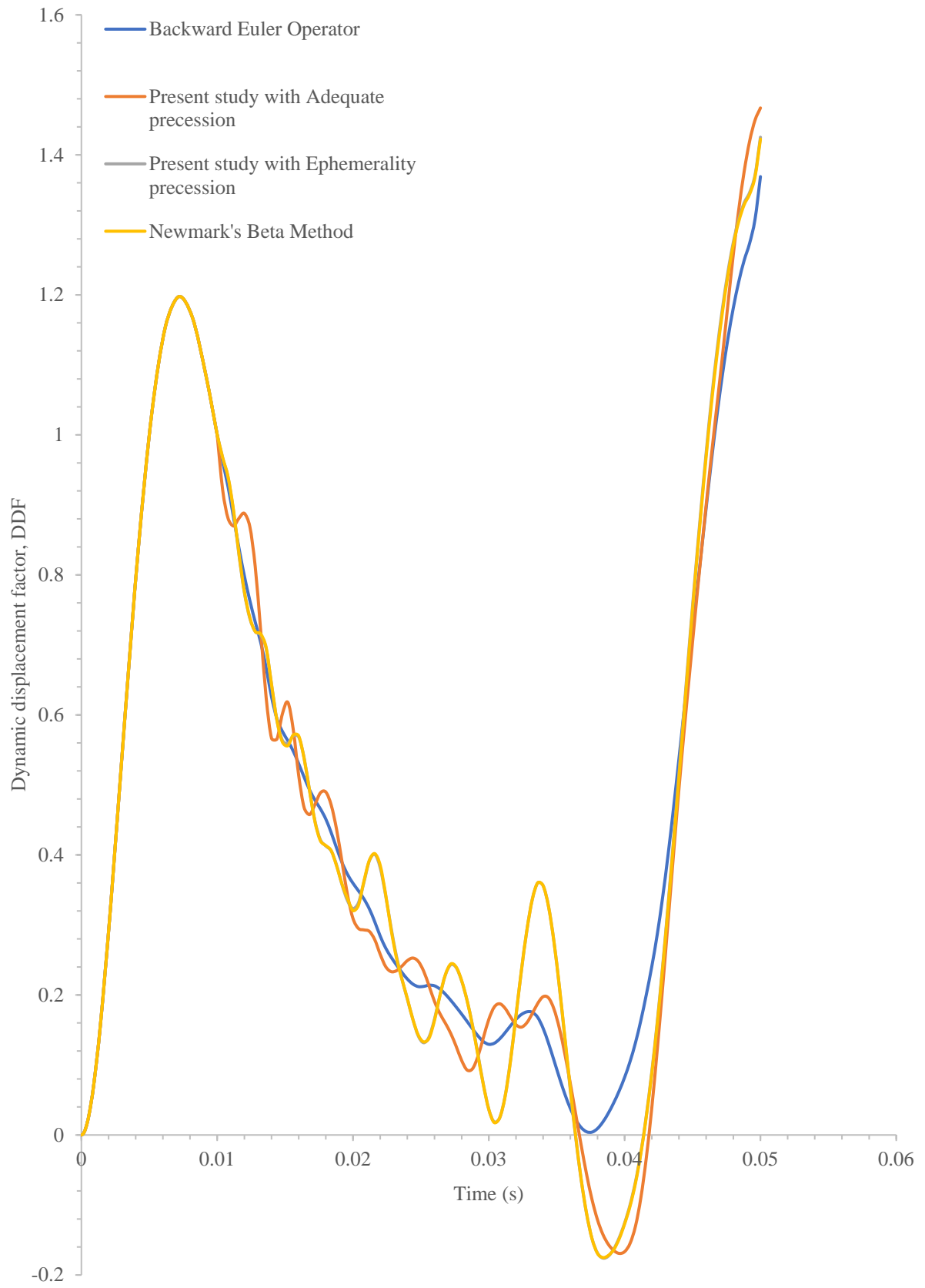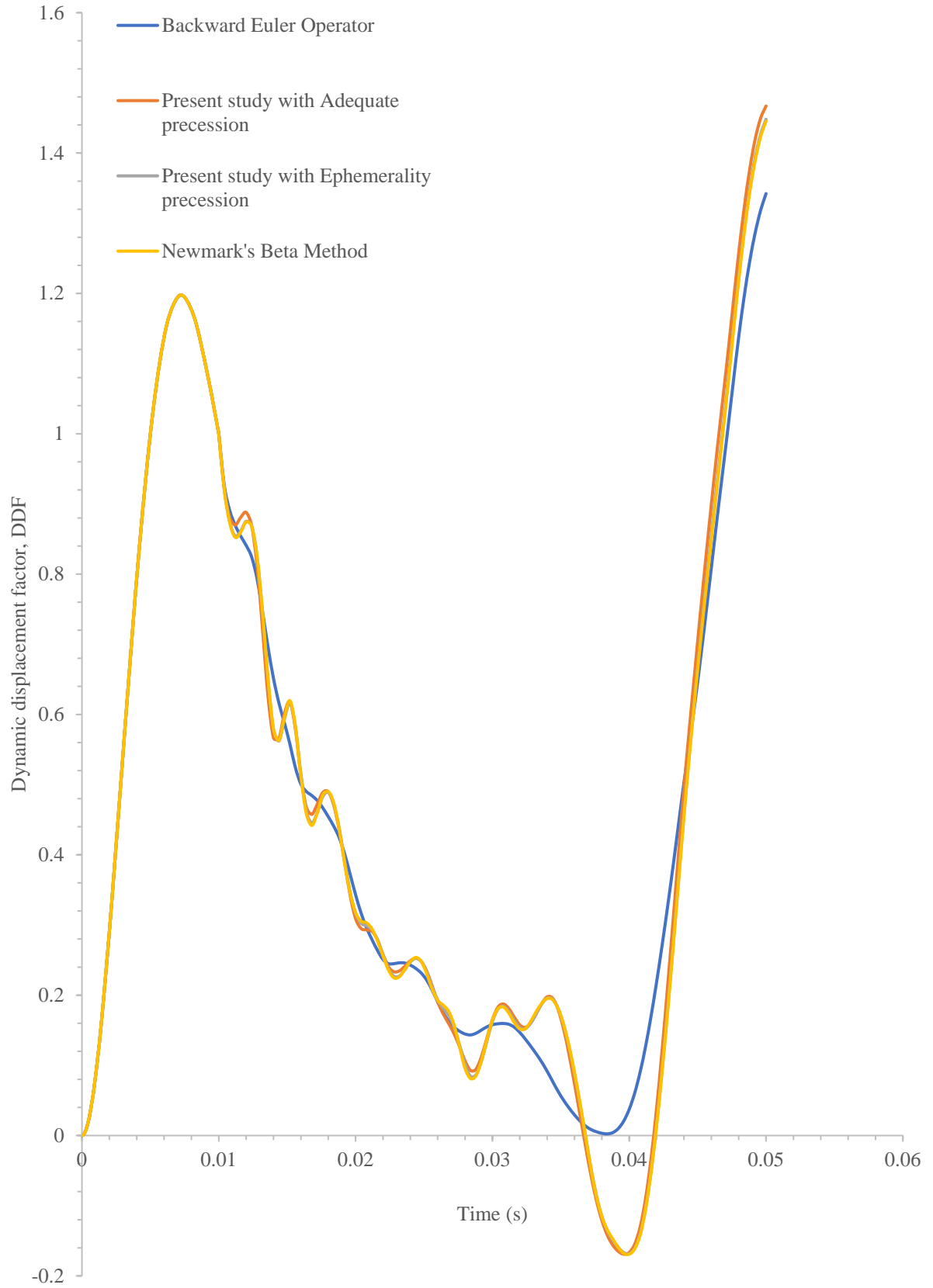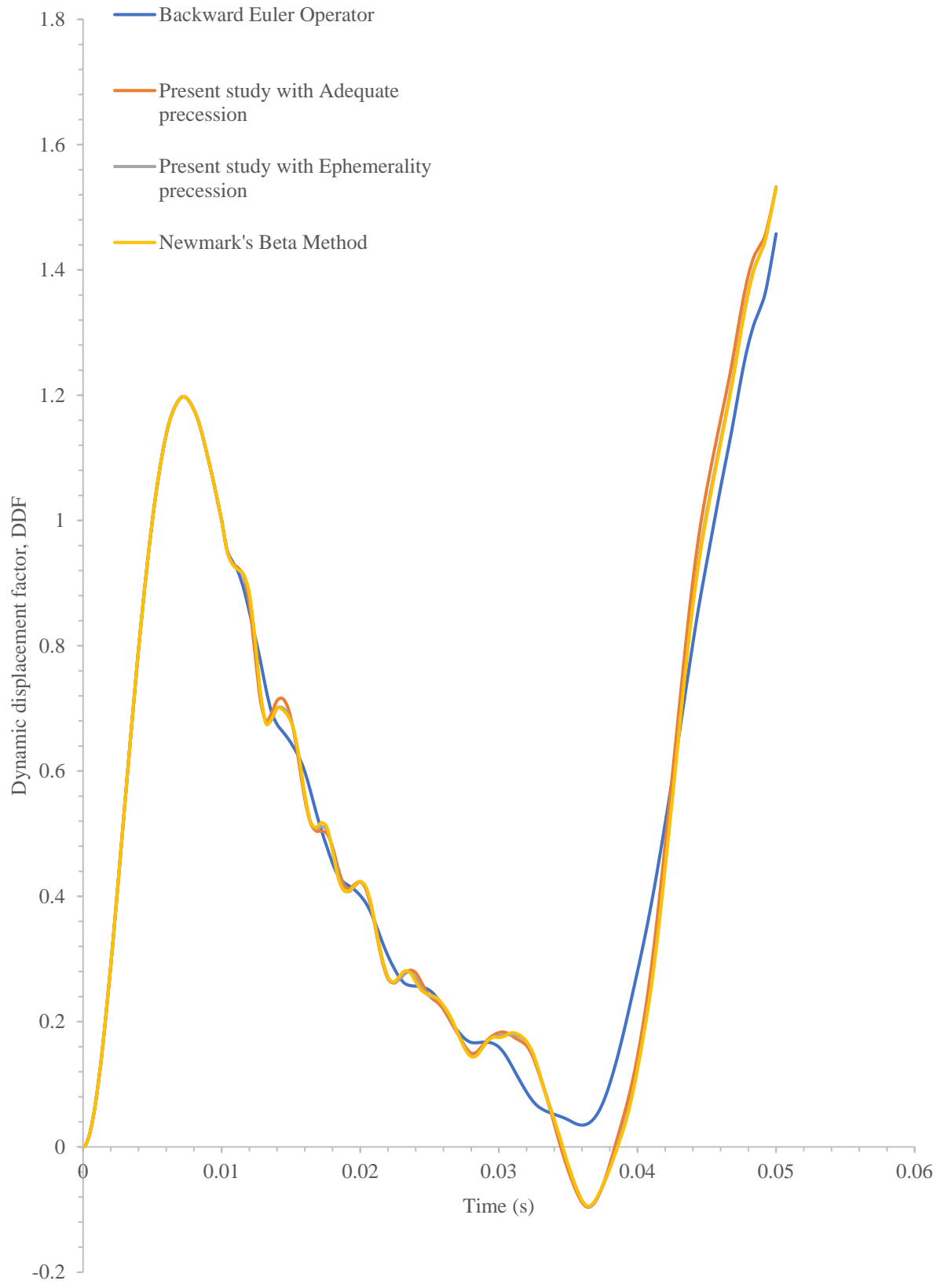
Figure 22 (a)
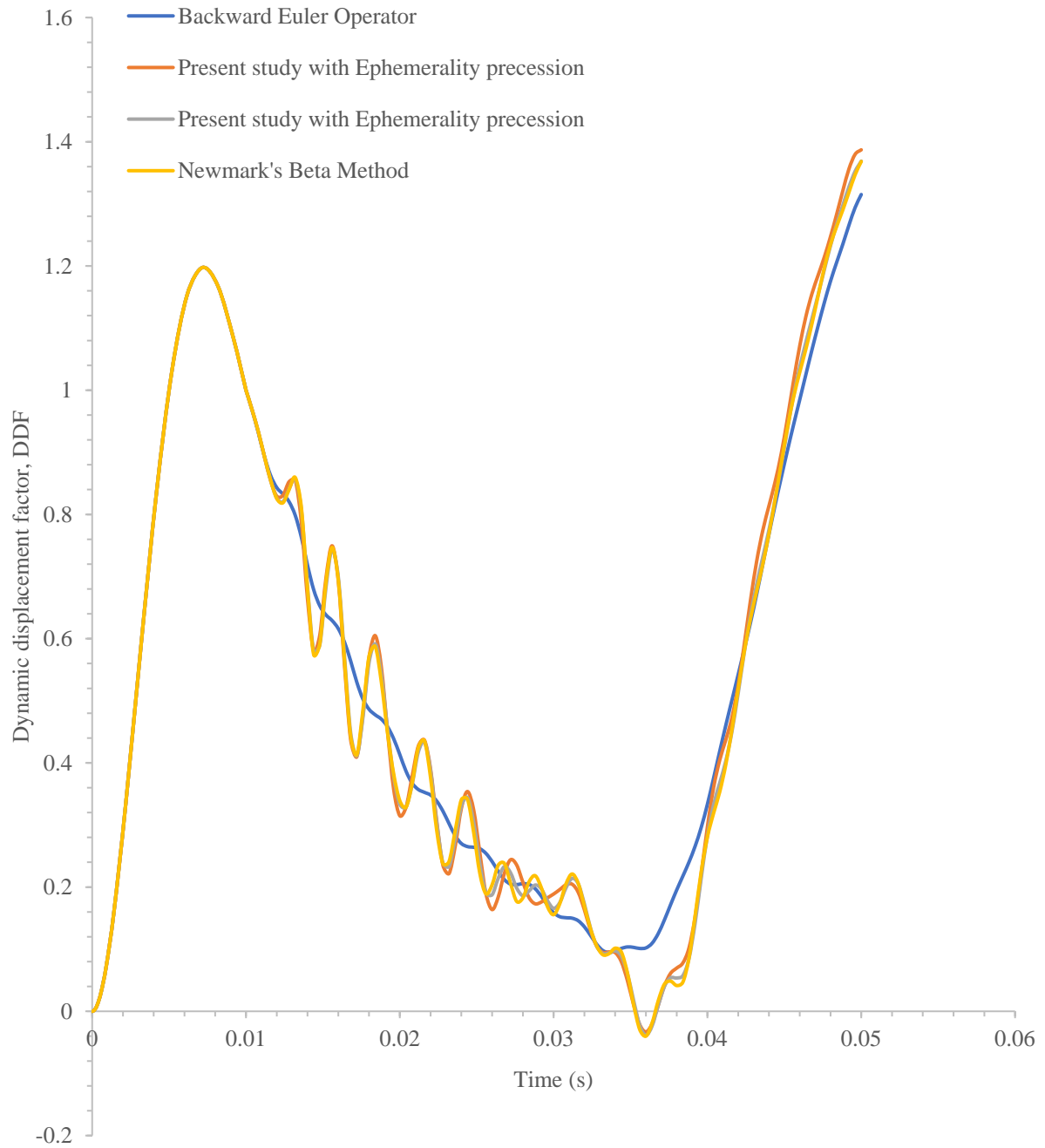
Figure 22 (b)

46

Figure 22(c)

Figure 22 (d)

Figure 22: Variation of DDF with time on pavement top at a velocity of 124.76 m/s using Backward Euler operator, HHT moderate dissipation operator, HHT transient fidelity operator, and Newmark's beta method for the present study in data convergence test as per global seeding mesh profile shown in figures (a) Global seeding 0.5, (b) Global seeding 0.4, (c) Global seeding 0.3, and (d) Global seeding 0.2.

It was observed that in the step time integration for the solver considered in the present study (both Adequate precision and Ephemerality precision) and Newmark's beta method shows the negative value of DDF for the velocity of 62.38 at global seeding of 0.4 and velocity of 124.76 m/s at global seeding of 0.5 to 0.2. The negative value of DDF indicates that a vacuum action was created due to high speed moving mass leading towards levitation.
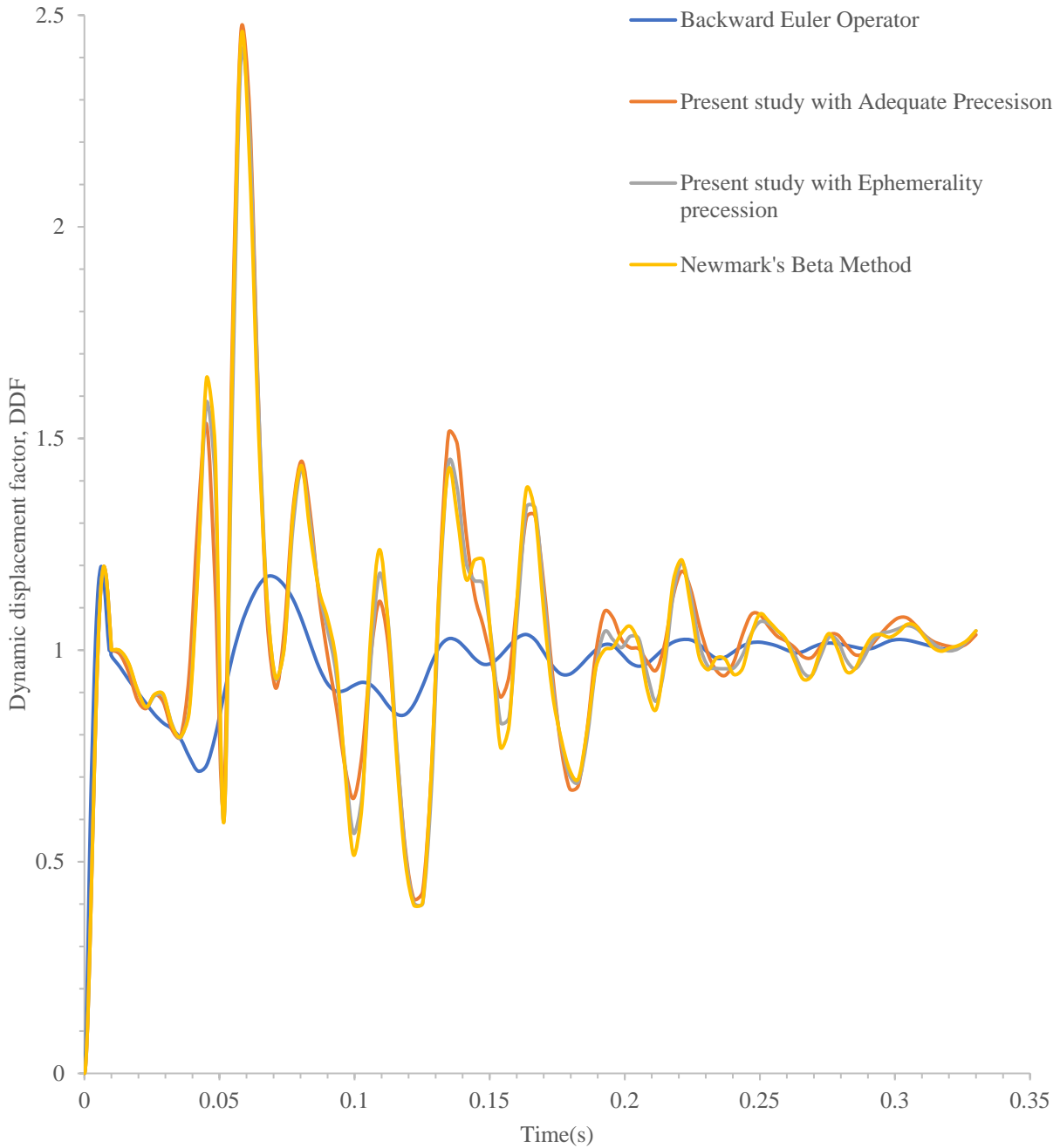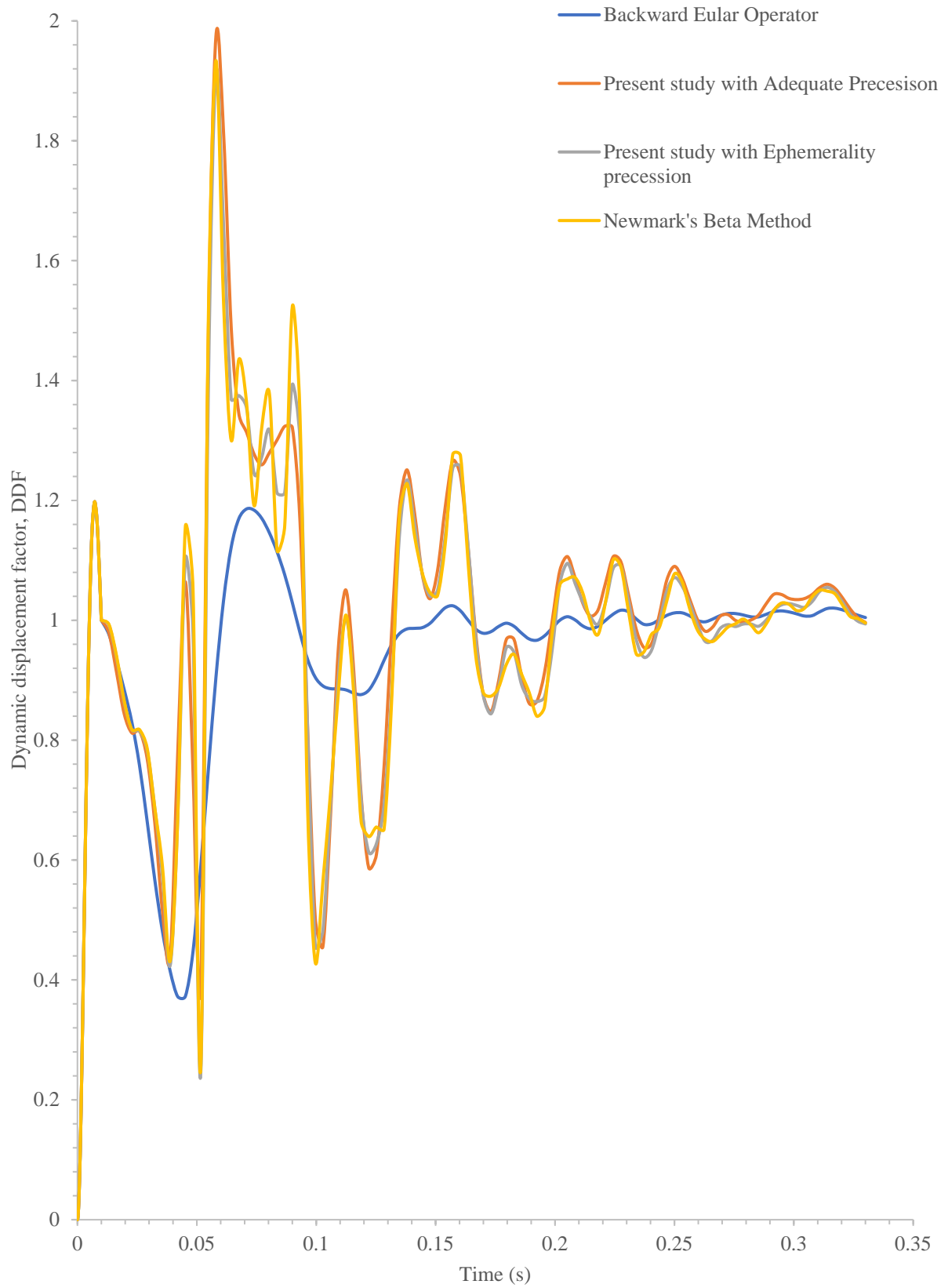

Figure 23 (a)

Figure 23 (b)

Figure 23 (c)

Figure 23 (d)

Figure 23: Variation of DDF vs time on retaining wall at a velocity of 15.6 m/s using backward Euler operator, HHT-moderate dissipation, HHT-transient fidelity, and Newmark's beta method for the present study and mesh convergence results as per global seeding mesh profile shown in figures (a) Global seeding 0.5, (b) Global seeding 0.4, (c) Global seeding 0.3, and (d) Global seeding 0.2.
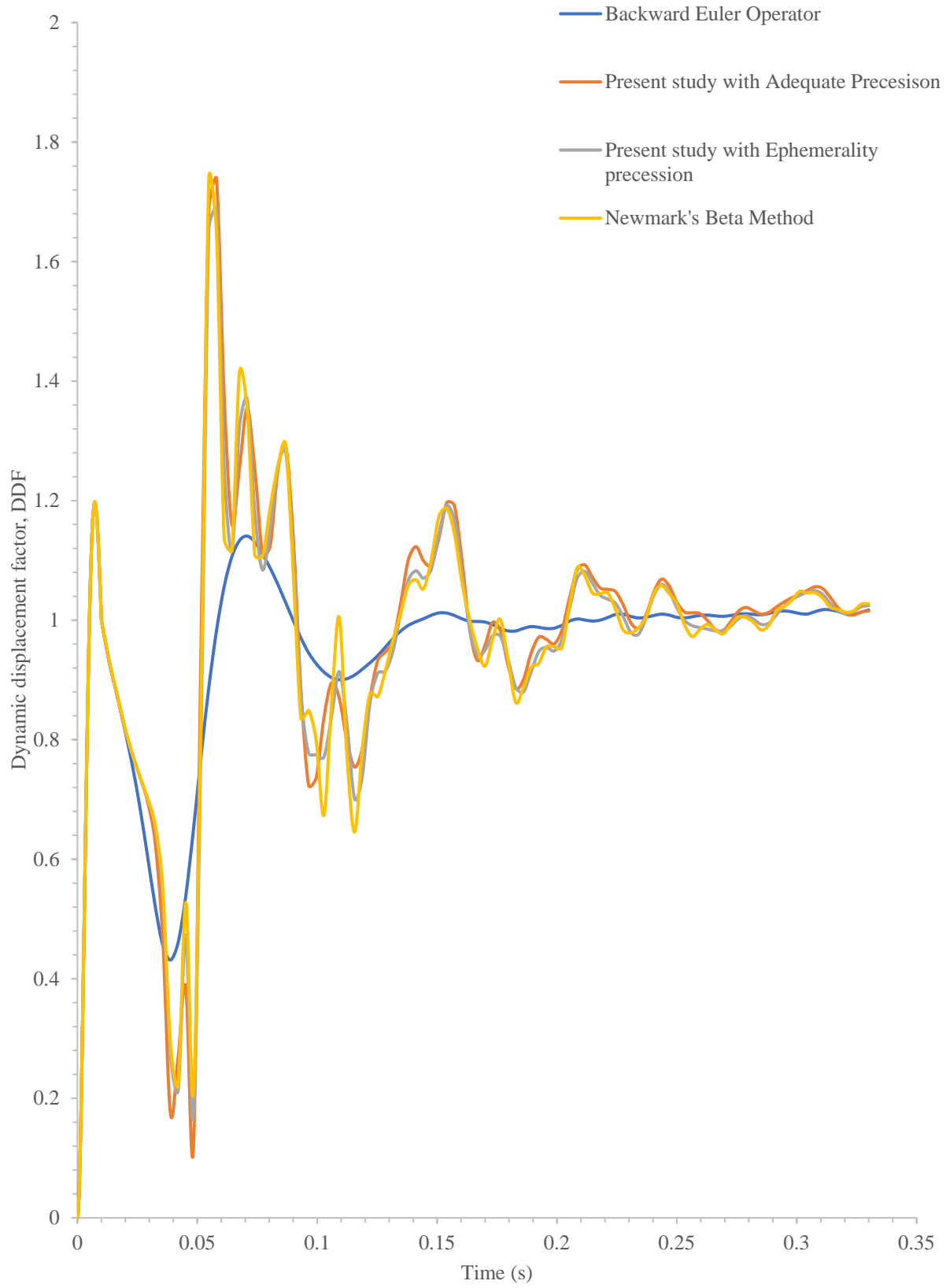
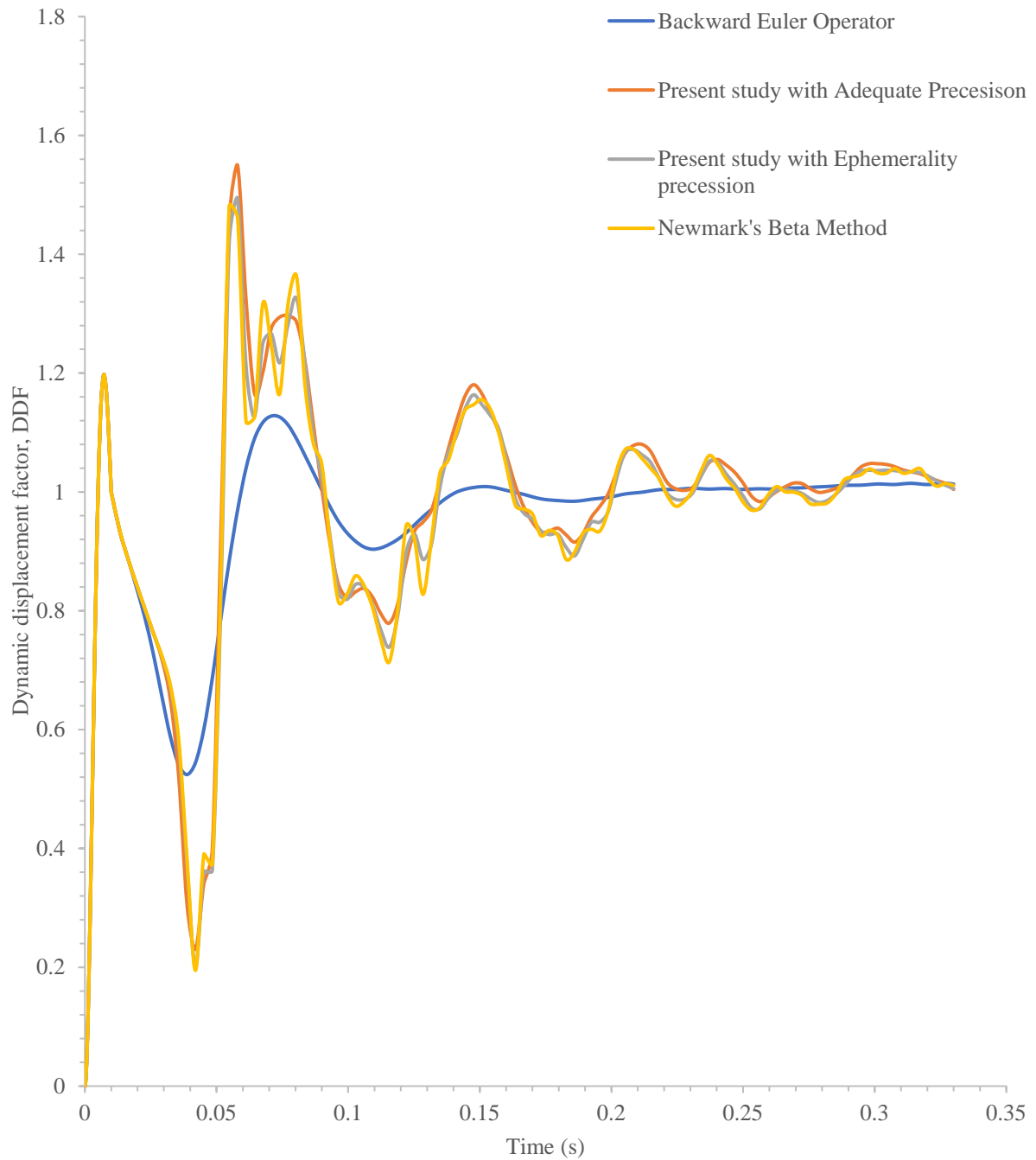Figure 24 (a)

Figure 24 (b)

Figure 24 (c)

Figure 24 (d)

Figure 24: Variation of DDF vs time on retaining wall at a velocity of 31.19 m/s using backward Euler operator, HHT-moderate dissipation, HHT-transient fidelity, and Newmark's beta method for the present study and mesh convergence results as per global seeding mesh profile shown in figures (a) Global seeding 0.5, (b) Global seeding 0.4, (c) Global seeding 0.3, and (d) Global seeding 0.2.
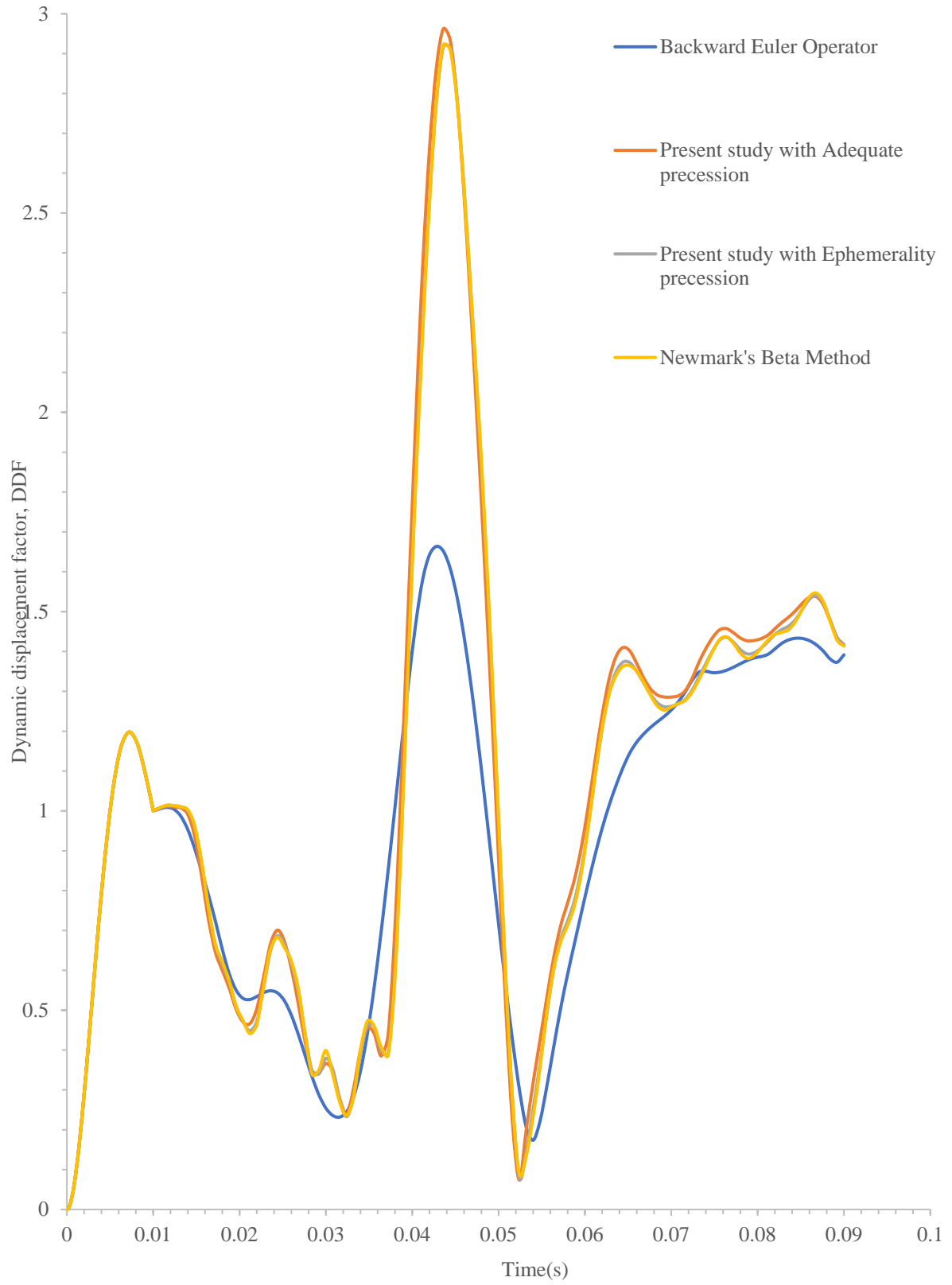
Figure 25 (a)
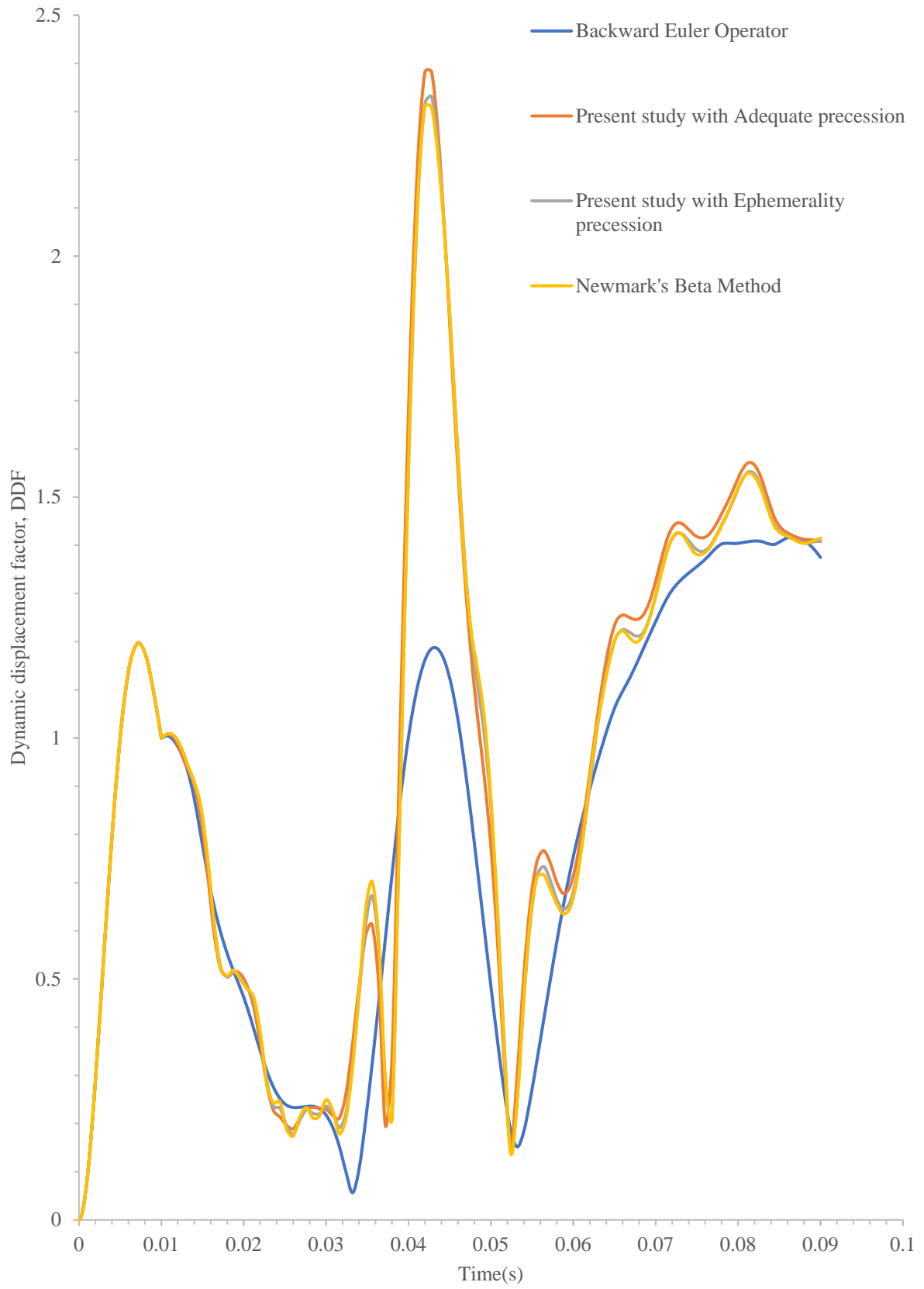
Figure 25 (b)
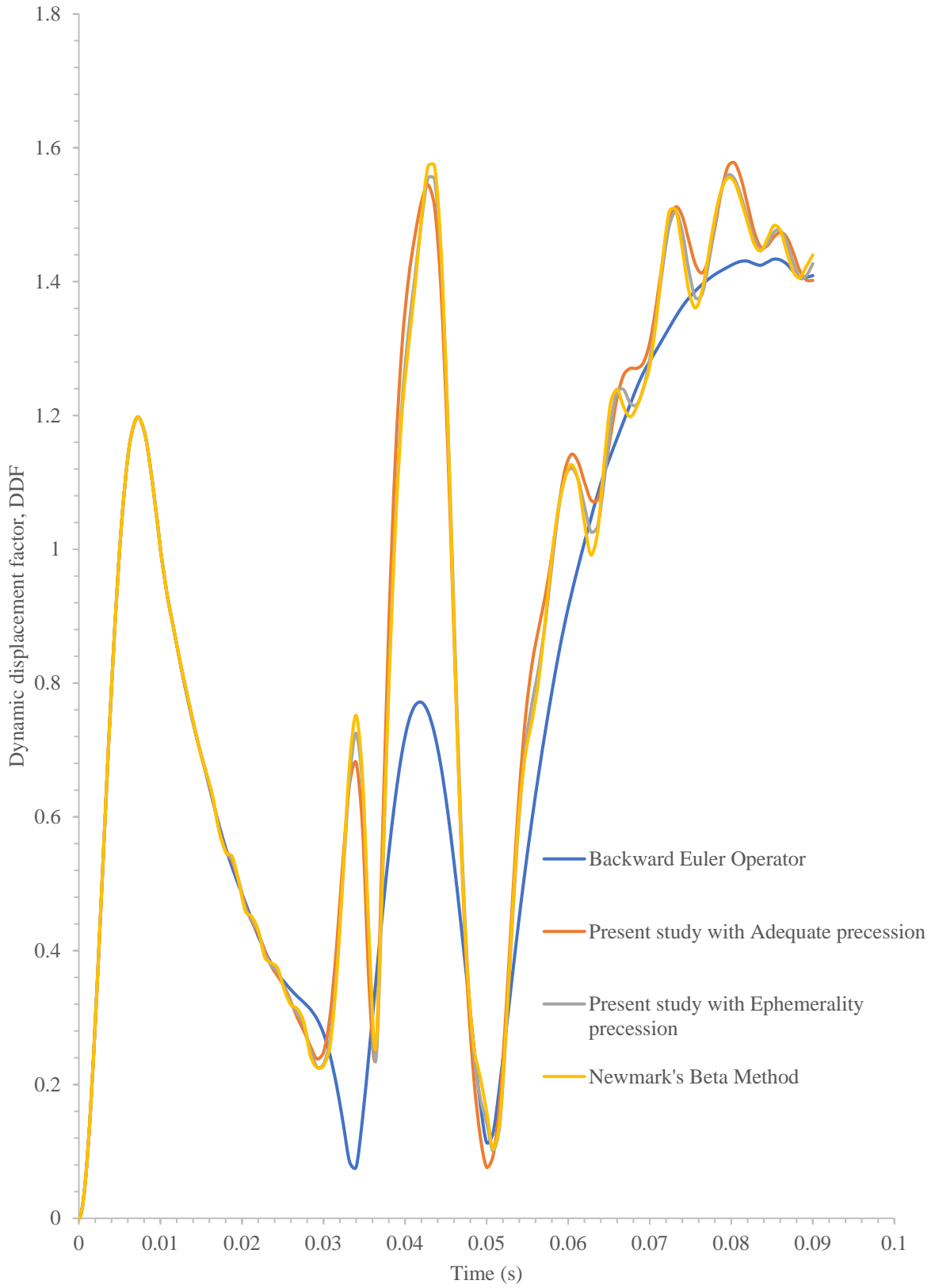
Figure 25(c)
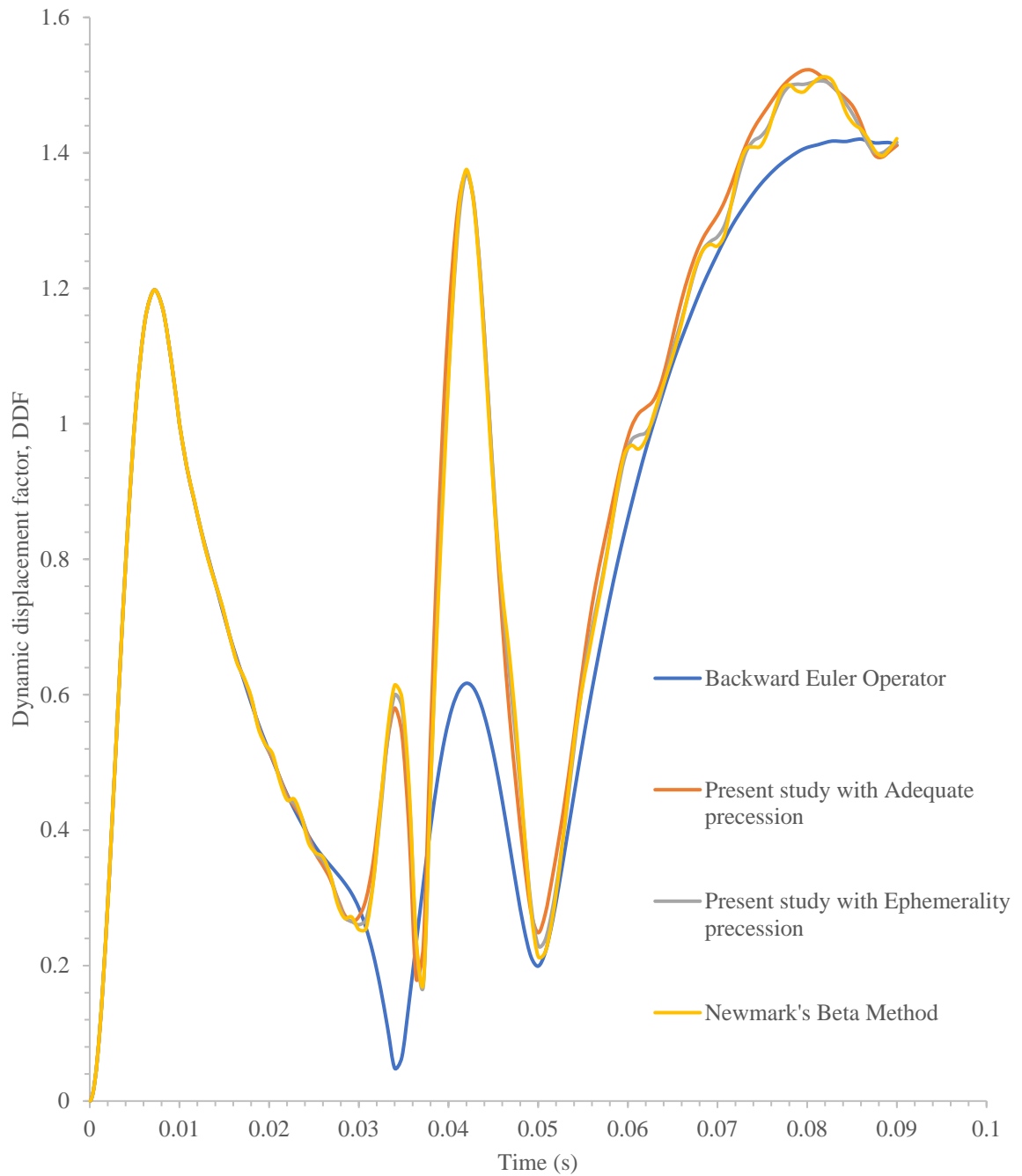
Figure 25 (d)

Figure 25: Variation of DDF vs time on retaining wall at a velocity of 62.38 m/s using backward Euler operator, HHT-moderate dissipation, HHT-transient fidelity, and Newmark's beta method for the present study and mesh convergence results as per global seeding mesh profile shown in figures (a) Global seeding 0.5, (b) Global seeding 0.4, (c) Global seeding 0.3, and (d) Global seeding 0.2.
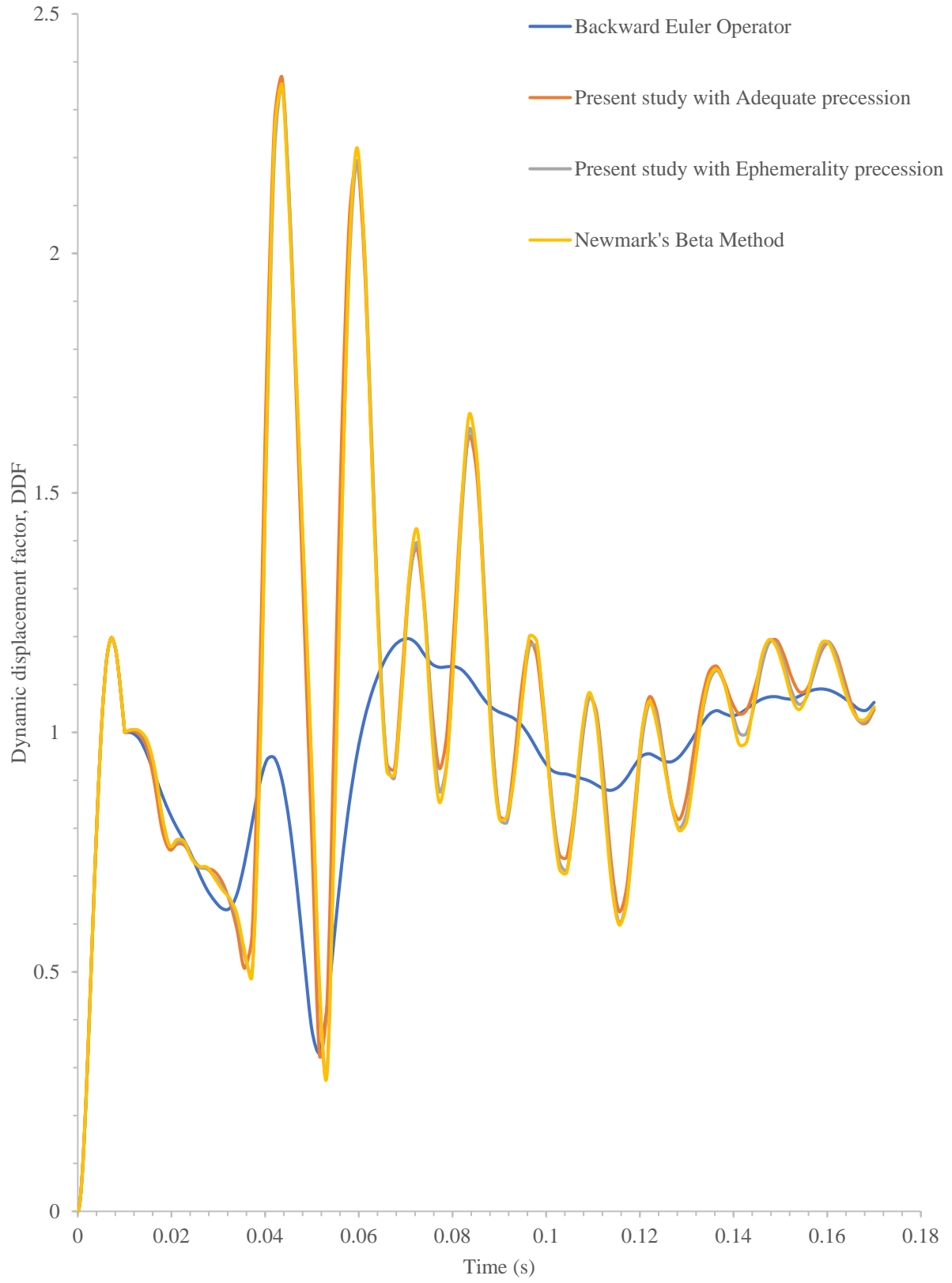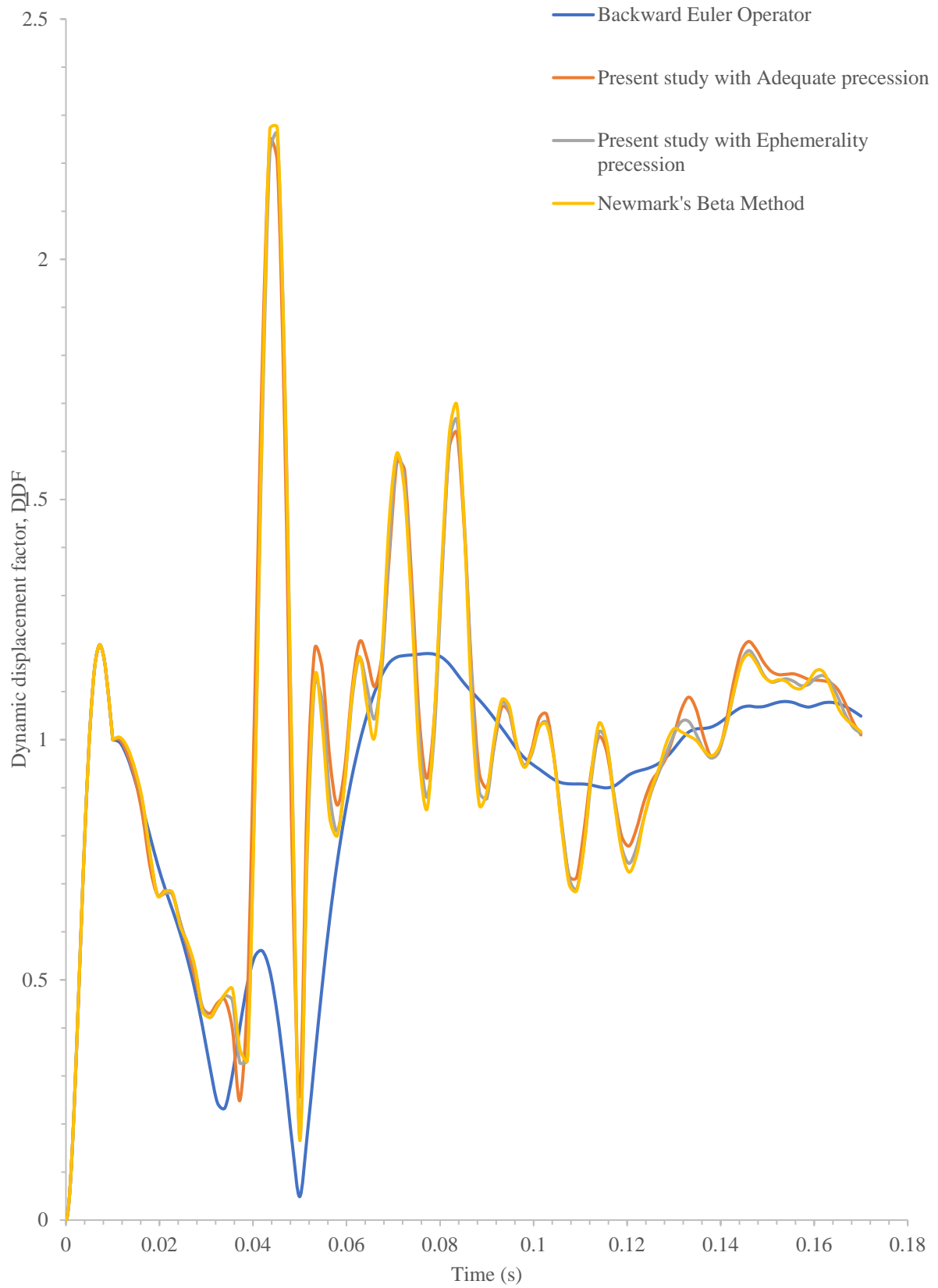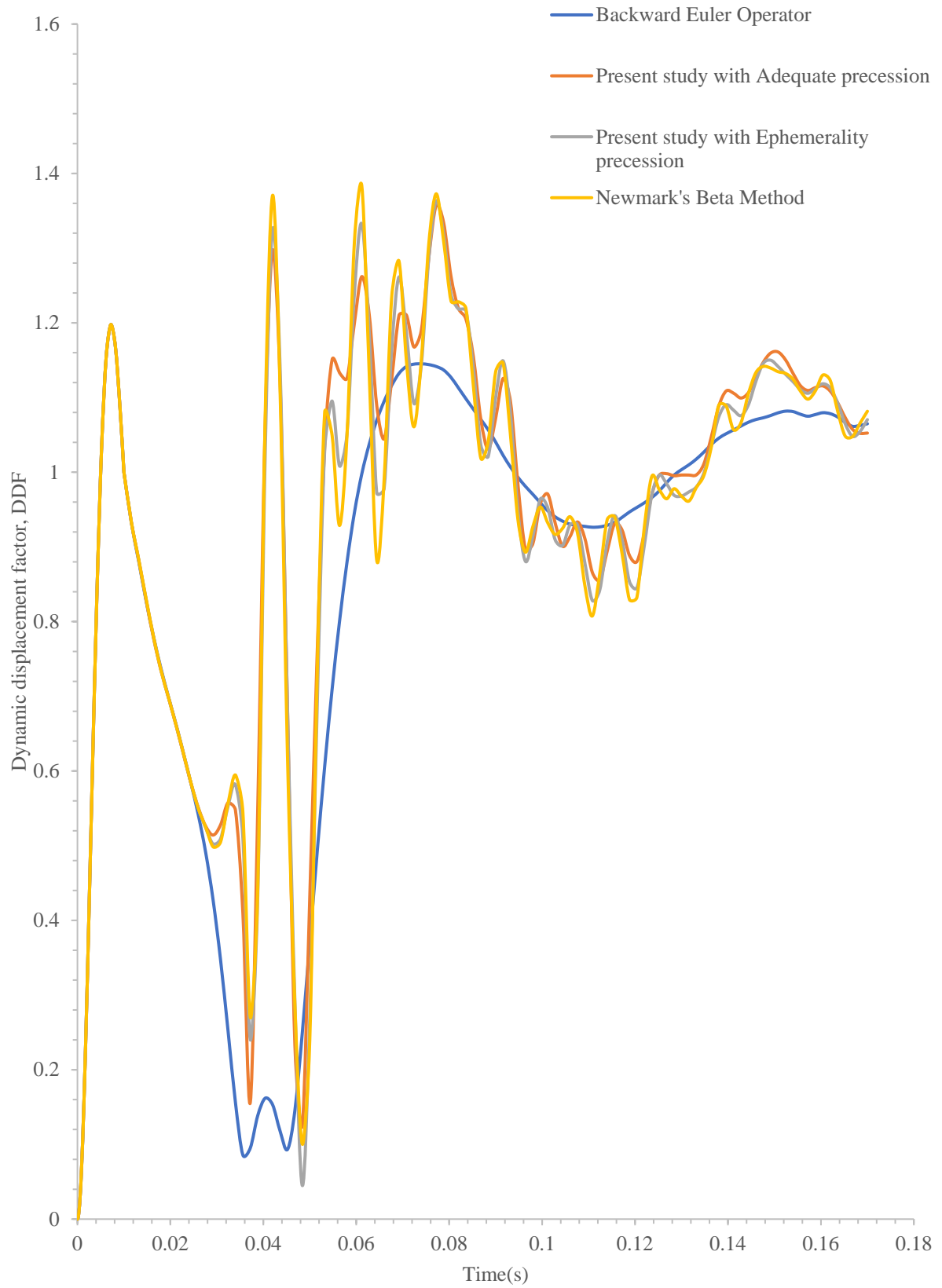
Figure 26 (a)
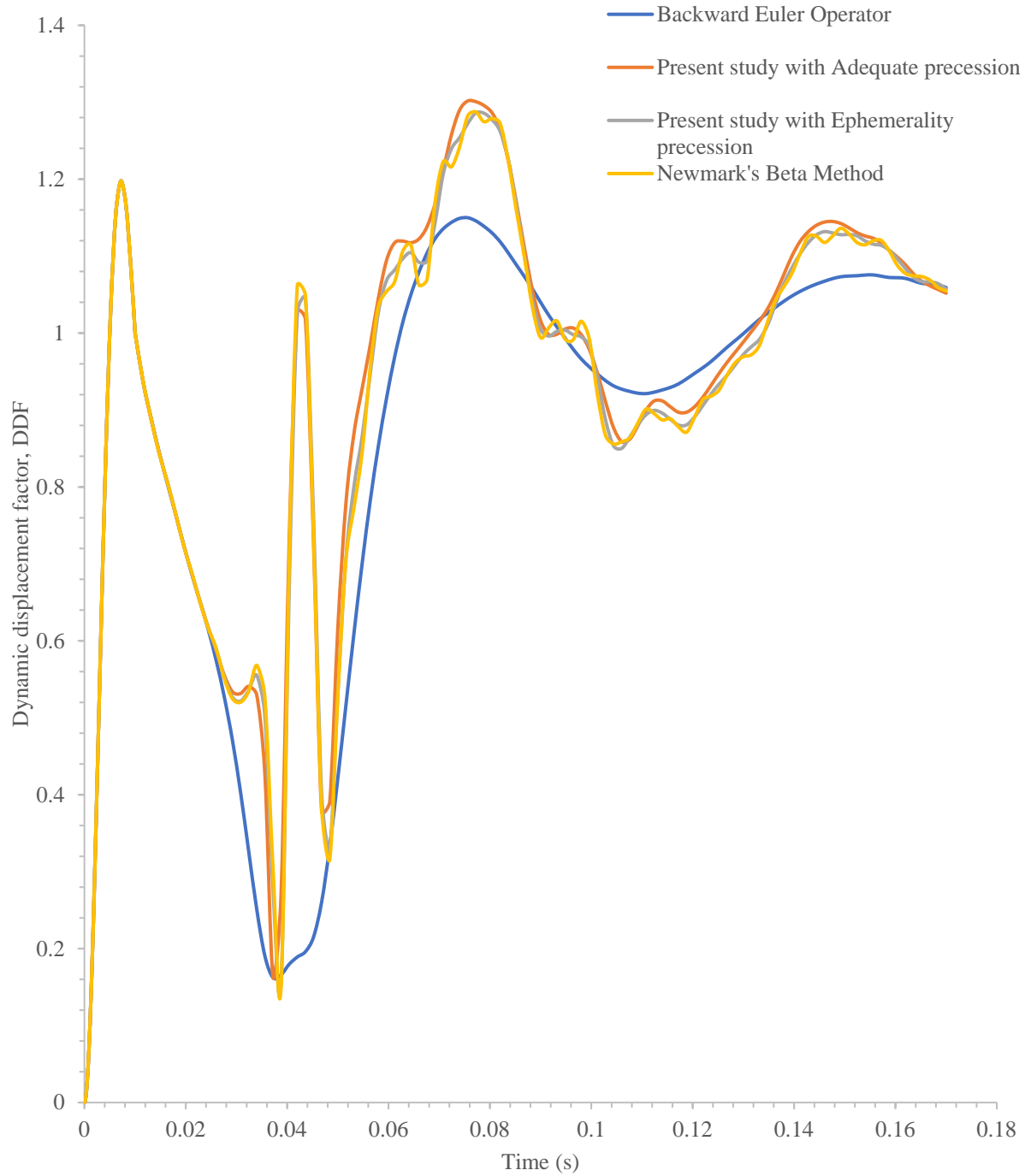
61
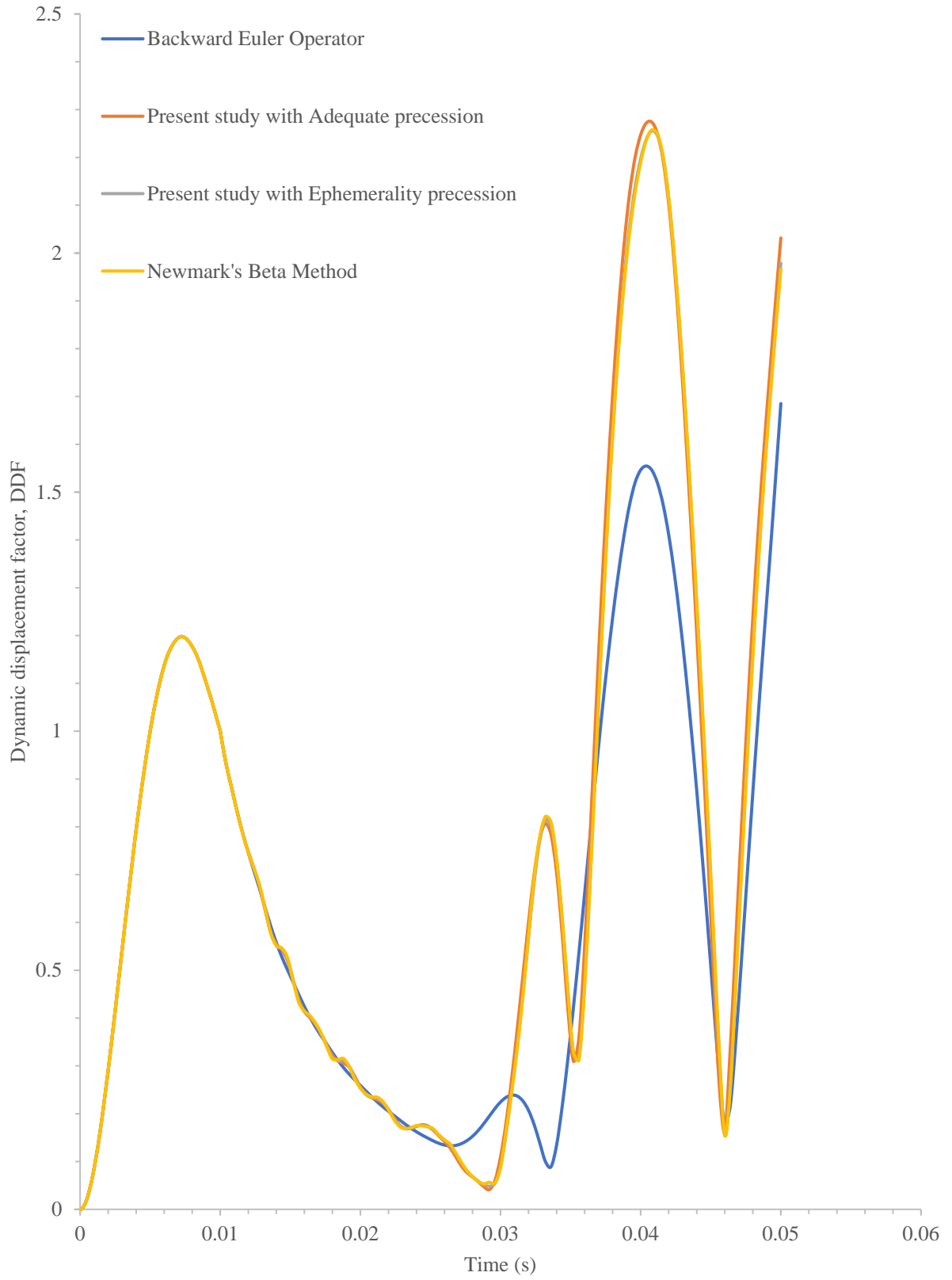
Figure 26 (b)

Figure 26 (c)
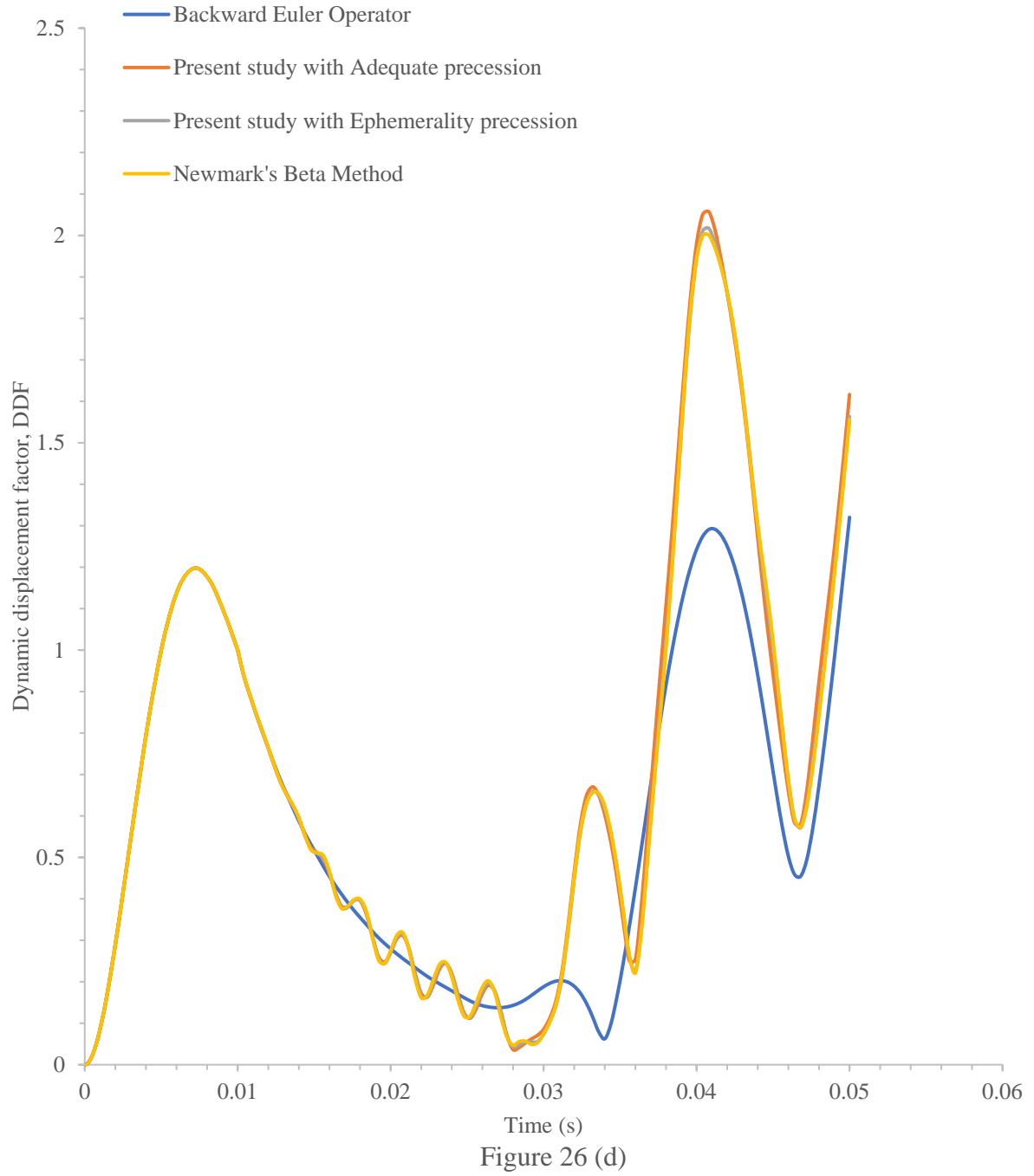
Figure 26 (d)

Figure 26: Variation of DDF vs time on retaining wall at a velocity of 124.76 m/s using backward Euler operator, HHT-moderate dissipation, HHT-transient fidelity, and Newmark's beta method for the present study and mesh convergence results as per global seeding mesh profile shown in figures (a) Global seeding 0.5, (b) Global seeding 0.4, (c) Global seeding 0.5, and (d) Global seeding 0.2.

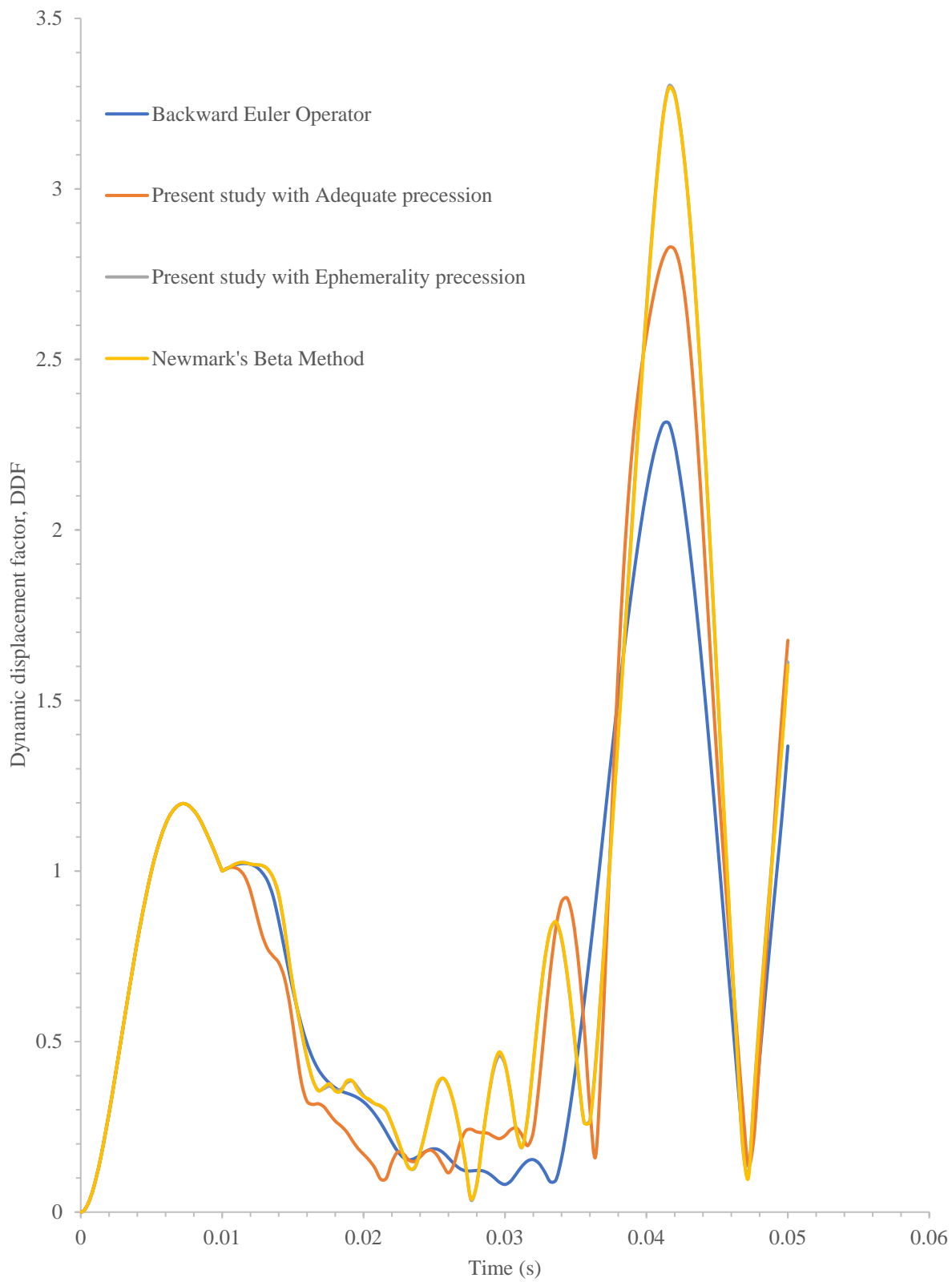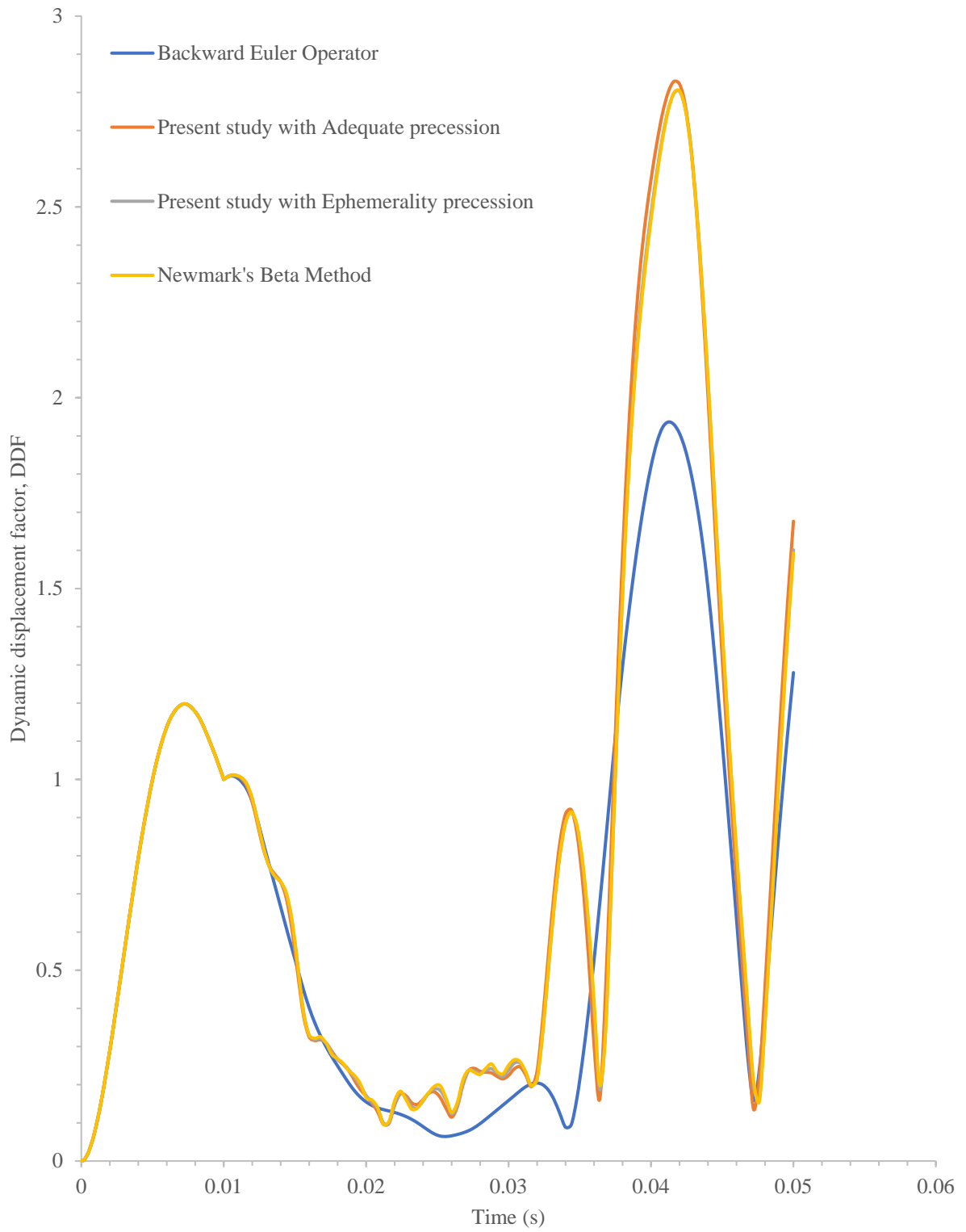As shown in Figure 23 to Figure 26 DCT in the lateral direction is performed and it was observed that in the step time integration for the solver considered in the present study (both Adequate precision and Ephemerality precision) and Newmark's beta method, shows the abrupt high values of DDF. Approximately 250% higher value in dynamic displacement is observed for coarse mesh as compared with static displacement for the velocity of 15.16 m/s. Similarly, for the velocity of 31.19 m/s, 62.38m/s, and 124.76 m/s the rise in dynamic displacement as compared to static displacement was observed to be 250%, 300%, and 350% respectively for coarser mesh size. With further reduction in mesh size, stability tends to increase. These abrupt changes indicate higher noise while integrating from one-time step integration to subsequent next time integration. Patterns observed in curves were highly noisy and the solver is stabilized using numerical damping.

No severe variation was observed in the finest mesh size adopted in this study. Hence the converged results obtained at the fine mesh size corresponding to global seeding of 0.2 are considered in this study for the analysis.

CHAPTER 6
Conclusion

A study of the dynamic response of rigid pavement constrained with retaining wall subjected to moving mass is done using a finite element model. The stability of the numerical model was studied in terms of numerical damping and results reported are compared with the case studies available in the literature. The effect of moving mass on the pavement top and retaining wall is reported in terms of load-dependent dynamic magnification factor (DMF) and displacement-dependent dynamic displacement factor (DDF). Further, a non-dimensional stiffness factor that accounts for dynamic stiffness produced due to moving load is reported in both lateral as well as in the vertical direction. The main conclusion from the present study are presented as follows,

1. With the increase in velocity magnification in load, displacement, and stress increases, and with an increase in damping magnification decreases.

2. Damping property has a significant contribution to harmonic response. With the decrease in damping, harmonic variation increases for stress response and dynamic deflection towards the end of the observation line and an increase in damping decreases the magnitude of stress with the harmonic response.

3. The effect of moving mass on stiffness property showed Harding and softening effects in the vertical and lateral direction.

4. For higher ranges of velocities (more than 115 m/s), the effect of levitation is observed because of which irregular shape in displacement bulb contours are observed and dynamic displacement lags behind the static displacement.

5. Maximum magnification in stiffness value is observed at a velocity of 124.76 m/s, indicating damper control across the retaining wall in the process of energy harnessing.

66

References

1. Achenbach, J.D., Sun, C.T., 1965. Moving load on a flexibly supported Timoshenko beam. Int. J. Solids and Struct., 1(4): 353-370.

2. Bowles, J.E., 1996. Foundation analysis and design, 5th Ed., McGraw Hill, New York, London.

3. Chiu, W.S., Smith, R.G., Wormley, D.N., 1971. Influence of vehicle and distributed guideway parameters on high speed vehicle guideway dynamic interactions. J. Dyn. Sys., Measurement, Control, 93(1): 25-34.

4. Ding, H., Yang, Y., Chen, L.Q., Yang, S.P., 2014. Vibration of vehicle pavement coupled system based on a Timoshenko beam on a nonlinear foundation. Journal of Sound and Vibration, 333 (24): 6623–6636.

5. Fryba, L., 1972. Vibration of solids and structures under moving loads, Noordhoff Int. Publ., Holland, The Netherlands.

6. Hilber, H.M., Hughes, T.J.R., Taylor, R.L., 1977. Improved Numerical Dissipation for Time Integration Algorithms in Structural Dynamics. Earthquake Engineering and Structural Dynamics, 5(3): 283–292.

7. Hinton, E., Owen, D.R.J., 1979. An introduction to finite element computations, Pineridge Press Limited, Swansea, United Kingdom.

8. Ioannides, A.M., Donnelly, J.P., 1988. Three-dimensional analysis of slab on stress-dependence foundation. Transp. Res. Rec., 1196: 72-84.

9. Kim, S.M., McCullough, B.F., 2003. Dynamic response of plate on viscous Winkler foundation to moving loads of varying amplitude. Engineering Structures, 25(9): 1179-1188.

10. Kumari N., Trivedi A. (2020). Vibration Control of Flexible Retention Systems. Advance in Computer Methods and Geomechinics. Lecture Notes in Civil Engineering, 56: 71-79 Springer, Singapore.

11. Lewis, K.H., Harr, M. E., 1969. Analysis of concrete slabs on ground subjected to warping and moving loads. Hwy. Res. Bull., 291(17): 194-211.

12. Liao, G.Y., Huang, X.M., 2008. Application of ABAQUS finite element software in road engineering, Southeast University Press, Nanjing, China.

13. Mejlun, L., Judycki, J., Dolzycki, B., 2017. Comparison of elastic and viscoelastic analysis of asphalt pavement at high temperature. Procedia Engineering, 172: 746–753.

14. Taheri, M.R., Ting, E.C., 1989. Dynamic response of plate to moving loads: structural impedance method. Compo and Struct., 33(6): 1379-1393.

15. Taheri, M.R., Ting, E.C., 1990. Dynamic response of plates to moving loads: finite element method. Compo and Struct., 34(3): 509-521.

16. Taheri, M.R., Zaman, M.M., Alvappillai, A., 1990. Dynamic response of concrete pavements to moving aircraft. J. Appl. Math. Modelling, 31(3): 562-575.

17. Tang, C., Lu, Z., Duan, Y., Yao, H., 2020. Dynamic responses of the pavement-unsaturated poroelastic ground system to a moving traffic load. Transportation Geotechnics, 33: ISSN 2414 – 3912.

18. Thompson, W.E., 1963. Analysis of dynamic behaviour of roads subject to longitudinally moving loads. Hwy. Res. Bull., 39: 1-24.

19. Wang, B., Yang, J., 2008. Effects of vehicle dynamic loading on CRCP by 3D finite element method. Journal of Southeast University: Natural Science Edition, 38(5): 850-855.

20. Wang, J.C., Chen, Y.K., 2006. Application of ABAQUS in civil engineering, Zhejiang University Press, Hangzhou, China.

21. Wang, Y.S., Fu, C.G., 2010. ABAQUS structural engineering analysis and example explanation, China Architecture and Building Press, Beijing, China.

22. Wu, C., Shen, P.A., 1996. Dynamic Analysis of Concrete Pavements Subjected to Moving Loads. Journal of Transportation Engineering, 122(5): 367–373.

23. Yang, S., Lu, Y., Li, S., 2013. An overview on vehicle dynamics. International Journal of Dynamics and Control, 1 (4): 385–395.

24. Yoshida, D.M., Weaver, W., 1971. Finite element analysis of beams and plates with moving loads. Publ. Int. Assn. Bridge Struct. Engrg., 31(1):179-195.

25. Zaman, M., Taheri, M. R., Alvappillai, A., 1991. Dynamic response of a thick plate on viscoelastic foundation to moving loads. Int. J. Numer. Anal. Methods Geomech., 15(9):627-647.

26. Zhuang, Z., You, X.C., Cen, S., 2009. Finite element analysis and application based on the ABAQUS, Tsinghua University Press, Beijing, China.